UNIVERISDAD DE COSTA RICA

SISTEMA DE ESTUDIOS DE POSGRADO

Caracterización del efecto del veneno del escorpión endémico de Costa Rica *Tityus championi* y sus neurotoxinas sobre la excitabilidad neuronal y las corrientes iónicas de sodio y potasio generadas por canales voltaje dependientes de moluscos, mamíferos e insectos

Tesis sometida a la consideración de la Comisión del Programa de Estudios de Posgrado en Biología para optar al grado y título de Maestría Académica en Biología con énfasis en Genética y Biología Molecular

CANDIDATA

Johanna Galit Akerman Sánchez

Ciudad Universitaria Rodrigo Facio, Costa Rica

2024

AGRADECIMIENTOS

Hacer ciencia como la que se encuentra en esta tesis ha sido un verdadero privilegio y regalo. Puedo decir que, en su gran mayoría, me sentí plena y descubrí nuevas fases de mí. Esto jamás lo hubiera podido lograr sin la ayuda de muchas personas. Personas que me dieron algo que cambió una parte de mí. Primero, quisiera agradecer a mi papá y a mi mamá, los más importantes. A mi padre, Jorge, por llenarme de preguntas y curiosidad desde que estaba pequeña, viendo bichos en el bosque y células en el microscopio. No es casualidad que cada vez me convierta en la científica que inspiró mi padre. A mi madre, Lorena, por darme toda la fuerza y amor que una persona puede necesitar, con tan solo un abrazo. Por esas noches que nos acompañamos juntas estudiando, y me hiciste saber que era capaz de todo lo que quisiera lograr. A Daniel, mi querido novio, quien me ha apoyado incondicionalmente, desde trabajar en códigos, escucharme hablar por horas, hasta atravesar el océano Atlántico y disfrutar de la vida juntos. Gracias Dani, no hay palabras con las que pueda expresar mi gratitud hacia vos.

Al Dr. Oscar Brenes, mi tutor y mentor, gracias por todo lo que ha compartido conmigo, gracias por darme la bienvenida al mundo de la electrofisiología y hacerla hermosa y cautivante sin importar cuan difícil sea. Comunicar la ciencia y lograr que las personas se enamoren así, es un don. Gracias por la confianza que ha depositado en mí, por las oportunidades que ha hecho florecer en mi camino. Por hacerme una mejor científica con cada conversación, mientras comemos pollo frito en el Mall San Pedro. Gracias a la Dra. Adarli Romero, por darme un ejemplo tan claro de la mujer fuerte científica que quiero ser. Por enseñarme a usar mis manos y construir lo que necesito. Gracias por esa primera clase de fisiología animal en donde con sus palabras yo dije, esto es lo que finalmente andaba buscando. Muchas personas pueden enseñar en la universidad, pero no todas van a cuidar y enseñar como usted lo hace, profe.

También, quisiera agradecer a mi profesor en Bélgica, Dr. Jan Tytgat, quien abrió las puertas de su laboratorio para poder responder las preguntas con las cuales no dejaba dormir a Daniel. Esas respuestas que me apasionaba descubrir, las encontré a su lado, Dr. Jan. Gracias por su amabilidad, por las numerosas discusiones en el laboratorio al lado de registros, por todas las

aventuras en bicicleta, donde me mostró realmente cómo es Leuven. Por abrir mi mente a una cantidad inmensurable de más preguntas, que no me paralizan, más bien me dan fuerza.

Sin embargo, no me puedo ir sin mencionar a dos personas que siempre han celebrado mi camino en la ciencia. Ellas han sido mis abuelas, Diana y Zulma. Para el cielo, mando muchos besos hacia mi Dianita, quien siempre me escuchó con emoción cuando le decía que venía del laboratorio. A Zulma, quien siempre está ansiosa por escuchar lo que hago en la universidad. Siempre sentí que mis abuelas estaban orgullosas de mi con solo decirles que quería ser científica. De vez en cuando escuchaba decirse una a la otra "que dichosa, ¿verdad?". Me decían sutilmente "aproveche mamita", "me hubiera encantado…". Esas frases siempre calaron en mí. Creo fielmente que, hoy tengo la posibilidad de hacer esto, gracias al camino que mujeres como mis abuelas han recorrido y pavimentado.

Espero hacerla sentir orgullosa, Tita Diana.

Espero hacerla sentir orgullosa, Zuli.

Gracias por darme la vida, esta vida.

Con gratitud y amor,

Galit

"Esta tesis fue aceptada por la Comisión del Programa de Estudios de Posgrado en Biología de la Universidad de Costa Rica, como requisito parcial para optar al grado y título de Maestría Académica en Biología con énfasis en Genética y Biología Molecular."

[Dra. Mariela Arias Hidalgo, Ph.D]
Representante de la Decana
Sistema de Estudios de Posgrado

[Dr. Oscar Brenes García, Ph.D]

Director de Tesis

[Dra. Cecilia Díaz Oreiro, Ph.D]

Asesora

[Dra. Adarli Romero Vasquéz, Ph.D]

Asesora

[Dr. Andrey Sequeira Cordero, Ph.D]

Representante Programa de Posgrado en Biología

[Johanna Galit Akerman Sánchez]

Candidata

RESUMEN

El objetivo de esta investigación fue caracterizar electrofisiológicamente el veneno y las neurotoxinas del escorpión *Tityus championi*, una especie endémica de Costa Rica, enfocándose en los canales iónicos voltaje-dependientes de Na^+ (Na_V) y K^+ (K_V), que son los blancos selectivos de las neurotoxinas de escorpión. Se utilizaron dos modelos celulares: *(i)* una neurona del caracol *Helix aspersa*, que expresa el canal $Na_V1.7$-like, relacionado con nociceptores, y *(ii)* ovocitos de rana *Xenopus laevis*, donde se expresaron de forma heteróloga isoformas de canales iónicos de humanos, ratas e insectos. Los resultados mostraron que el veneno disminuye la excitabilidad neuronal, y puede afectar tanto las corrientes de Na^+ como de K^+, en la neurona del caracol y en canales de mamíferos e insectos. Se identificaron toxinas que aumentan la sensibilidad de los Na_Vs y una toxina que los inhibe, siendo probablemente la toxina Tch3 una de las principales responsables de la inhibición de la corriente de Na^+ y la disminución de la excitabilidad neuronal. Se identificó una nueva toxina selectiva para K_Vs, denominada TchKTx7, que mostró un bloqueo prácticamente completo en $K_V1.2$ y parcial en ShakerIR. Además, se observaron efectos de α-toxina sobre los canales $Na_V1.6$, $Na_V1.7$ y $BgNa_V1$. En el caso del $Na_V1.7$, aunque presenta efectos de α -toxina, también se observó una inhibición de la corriente máxima, congruente con lo observado en los canales de caracol. Este estudio representa un avance significativo en el entendimiento de las neurotoxinas de *T. championi*, siendo el primero en caracterizar los efectos funcionales de estas toxinas en diferentes canales iónicos y especies, abriendo nuevas oportunidades para la prospección farmacológica de estas potentes moléculas.

LISTA DE CUADROS

CAPITULO I

CAPITULO II

ANEXOS

CAPÍTULO I

CAPÍTULO II

LISTA DE FIGURAS

CAPITULO I

CAPITULO II

ANEXOS

CAPÍTULO I

LISTA DE ABREVIATURAS

AIS: Axon Initial Segment

AP: Action Potential

BSA: Bovine Serum Albumin

CNS: Central Nervous System

G: Conductance

GFL: Giant Fiber Lobe

g_{Na}: Na^+ conductance

I: Current

IFF: Instantaneous Firing Frequency

I_P: Steady-state Persistent current

I_T: Transitory current

KTx : K^+ Toxin

K_V : Voltage-dependent K^+ channel

MFF: Mean Firing Frequency

MWM: Molecular Weight Markers

NaTx : Na^+ Toxin

Na_V : Voltage-dependent Na^+ channel

PNS: Peripheral Nervous System

Po: Channel opening probability

PP: Propeptide

s.e.m: Standard error of the mean

TEVC: Two-Electrode Voltage Clamp

V: Voltage

INTRODUCTION

Scorpion envenomation is a global health concern, affecting over 1.2 million people annually and resulting in more than 3,000 deaths (Chippaux & Goyffon, 2008). Among the many scorpion species, the genus *Tityus* (Buthidae) is particularly notorious for causing severe envenomation in Central and South America, including the Amazon region (Borges *et al.,* 2020). The venom of these scorpions contains peptide toxins that primarily target the nervous and muscular systems, altering excitability and leading to potentially life-threatening effects (Goudet *et al.,* 2002).

The bioactivity of scorpion neurotoxins is both potent and specific, enabling these toxins to effectively immobilize prey by targeting key cellular components such as ion channels (Gwee et al. 2002). These peptide toxins interact with excitable cells by modulating the activity of various ion channels, including those that regulate the flow of Na^+, K^+, Ca^{2+}, and Cl^- ions (Srinivasan *et al.,* 2002). Scorpion toxins are known to modulate more than 40 types of ion channels, with more than 1.300 specific toxins identified to date (Housley *et al.,* 2017; UniProtKB, 2024). This broad range of activity is what makes scorpion venom such a potent agent, capable of eliciting severe physiological responses.

The primary molecular targets of scorpion toxins are voltage-dependent Na^+ and K^+ channels (Na_V and K_V, respectively), which play critical roles in cellular signaling and electrical activity, particularly in excitable cells, such as neurons and muscle fibers (García *et al.,* 2001; de la Vega & Possani, 2007). Na_V channels are transmembrane proteins essential for transmitting electrical signals in the central and peripheral nervous systems, with their rapid activation and inactivation regulating the flow of Na^+ ions (Clairfeuille *et al.,* 2019). Na^+ channel toxins (NaTxs) from *Tityus* scorpions can disrupt this process by either delaying channel inactivation (α-toxins) or promoting channel opening at more negative voltages (β-toxins), mostly leading to increased neuronal excitability and altered muscle function (Chow *et al.,* 2020). These disruptions can result in paralysis, cardiac arrhythmias, and even death (Hanck & Sheets, 2007).

Similarly, K^+ channel toxins (KTxs) from scorpions affect K_V channels, which are essential for the cell's repolarization after action potentials (APs) (Kuang et al. 2015). These channels are highly selective for K^+ ions due to their unique pore structure, which filters out other ions (Doyle *et al.,* 1998). By binding to K_V channels, KTxs block their function, prolonging APs and

contributing to abnormal cellular activity (Mouhat *et al.,* 2008). Both NaTxs and KTxs are valuable tools in studying ion channel function and have potential therapeutic applications in treating conditions such as cancer, pain, and autoimmune diseases (Bergeron & Bingham, 2012).

Given the medical relevance of scorpion toxins, particularly from the *Tityus* genus, which is responsible for the most severe and fatal envenomation in Latin America (Guerra-Duarte *et al.,* 2023), it is crucial to expand our understanding of how these toxins affect ion channel function. In this study, we aimed to investigate the effects of the venom and toxins from *Tityus championi*, a species endemic to Costa Rica and Panama that is known to cause severe cases of envenomation in Panama (Salazar *et al.,* 2018). The venom of *T. championi* likely targets Na^+ and K^+ channels, as seen in other *Tityus* species, and could provide insights into the mechanisms of toxin-channel interaction. This research could also contribute to therapeutic application development for conditions involving ion channel dysfunction.

CAPÍTULO I

Effect of the venom and purified neurotoxins of Costa Rican scorpion Tityus championi on invertebrate cation channels

Galit Akerman-Sánchez[1,2], Cecilia Díaz[3,4], Natalia Ortiz [3,4], Oscar Brenes[1,5]

[1] Department of Physiology, School of Medicine, University of Costa Rica, San José, Costa Rica

[2] SEP, School of Biology, University of Costa Rica, San José, Costa Rica

[3]Clodomiro Picado Institute, Faculty of Microbiology, University of Costa Rica, Coronado, Costa Rica

[4] Department of Biochemistry, School of Medicine, University of Costa Rica, San José, Costa Rica

[5] Neuroscience Research Center, University of Costa Rica, San José, Costa Rica

ABSTRACT

Scorpion neurotoxins are small peptides with significant bioactive potential, targeting ionic channels and offering opportunities for novel therapeutic discoveries. This study analyzed the functional electrophysiological effects of newly discovered toxins from the Costa Rican endemic scorpion *Tityus championi*. Using the C1 neuron from the land snail *Helix aspersa* as a cellular model, whole-cell patch-clamp techniques in both voltage- and current-clamp configurations were employed to analyze sodium and potassium currents, action potential generation and morphology in exposure to crude venom and purified toxins. Results revealed that scorpion crude venom was inhibitory on neuron activity, affecting both depolarization and repolarization. The venom toxins (2 μM) exhibited different effects and mechanisms on sodium currents mediated by the $Na_V1.7$-like channel. Specifically, Tch2 and Tch4 toxins increased both transient and persistent currents. In transient currents, both induced activation and inactivation changes in voltage sensitivity and dependency, ultimately widening the current window and increasing currents at more negative voltages but decreasing channel availability. Conversely, Tch3 behaved as an inhibitory toxin, affected only the transient current, closed the window current, and decreased cellular excitability. Since similar effects were also observed with the complete venom, results suggested that this inhibitory toxin is predominant within the venom's effect. Additionally, partial blocking effects were noted for the K^+ toxin TchKTx5. This study provides new insights into the toxins of Costa

Rican scorpions, elucidating their complex mechanisms of action and their effects, thus advancing our understanding of their bioactive potential.

INTRODUCTION

Scorpion neurotoxins are peptides that interfere with the normal function of the nervous system, exhibiting potent and specific activity to attack a possible offender or prey, by immobilizing or killing it (Gwee *et al.,* 2002; Stevens *et al.,* 2011). In scorpions, evolutionary pressure has selected these peptides to modulate different ion channels (Zhang *et al.,* 2015), especially Na^+ and K^+ ion channels, which play crucial roles in numerous cellular processes, such as action potential (AP) generation and muscle contraction (García *et al.,* 2001; de la Vega & Possani, 2007).

Scorpion toxins selective for Na^+ voltage-gated channels (Na_V) (NaTxs) consist of 60-76 amino acids with disulfide bridges in their tertiary structure and can be distinguished into two types (Chow *et al.,* 2020; Ghosh *et al.,* 2019). The α-toxins (α-NaTxs) prevent rapid channel inactivation by binding to the extracellular loop called receptor site 3 (Cestéle *et al.,* 1998). Due to their proximity to the S4 voltage sensor in the motive IV (IVS4), the toxin keeps the sensor in an internal, non-active position, delaying inactivation (Gwee *et al.,* 2002). Functionally, this prolongs the duration of the AP and reduces cellular firing frequency (Clairfeuille *et al.,* 2019; Zhu *et al.,* 2020). On the other hand, the β-toxins (β-NaTxs), promote channel opening by binding to receptor site 4. During channel activation, the S4 voltage sensor of motive II is translocated extracellularly, where it interacts with the β-NaTxs, anchoring it in an external, active position (Gwee *et al.,* 2002). This leads to increased channel activation and negative voltage dependence shift in future activations, opening at more negative voltages (Rogers *et al.,* 1996). Functionally, a shift toward more negative membrane potentials results in increased AP firing frequency (Chow *et al.,* 2020). These two types of NaTxs, with different action mechanisms, ultimately increase Na^+ currents, probably causing massive neurotransmitter release (Gordon & Gurevitz, 2003; de la Vega & Possani, 2005). Consequently, α and β-NaTxs can cause paralysis, cardiac arrhythmias, and death (Hanck & Sheets, 2007).

Scorpion toxins selective for K^+ voltage-gated channels (K_V) (KTxs) consist of 25-45 amino acid residues, with three or four disulfide bridges (Mouhat *et al.,* 2008). KTxs reversibly

bind to the K_V channel's negatively charged residues with their positively charged residues (Gwee *et al.,* 2002). As a result, the channel is blocked, prolonging action potentials, and leading to abnormal nerve function (Mouhat *et al.,* 2008).

Together, NaTxs and KTxs modify the activity of their respective channels, collectively altering cell excitability, neurotransmitter release, and ultimately, neuronal function and animal behavior (Mouhat *et al.,* 2008).

In the present study, we aim to characterize the effect of the crude venom and isolated toxins from the scorpion *Tityus championi* (Pocock, 1898) on Na^+ and K^+ invertebrate ion channels and their impact on neuronal excitability.

EXPERIMENTAL PROCEDURES

Animals

Juvenile specimens of terrestrial snails *H. aspersa* (NCBI taxonomic ID: 6535) were provided by local breeders. The snails were housed in plastic boxes in a room with a regulated temperature (20°C) and a 12:12 h light:dark cycle. Snails were fed once a week with a calcium-rich diet and lettuce or cucumber. Before procedures, a 0.1M $MgCl_2$ solution was injected into the snail's foot to anesthetize and induce muscle relaxation, subsequently, they were sacrificed by evisceration. All methodologies were previously validated by the Institutional Animal Care and Use Committee (CICUA-026) of the University of Costa Rica, and efforts were made to minimize the number and suffering of animals in accordance with guidelines established by the Ethical-Scientific Committee on the protection of animals for scientific purposes.

C1 Neuron Isolation

Cell isolation was performed as previously described (Brenes *et al.,* 2015). Briefly, to isolate the cerebral ganglion, nerves, and surrounding tissue were carefully cut. Once isolated, the ganglia were incubated for enzymatic digestion using protease type XIV (Sigma-Aldrich) in L15 isotonic medium (0.4 U/mL) at 34°C for 4 h. Following digestion, the ganglia underwent two washes with L15 medium to proceed with the isolation of C1 neurons via microsurgery. This

neuron was identified by its position, size, and distinctive morphology in the cerebral ganglion. Neurons were gently isolated with segments of the axon still attached to the soma and subsequently placed in dishes pre-coated with 5% bovine serum albumin (BSA) until the axon was reabsorbed, resulting in a configuration known as the soma configuration as previously described (Fiumara et al. 2005).

Venom

The venom of *T. championi* was obtained from the Dangerous Animals Research Laboratory (LIAP) at the Clodomiro Picado Institute (ICP) through the sorting of specimens maintained in its animal facility. This part of the study was approved by the Biodiversity Commission of University of Costa Rica (No. 293-2021). The lyophilized venom (81 mg) was reconstituted in 1 mL of distilled water. Subsequently, protein quantification was performed in the Institute of Health Research (INISA), using the BCA method with the Thermo Scientific microBCA kit #23235 and the spectrophotometer (Nanodrop 2000, Thermo Scientific) in triplicate.

Following this, venom samples were separated by SDS-PAGE (15% polyacrylamide) under reducing conditions (prior step of 10-min incubation at 98 degrees Celsius with 5% 2-mercaptoethanol) (Isotemp, Fischer Scientific). The low molecular weight ladder BLUeye Prestained Protein (94964, Sigma-Aldrich) was used to determine the mass of the main components. Subsequently, the gel was allowed to run for 1 h at 150 V using a Mini-Protean Tetra System coupled with PowerPac Basic power supply (BioRad), and proteins were stained with Coomassie Blue R-250.

Toxins

The toxins were isolated from the venom through reverse-phase HPLC and mass spectrometry was used to identify their sequences at the ICP. It was decided to proceed with the functional analysis of four of the most abundant toxins in the venom, Tch2, Tch3, Tch4, and TchKTx5. The amino acid sequence of these toxins is presented in Table I.

The putative toxins used in the electrophysiological studies were dissolved in distilled water and stored at -20°C until use. During experiments, each toxin was added directly to the culture dish where the cell was located in a 2 μM final concentration.

Electrophysiology recordings

Standard intracellular recording techniques, such as whole-cell patch-clamp, in current and voltage clamp configurations were used with isolated cells under a Nikon inverted microscope (Eclipse TS100). A borosilicate electrode manufactured at the time of use (with a puller Flaming-Brown P-1000), with a resistance between 1.5 and 2.8 MΩ, was brought close to the cell until a connection with the cytosol was established. Signals were amplified using a Multiclamp 700B amplifier (Axon Instruments) and converted to digital signals through the analog/digital interface Digidata 1322A (Axon Instruments). Data were collected using pClamp 11 software (Axon Instruments) on a personal computer. Series resistance compensation between 60 and 80% was performed before data collection, depending on each cell.

Table I. Neurotoxins purified from the venom of the scorpion T. championi and their primary structure (Díaz *et al.,* 2023).

Neurotoxin	Sequence of amino acids
Tch2	EAIDGYPLSKNNYCKIYCPDDAVCKDTCKNRAGATNGKGDCINKGCY CYDVAPSTKMYPGRLPCNPY
	EALDGYPLSKNNYCKIYCPDDAVCKDTCKNRAGATNGKGDCINKGC YCYDVAPGTKMYPGRLPCNPY
Tch3	EALDGYPLSKNNYCKIYCPNDEVCKDTCKHRAGATNGKGDCIWQTC YCYDVAPGTKMYPGSSPCYA
Tch4	GIKNGYPRDSKGCTFKCGQDAKHGDDYCDKMCKTTLKGEGGDCDFE YAECWCDNIPDTVVTWKNKEPK
TchKTx5	MHFSGVAFILISMVLINSIFETTAEAGDGPKSDCKPDLCEKACKEEKGK PMDFCKGDICKCKD

Electrodes were filled with different solutions depending on the current of interest, Na^+ or K^+. The composition of the intracellular solution used for K^+ current recording was as follows (mM): 100 KCl, 10 HEPES, 1 MgCl2 – 6H2O, 5 EGTA; while the extracellular solution in the dish was composed of (mM): 5 KCl, 90 cholineCl, 1 $CaCl_2$-$2H_2O$, 5 $MgCl_2$-$6H_2O$, 10 Tris-Cl. The composition of the intracellular solution used for Na^+ current recording was (mM): 110 CsCl, 10 HEPES, 2 $MgCl_2$, 1 NaCl, 2 EGTA; while the extracellular solution was (mM): 4 KCl, 90 NaCl, 1 $CaCl_2$, 5 $MgCl_2$, 10 Tris, 30 TEA-HCl, 4 4-AP. All solutions were adjusted to a pH of 7.4 before use.

Ion Current Evaluation

We evaluated the effects of the toxins on the three Na_V gating processes (activation, inactivation, and recovery), and on K_V activation.

To evaluate the activation of Na_V and K_V channels, currents were measured at different voltages from -60 mV to +60 mV (ΔV =10 mV) for 200 ms, from a resting potential of -50 mV (Supplementary material Fig. S1A). For Na^+ currents, data of the maximal transitory current (I_T) and steady-state persistent current (I_P) were extracted. Additionally, from these recordings, the inactivation time constants (τ of inactivation) were obtained by fitting the inactivation phase of the current curve to a standard exponential equation (Supplementary material SE.1) using Clampfit software (Axon Instruments). For K^+ currents, data were extracted solely from I_P, corresponding to the K^+ current through K_V channels.

I_T and I_P were plotted against their respective voltage to generate standard IV curves. For the voltage-dependent activation, the conductance (g_{Na}) and the channel opening probability (Po) were obtained using the standard approaches (Supplementary materials SE.2 and SE.3). Steady-state inactivation was evaluated by a two-pulse voltage protocol, quantifying the maximal Na^+ current generated during a test pulse at -20 mV after channel inactivation caused by conditioning step pulses ranging from -60 mV to +60 mV (ΔV = 10 mV), each pulse lasting 200 ms (Supplementary material Fig. S1B) (Abd El-Aziz et al. 2021). Maximal test pulse I_T was normalized to the maximal current (similar to SE.3).

The voltage-dependent activation and steady-state inactivation were plotted as a function of voltage and the data were fitted using the Boltzmann equation (Supplementary materials SE.4), to obtain $V_{1/2}$ and k values, where $V_{1/2}$ represents the voltage of half-maximal

activation/inactivation and k is the slope factor of the voltage dependence of the open probability. The area subtended by the intersection of the activation and inactivation curves was calculated (window current). RStudio (Version 2023.06.0+421) was used for window current calculation (Calculation Code).

The time required for the channel to recover from the inactive state (recovery from inactivation) was measured using two voltage steps at -20 mV, separated by an increasing time interval starting from 5 ms to 100 ms with a $\Delta t = 5$ ms (Supplementary material Fig. S1C) (Kiss 2003), assessing in this way the impact of toxins on the Na_V channels availability.

Action Potential Assessment

The current-clamp technique was employed to identify possible changes in APs due to the effect of toxins. The stimulation protocol consisted of three stimuli of increasing intensity (0.5, 1.0, and 1.5 nA), each lasting 500 ms (Brenes *et al.,* 2015). Mean Firing Frequency (MFF) was calculated as the average number of APs fired during the 500 ms stimulus, multiplied by two to report in Hz. Instantaneous Firing Frequency (IFF), where the IFF is the frequency between each AP.

Also, several parameters of AP waveform morphology were reported (Supplementary material Fig. S2), the morphological variables of the AP analyzed include: (i) AP amplitude (mV), determined as the difference between the maximal depolarizing potential and the resting membrane potential before stimulation; (ii) half-width, measured as the duration (ms) at half of the maximal amplitude; (iii) maximal depolarization rate (mV/ms); (iv) depolarization rate (mV/ms) between 10% and 90%; (v) depolarization time constant (rise τ, ms), corresponding to the time required to reach 63% of the maximal magnitude of the AP.

Data

Data was reported as mean ± standard error of the mean (s.e.m.). Figures were made with GraphPad Prism version 10 (GraphPad Software).

RESULTS

A clear inhibitory effect on neuronal excitability due to the cocktail of a complex mix of components and neurotoxins present in crude venom

Starting with the crude venom, we observed a distinct pattern of proteins with varying molecular weights. The dominant components are low molecular weight peptides, primarily below 8 kDa, which are typically associated with small peptides present in the venom, such as neurotoxins (Fig. 1). We identified in this sense three prominent bands: two thicker bands representing peptides smaller than 8 kDa and a thinner band between 8 and 15 kDa. Discrete bands were also observed between 24 and 72 kDa, while bands representing higher molecular weights (>72 kDa) appeared faint, indicating lower concentrations of high molecular weight proteins in the venom.

Given the dominant presence of low-weight peptides, including NaTxs and KTxs, we evaluated the Mean Firing Frequency (MFF) and the morphology of APs. Interestingly, exposing the cells to the complete venom (10 µg/ml) completely abolished firing induced by the smallest stimulus (0.5 nA), and decreased the firing frequency in a time-dependent manner with the highest stimulus (1.0 and 1.5 nA) (Fig. 2A).

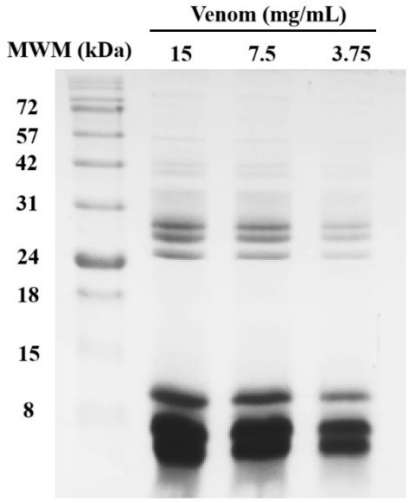

Figure 1. Protein pattern of *T. championi* venom. Complete venom was analyzed by SDS-PAGE (15% acrylamide) under reducing conditions. MWM = Molecular Weight Markers.

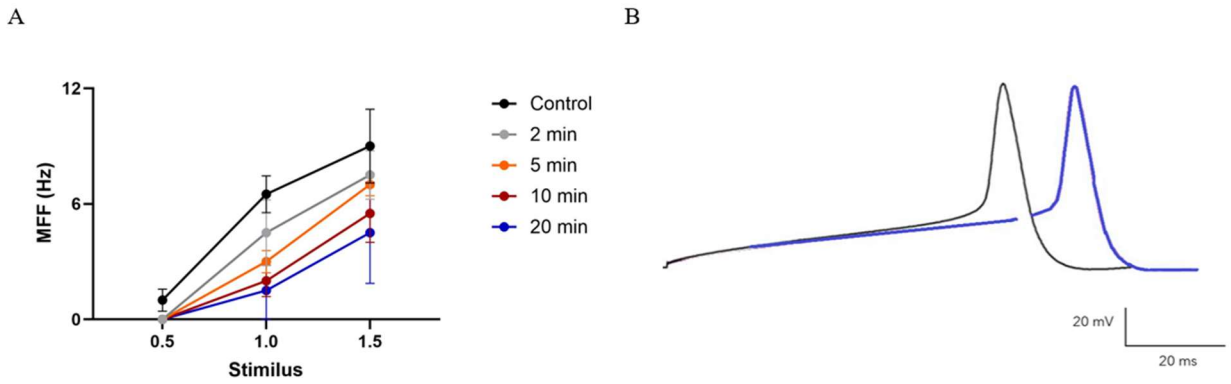

Figure 2. Effect on the action potential firing upon exposure to *T. championi* venom (10 µg/ml). A. Mean Firing Frequency (MFF) (Hz) under stimuli of 0.5, 1.0, and 1.5 nA before (Control) and after 2 (grey), 5 (orange), 10 (red), and 20 (blue) min of venom exposure (n=4). B. Representative recording of the first action potential induced by 1.5 nA stimulus before (black) and after 20 min (purple) of venom exposure. Each value indicates mean ± s.e.m.

Together with a decrease in the number of AP fired by the cells, we observed changes in AP waveform (Fig. 2B). Hence, we proceeded to examine in detail the effect on different parameters describing the morphology of individual AP induced by 1.5 nA current pulse (Fig. 3). The AP amplitude was not affected (Fig. 3A), and there was a slight reduction in half-width after 20 min of venom exposure (Fig. 3B). During depolarization, there was a small decrease in the rise slope from the second minute of exposure, consistent with an increase in rise time (Fig. 3C and D, respectively). On the other hand, during repolarization, no clear patterns were observed. In the first APs, there was a small increase followed by a small decrease in the decay slope during the first 2, 5, and 10 min of exposure, however with no strong changes in the decay time (Fig. 3E and F, respectively). Nevertheless, after 20 min of exposure, a clear increase in decay slope with a decreased decay time was evident. This suggests a reduction of AP duration, possibly explaining the smaller half-width after 20 min of venom exposure (Fig. 3B).

The inhibitory effect of the crude venom is consistent with the effect of the predominant toxin Tch3 within it

To achieve a deeper understanding of the venom components effects on cells, we studied the effects of one of the most abundant toxins present in this venom, Tch3 (Diaz *et al.,* 2023). Given that very little quantity of toxins can be isolated in a pure form from the venom, one single cell was used to test toxin effects on cell firing. In Figure 4A, it can be observed that, before toxin exposure, the cell fired APs in response to 1.0 and 1.5 nA. However, under the influence of the toxin, the cell only fired when the higher-intensity stimulus (1.5 nA) was applied. Similarly, it is noticeable that the IFF, decreased under toxin exposure, especially in the first APs, also decreasing AP adaptation (Fig. 4B).

Regarding the action potential waveform, we observe a slight increase in the amplitude of APs, reaching a difference of approximately 10 mV between the control and the 30-min toxin exposure for the last AP generated (Fig. 5A). In the half-width, an increase in width was noted in the first APs fired (Fig. 5B).

Since the sequence of Tch3 indicates that it is a putative NaTx, we analyzed the depolarization phase, which is governed by Na^+ conductance. In the control cell, we observed a small decrease in the rise tau of each AP evoked. Regarding the maximal rise slope, the first AP was notably fast, but this slope decreased in the following four APs. A similar trend was observed in the rise slope 10-90%. In the presence of the toxin, the rise tau showed a progressive increase with the exposure time (Fig. 5C). The maximal rise slope of the first AP was lower in the presence of the toxin, and the pattern of slope reduction in the following four APs was not as pronounced. Finally, we observe that the rise slope 10-90% mostly decreased with exposure to the toxin (Fig. 5E).

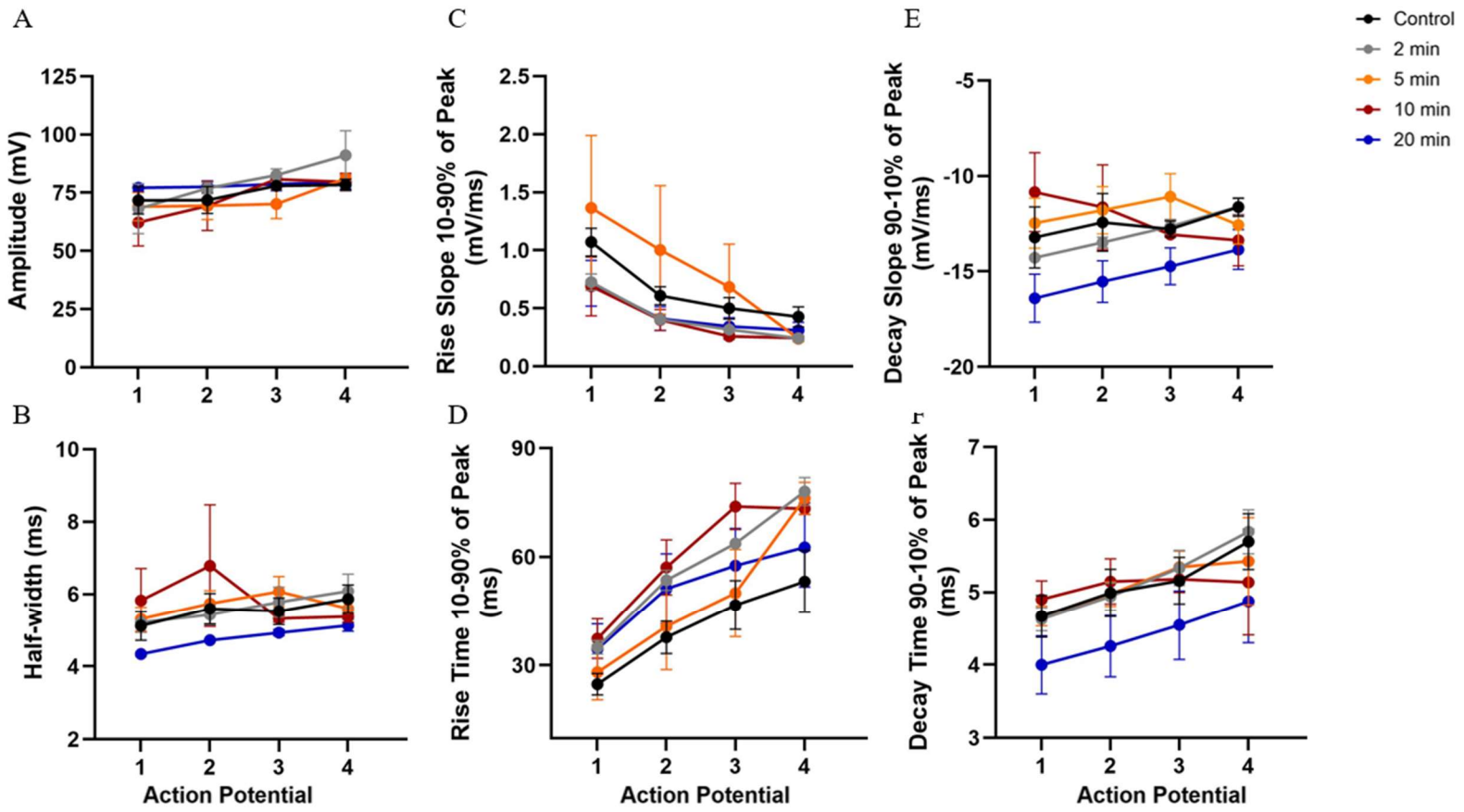

Figure 3. Effect of *T. championi* venom on the morphology of evoked action potentials. All action potentials were evoked by a 1.5 nA stimulus for 500 ms, in control (black), and after 2 (grey), 5 (orange), 10 (red), and 20 (blue) min of venom exposure. The variables observed were Amplitude (A), Half-width (B), Rise Slope 10-90% (C), Rise Time 10-90% (D), Decay Slope 90-10% (E), and Decay Time 90-10% (F). Each value indicates mean ± s.e.m.

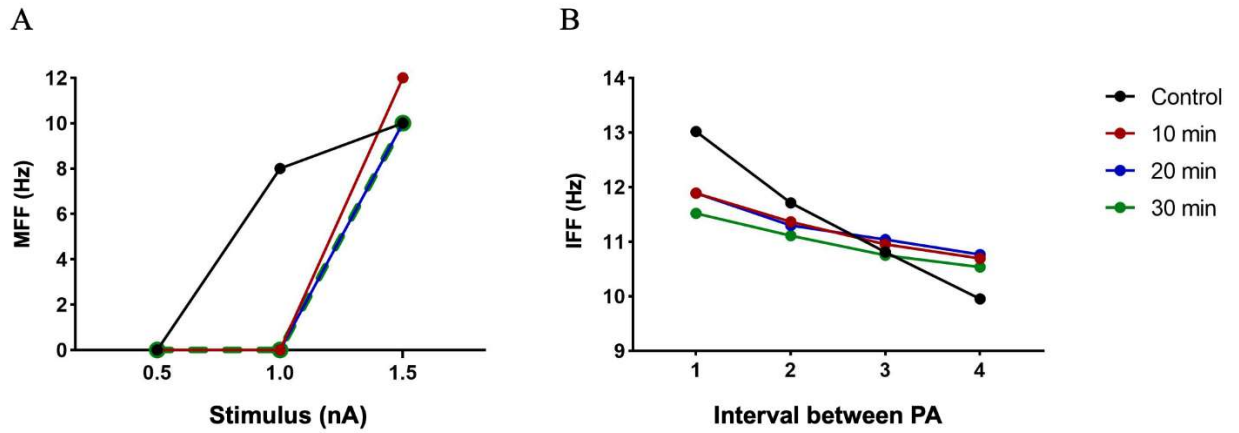

Figure 4. Effect of the toxin Tch3 on the cellular firing frequency. A. Mean Firing Frequency (MFF) (Hz) under increasing current stimuli, 0.5, 1.0, and 1.5 nA. In control (black), and after 10 (red), 20 (blue), and 30 min (dotted green) of toxin exposure. B. Instantaneous Firing Frequency (IFF) (Hz) in the intervals between action potentials. Firing frequency was measured before (control, black), and 10 (red), 20 (blue), and 30 min (green) after toxin exposure.

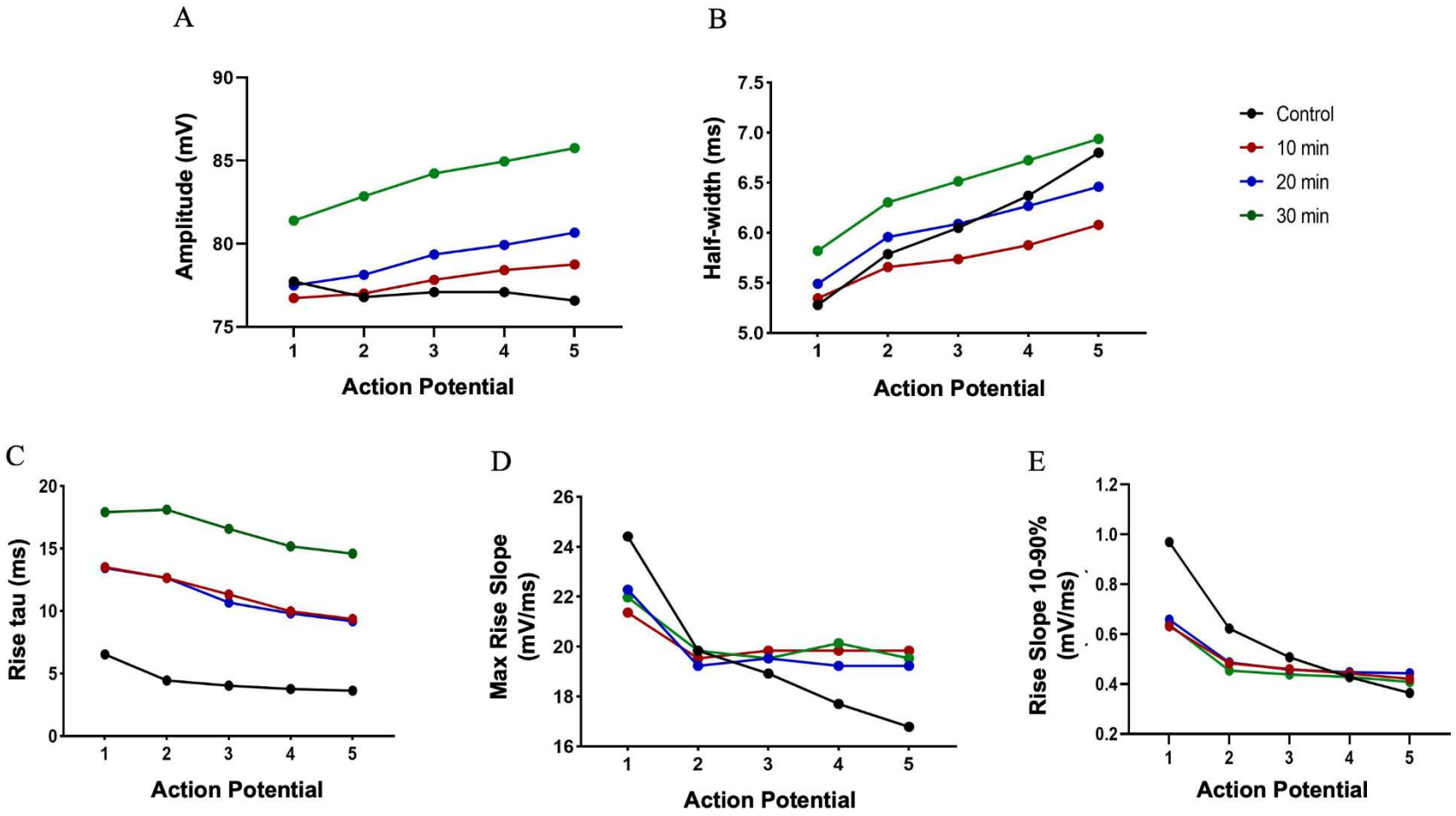

Figure 5. Effects of Tch3 on the evoked action potentials waveform. Action potentials were evoked by a stimulus of 1.5 nA for 500 ms, in control (black), and after 10 (red), 20 (blue), and 30 min (green) of toxin exposure. The variables measured were Amplitude (A), Half-width (B), rise tau (C), maximal rise slope (D), and rise slope from 10 to 90% of the action potential (E).

Distinction of two types of Na^+ inward currents with distinct behavior in C1 neuron

Being that we observe a noticeable effect on the depolarization, suggesting an alteration in Na^+ conductance, and several neurotoxins in *T. championi* venom are putative NaTxs (Díaz *et al.,* 2024), as a starting point, we characterized C1 Na^+ currents. In this matter, different components were observed in the C1 macroscopic current (Figure 6A) probably composed of two distinct currents, a transient current called I_T, and a steady-state persistent current called I_P.

The IV relationship of the I_T current showed that activated from -30 mV, reached its maximal peak at -20 mV, with a maximal average amplitude of up to 10 nA, and its average reversal potential was around +40 mV (Figure 6B). On the other hand, the I_P current showed smaller amplitudes (less than 2 nA), also started at -30 mV, but reached its peak at -10 mV and had a reversal potential close to 0 mV (Figure 6C).

Using the I_T current values, the relative conductance was plotted as a function of membrane potential (Figure 6D), and the mean activation of these channels was characterized by a $V_{1/2}$ of -29.7 mV and a k of 2.29. Regarding the inactivation of the I_T, the relative current was plotted as a function of membrane potential (Figure 6E), reaching a complete inactivation at 0 mV, and with a $V_{1/2}$ of -22.1 mV and a k of 6.63. By merging the activation and inactivation open probability curves, the window current reached an area value of 12.6.

Comparative analysis of purified toxins on transient and persistent Na^+ currents

Subsequently, understanding the behavior of the Na^+ currents in *Helix* snails, we proceed to analyze the effects of three purified toxins, which share primary structural homology with NaTxs, called Tch2, Tch3, and Tch4 (Díaz *et al.,* 2023).

As shown in Figure 7, the three NaTxs targeted the same channels but exhibited different effects. Tch2 and Tch4 increased transient current at -30 mV (Figure 7A and 7E, respectively). This effect becomes noticeable from five min of exposure. A slight increase in the Na^+ I_P was also observed at most of the voltages tested during Tch2 and Tch4 exposure (Figure 7B and 7F, respectively).

In contrast, the previously mentioned Tch3 was the only toxin that induced a trend of decrease in I_T with exposure time, especially at 20 min (Figure 7C). However, when tested on I_P Tch3 did not affect the currents, maintaining similar values at each voltage during exposure time (Figure 7D).

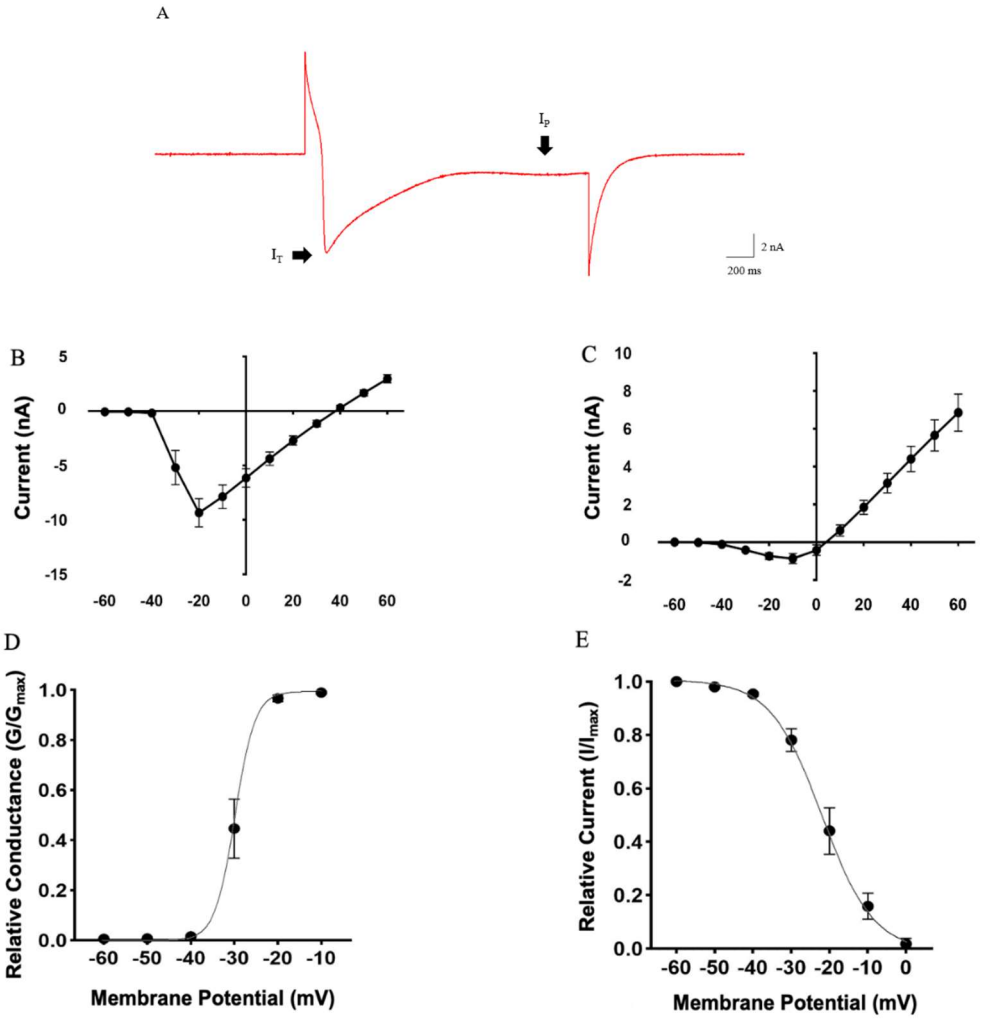

Figure 6. Macroscopic Na^+ currents in the C1 neuron of the snail *H. aspersa*. A. Representative macroscopic Na^+ current, indicating the transient (I_T) and persistent (I_P) components. B. IV relationship of transient Na^+ current (n=13). C. IV relationship of persistent Na^+ current (I_P) (n=12). D. Relative conductance as a function of membrane potential. E. Relative current as a function of the membrane potential of the preceding voltage pulse. Each value indicates mean ± s.e.m. Curve fittings in D and E were obtained by the Boltzmann equation.

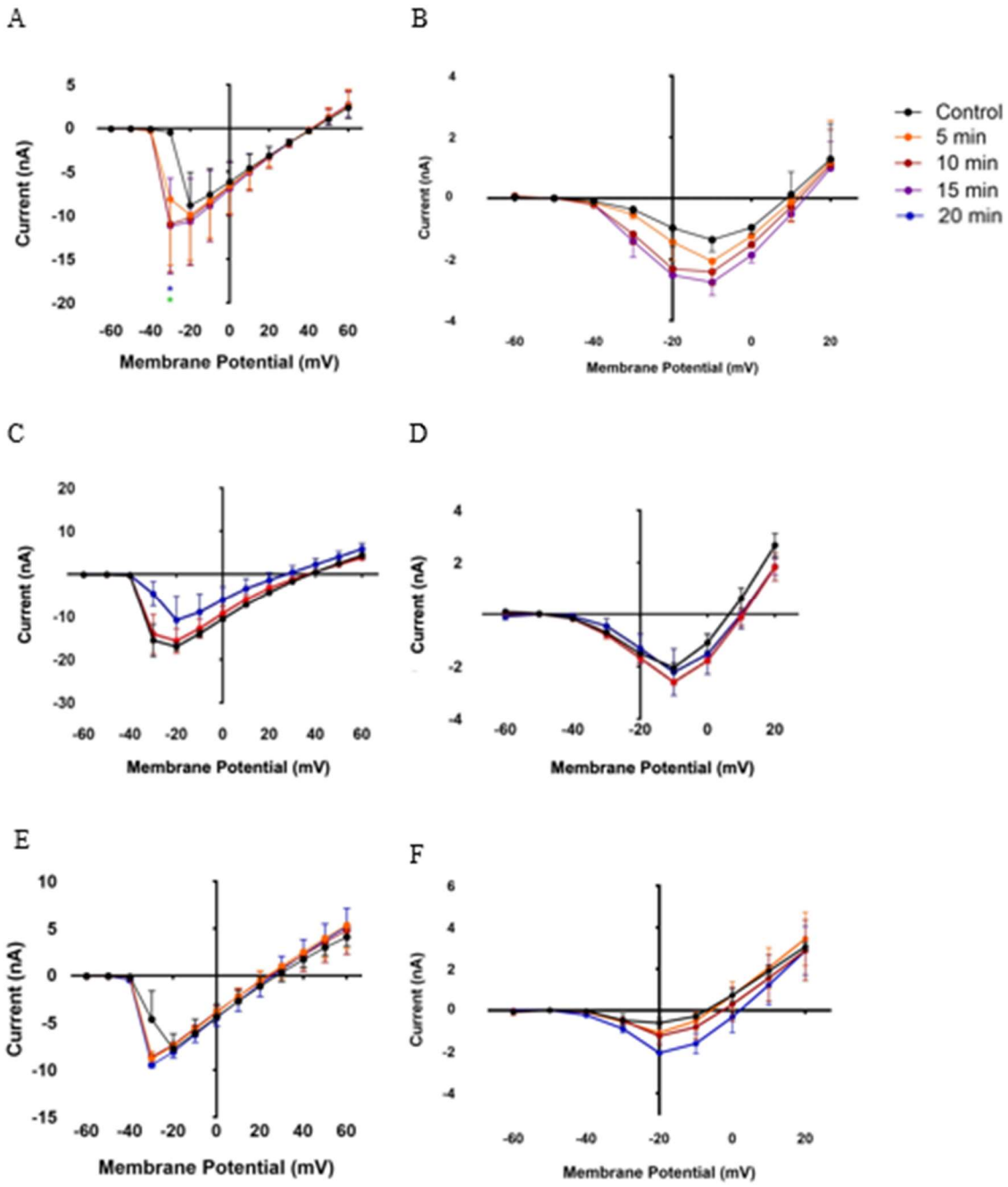

Figure 7. Tch2, Tch3, and Tch4 effects on transient and persistent currents. IV relationship of I_T is shown in A, C, and E. IV relationship of I_P is shown in B, D, and F. Tch2 effect (A and B) Tch3 effect (C and D), and Tch4 effect (E and F) ware shown before (Control, black) and after 5 min (orange), 10 min (red), 15 min (purple) and 20 min (blue) of toxin exposure (n=2). Each value indicates mean ± s.e.m.

Effect of three different toxins on the activation and inactivation kinetics

After observing the different effects on the Na^+ I_T when cells were exposed to the toxins, we proceeded to analyze the voltage dependency and sensibility by plotting the open probability of activation and inactivation particles as a function of voltage. With the exposure to Tch2, a ~10 mV negative shift in the activation curve was present after 5 and 10 min, which was then reversed by 5 mV at 20 min, and 30 min, a smaller voltage-dependency was also evident (bigger slope factor), especially at 30 min (Fig. 8A and Table II). Upon analyzing the inactivation curve, no strong effects of the toxin Tch2 were observed in voltage sensitivity (Fig. 8B, Table II). Still, a strong decrease in voltage dependency for inactivation was observed, evidenced by an increase in slope factor from 4.38 mV to 7.89 mV (Table III). These parallels with an increase in the inactivation time constant (τ) over exposure time (Table III), even leading to an incomplete inactivation (Fig. 8B, blue and green dots).

To simultaneously analyze the effects of the toxin on both activation and inactivation, window current was calculated (Fig. 9). An increase in the window current was observed from the first ten min of exposure to Tch2, nearly doubling its value (Fig. 9, upper panel, red plot). However, as mentioned before, after 20 and 30 min of toxin exposure, a slight reversal in the effect was observed, evidenced by a reduction in the area, even though with the incomplete inactivation the window current is still more than 60% bigger than before toxin exposure (Fig. 9, upper panel, blue and green plots). Altogether, the increased currents reported at -30 mV in Figure 7A correlate with the positive shift observed in activation, and this shift increased the window current.

Regarding the Tch3, the current decrease reported in Figure 7C was accompanied by a positive shift in voltage after 20 min of toxin exposure (Fig. 8C), the $V_{1/2}$ shift from -32.08 to -28.14 implied a decrease in voltage sensitivity with toxin exposure (Table II). Additionally, a strong decrease in the voltage dependency of the activation was identified (Table II).

In the other way, in the inactivation curve, it was shown a negative shift in the relative current with the exposure time to Tch3 (Fig. 8D), with a strong change in $V_{1/2}$ from -27.54 mV to -46.90 mV, a value very close to the resting membrane potential (Table III). Furthermore, the voltage dependence of the channel decreased, where the slope factor increased even after 5 min of toxin exposure (Table III). Finally, a change in the inactivation τ was observed, with a decrease also from 5 min of exposure (Table III).

It became evident that the current window gradually decreased with increasing exposure time, and the area was reduced by more than half at 20 min exposure (Fig. 9, middle panel). This reduction is consistent with previous observations, indicating that the toxin exerts an effect on the channel by decreasing its open probability and accelerating its inactivation at more negative membrane potentials, ultimately leading to the smaller currents reported in Figure 7C.

When Tch4 was analyzed, a notable difference between the control activation curve and the toxin exposure curve was observed, with a negative shift (Fig. 8E). These changes are elucidated in Table II, where we can notice a change in the $V_{1/2}$ value of -9 mV at 10 min of toxin exposure, that decreased to -4 mV after 20 min of exposure. Likewise, the slope factor decreased from 1.50 mV to 1.29 mV in the first 10 min of exposure, but then reversed and increased to 2.40 mV (Table II). There were also modifications in the inactivation curves compared to the control, not very clear in the plot of Figure 8F, however when analyzed through Boltzmann fitting, we saw a -6 mV negative shift, as well as a decrease in voltage dependency (increase in the k) and an increased inactivation τ (Table III).

Analyzing the window current in the lower panel of Figure 9, a notable change was observed in the first few minutes, in detail, before toxin exposure, the activation open probability at -30 mV was around 50%, and the inactivation open probability at -10 mV was around 20%. However, after just 5 min of exposure, activation probability at -30 mV increased to 100% and inactivation probability at -10 mV decreased to 0%. Inactivation correlated with the value of the area under the curve, which decreased at 5 min. The effect persisted after 10 min of exposure, but reversed 10 min later, where the inactivation curve shows an open probability at the membrane potential of -10 mV exceeding 10%, with a larger area under the curves. Altogether, similar to Tch2, the increased currents reported at -30 mV in Figure 7E correlated with the positive shift observed in activation, however, this shift does not correlate with an increase in the window current.

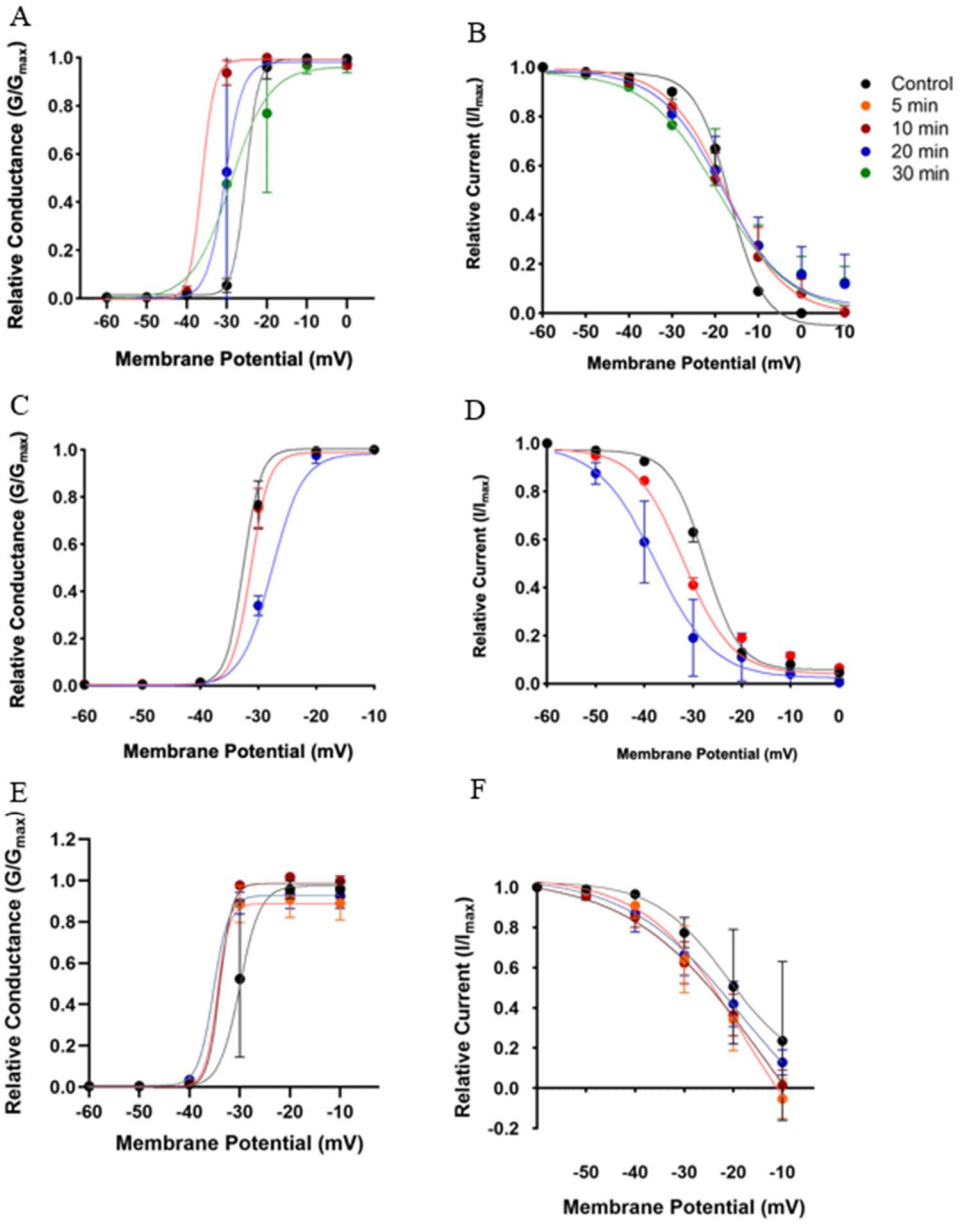

Figure 8. Activation and inactivation kinetics under Tch2, Tch3, and Tch4 exposure. Relative conductance was plotted as a function of membrane potential (A, C, and E.), the curve represents the data fitted to the Boltzmann equation. Relative current was plotted as a function of the membrane potential of the preceding voltage pulse (B, D, and F), curves fitted to the Boltzmann equation. A-B. Exposure of Tch2. C-D. Exposure to Tch3. E-F. Exposure to Tch4. Cells were analyzed before (Control, black) and after toxin exposure for 5 min (orange), 10 min (red), 15 min (purple), 20 min (blue), and 30 min (green) (n=2). Each value indicates mean ± s.e.m.

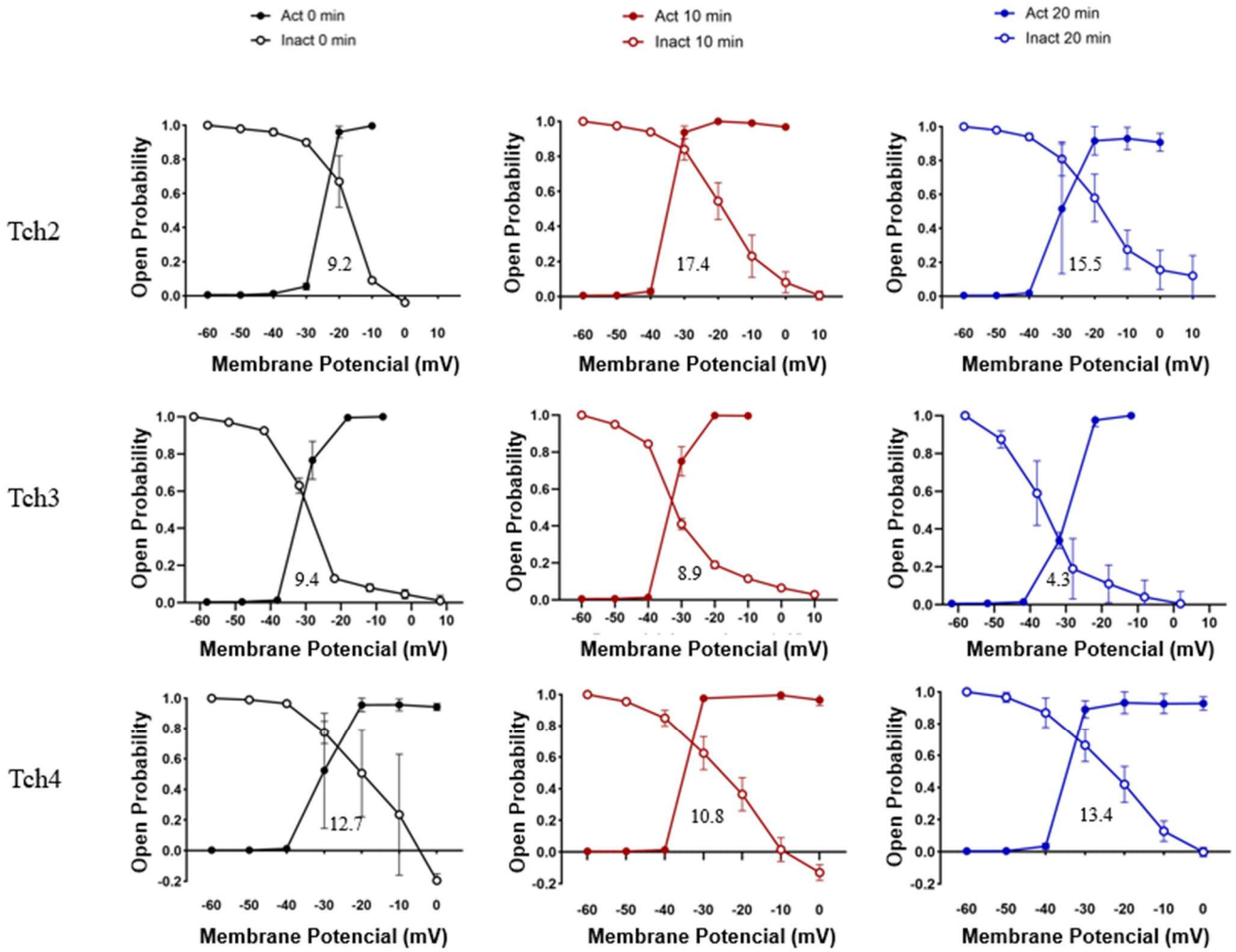

Figure 9. Window current changes depending on the toxin exposition. The window current is observed by combining the activation curves (closed circles) generated as relative conductance (G/G_{max}), and inactivation curves (open circles) calculated as relative current (I/I_{max}) in the same graph. The value of the window current area is denoted in each graph. The upper panel shows Tch2, the middle panel

shows Tch3, and the lower panel shows Tch4. Control (black) and toxin exposure for 10 min (red), 15 min (purple), 20 min (blue) (n=2). Each value indicates mean ± s.e.m.

Table II. Open probability parameters of activation. $V_{1/2}$ is the voltage corresponding to half-maximal activation, and k is the slope factor. All data are shown from n=2, as mean ± s.e.m.

	$V_{1/2}$ (mV)				k (mV)			
Toxin	Time (min)							
	0	5	10	20	0	5	10	20
Tch2	-25.55 ± 0.52	-30.08 ± 3.09	-34.75 ± 1.58	-29.69 ± 3.64	1.5 ± 0.35	1.40 ± 0.09	1.29 ± 0.16	1.85 ± 0.32
Tch3	-32.08 ± 0.77	-31.85 ± 0.71	-28.07 ± 0.46	-28.14 ± 1.61	1.72 ± 0.21	1.62 ± 0.005	2.66 ± 0.07	3.18 ± 0.41
Tch4	-29.57 ± 4.84	-34.72 ± 0.14	-34.02 ± 0.57	-34.30 ± 0.36	2.03 ±0.65	1.27 ±0.02	1.23 ± 0.03	1.63 ± 0.23

Table III. Open probability parameters of steady-state inactivation. $V_{1/2}$ is the voltage corresponding to half-maximal inactivation, and k is the slope factor. All data are shown from n=2, as mean ± s.e.m.

	$V_{1/2}$ (mV)				k (mV)				Normalized τ			
Toxin	Time (min)											
	0	5	10	20	0	5	10	20	0	5	10	20
Tch2	-16.22 ± 2.01	-16.77 ± 2.88	-17.82 ± 3.14	-18.79 ± 2.87	4.38 ± 1.25	4.72 ± 1.81	7.22 ± 0.43	7.89 ± 0.94	0.59 ± 0.15	0.79 ± 0.15	0.87 ± 0.11	1
Tch3	-27.54 ± 1.08	-32.00 ± 0.53	-38.00 ± 3.77	-46.90 ± 2.23	4.61 ± 0.20	6.24 ± 0.30	6.65 ± 1.71	6.85 ± 1.72	0.87 ± 0.13	0.49 ± 0.23	0.65 ± 0.35	
Tch4	-16.33 ± 6.63	-26.24 ± 5.46	-22.33 ± 2.90	-22.64 ± 4.16	3.06 ± 2.73	5.19 ± 0.08	9.31 ± 1.44	10.55 ± 1.74	0.34 ± 0.03	0.53 ± 0.13	0.60 ± 0.17	1

All NaTxs analyzed from the venom reduced the probability of finding closed channels.

The next step of the analysis was to examine whether the toxins affected the transition to the closed state using the degree of recovery from inactivation over the time spent at resting membrane potential. With the exposure to Tch2, an increase in the recovery was observed after 5 ms repolarization, reaching 50% of recovery within the first 10 min (Fig. 10A). This implies that the probability of finding closed channels, rather than inactive channels, is higher during this first 5 ms. However, a subsequent change in this pattern was observed, as the recovery percentage decreases with longer exposure time to Tch2, and longer times at resting membrane potentials, implying a 20% reduced availability of Na_V channels on the membrane even after 75 ms in the long term.

In the case of Tch3, a clear decrease in the recovery from inactivation was observed, especially after 20 min of toxin exposure (Fig. 10B), reaching almost 30% reduced availability of Na_V channels.

Then Tch4 was analyzed, and we saw a decrease in the recovery from inactivation after just 5 min of exposure, decreasing availability in the first milliseconds, however reaching a similar recovery to the control condition after 75 milliseconds at resting membrane potential (Figure 10 C).

TchKTx5 is a toxin that blocks the macroscopic outward K^+ current.

Lastly, in the venom of the scorpion *T. championi*, the presence of a dominant toxin named TchKTx5 has been identified, which shows homology with KTxs in other *Tityus* venoms (Díaz *et al.,* 2024). We tested the possible effects of this toxin on macroscopic K^+ currents. The IV relationship of these currents showed that when exposed to the toxin a decrease in the steady-state recorded currents was evident after only 2 min of exposure (Figure 11).

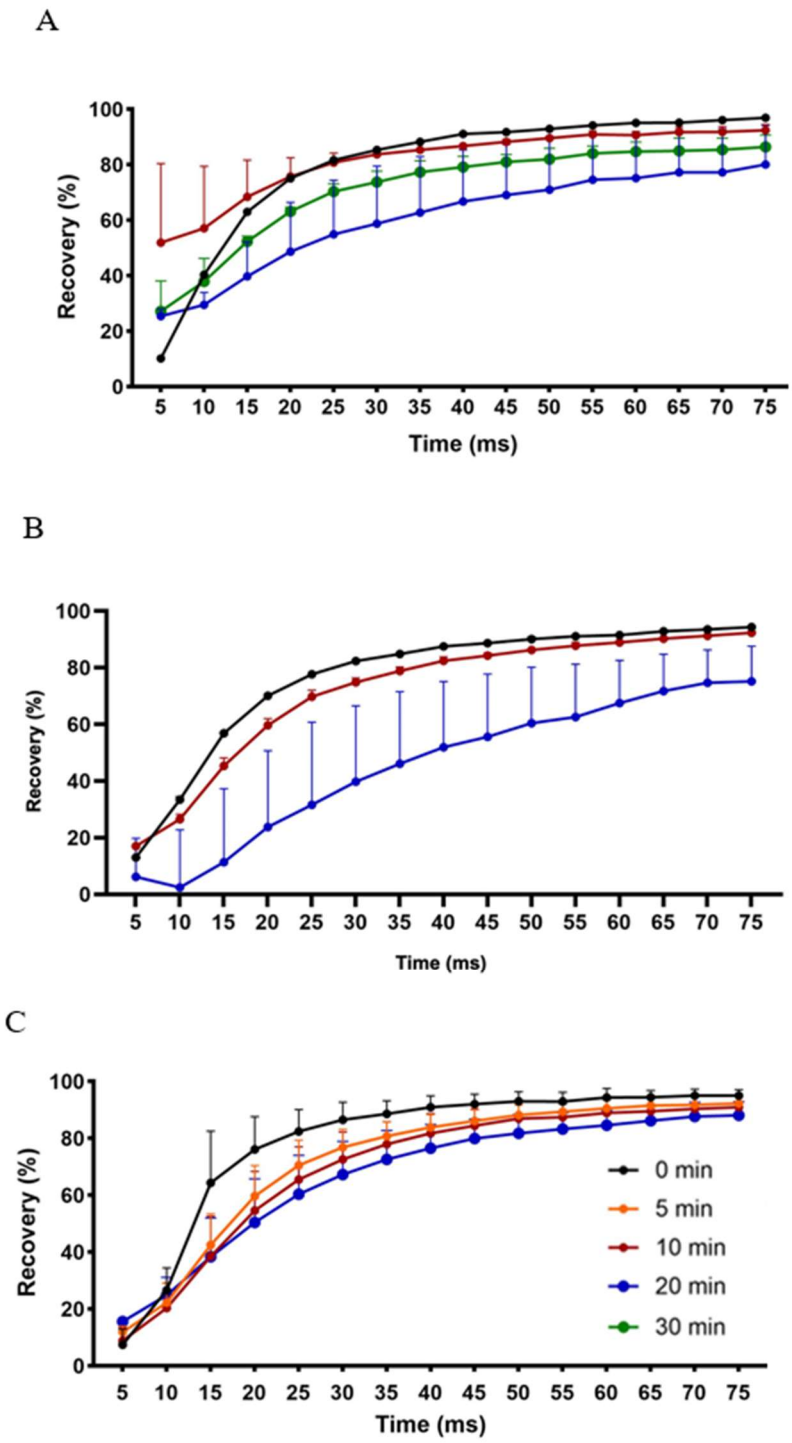

Figure 10. Reduction in the recovery from inactivation by all toxins applied. A. Exposure to Tch2. B. Exposure to Tch3. C. Exposure to Tch4. Control (black) and toxin exposure for 5 min (orange), 10 min (red), 20 min (blue) and 30 min (green) (n=2). Each value indicates mean ± s.e.m.

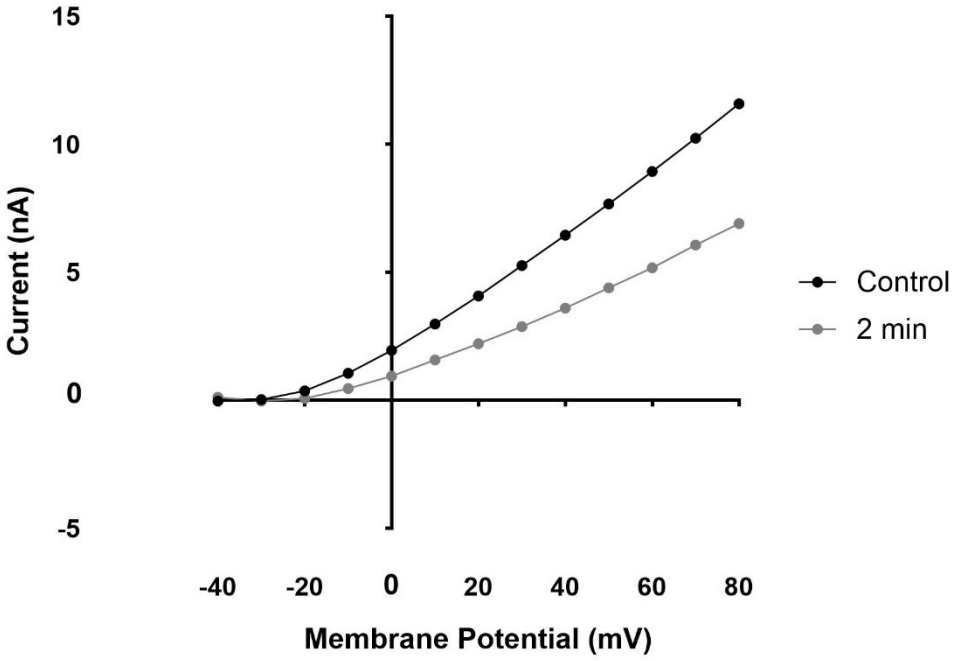

Figure 11. Fast reduction of K^+ current by toxin TchKTx5. Voltage-dependent K^+ current was measured at different voltage steps (IV relationship) before (control, black) and after 2 min of exposure (red) to TchKTx5 (n=1).

DISCUSSION

To analyze the electrophysiological effect of *T. championi* toxins, we used land snail C1 neurons as a cell model. Invertebrate neurons exhibit neuronal functioning similar to mammalian neurons (Lukyanetz & Sotkis, 1996). Given the high level of conservation in these processes, it is possible to study mechanisms in simpler systems and extrapolate them to more complex neuronal ones (Ierusalimsky *et al.,* 2020). In this context, the serotonergic neuron C1 from the cerebral ganglion of *Helix* snails is commonly used due to its easy identification and high resistance to manipulation *in vitro*, and the identification of $Na_V1.7$-like channel present in its membrane (Kiss *et al.,* 2012; Brenes, 2022).

The inhibitory effect on neuronal excitability of crude venom

The protein pattern of the scorpion venom agrees with the findings reported by Díaz and colleagues (2023), describing the characteristic electrophoretic pattern of *T. championi* among other species within the Buthidae family. The bands with lower molecular weight likely correspond to several neurotoxins for Na^+ and K^+ channels, with amino acid sequences ranging between 30 and 70 residues (Borges *et al.,* 2021), such as the toxins studied in the present work (Table I). The intense staining observed in these bands could suggest a higher concentration of these proteins or peptides in the sample, consistent with their attributed role as the primary molecules responsible for clinical effects in *Tityus* scorpion envenomation (Abroug *et al.,* 2020; de Oliveira *et al.,* 2018). On the other hand, in the middle section of the gel, distinct bands can be identified as hyaluronidases (46 kDa) and various proteases (37 kDa). And the higher molecular weight bands are probably enzymes, such as metalloproteases, serine proteases, endothelin-converting enzymes, angiotensin-converting enzymes, endopeptidases, among others identified in this venom through mass spectrometry (Supplementary Table SI). These enzymes may be associated with improved toxin dispersion in tissues, facilitating the degradation of extracellular matrix and enhancing the efficiency of toxin delivery to their target channels (Guerra-Duarte *et al.,* 2019; Díaz *et al.,* 2023).

Initially, what caught our attention, regarding the effects of complete venom, was the reduction in the MFF of the cells (Figure 2A). This effect has been documented in the literature, where venom from other scorpion species has been shown to decrease firing frequency (Narahashi *et al.,* 1972). Analyzing the major effect on AP morphology, a clear impact on depolarization was

observed (Figure 3C and D). In addition, when we tested the most abundant toxin in the venom (the NaTx Tch3) its effect on excitability agreed with the venom effect, decreasing Mean Firing Frequency and exhibiting reduced rise slope and increased depolarization time (Fig. 4 and 5). Since $Na_v1.7$ channels have been identified as threshold channels for AP initiation in cells as nociceptors (McDermott *et al.,* 2019; Alexandrou *et al.,* 2016), it is reasonable that the impact of Tch3 and venom on these channels holds the potential to influence cellular firing. This reduction in MFF can also be attributed to the slow recovery from inactivation, or slow repriming, characteristic of this isoform, reported in mouse spinal sensory neurons (Herzog *et al.*, 2003), with the venom making it harder for the channel to reopen, thereby reducing the macroscopic Na^+ current.

Collaço *et al.* (2019) tested venom from a sister species, *T. bahiensis*, at low (1 µg/ml) and high (10 µg/ml) concentrations, where low concentrations led to prolonged depolarization, enhancing neurotransmitter release and facilitating nerve-evoked muscle contraction. Conversely, at high concentrations, there was a blockade in AP generation and muscle twitches (Collaço *et al.,* 2019), consistent with our findings. Some of these findings also agree with observations from studies on synaptic transmission inhibitors derived from tarantula toxins, which evoked reductions in AP slopes (Schmalhofer *et al.,* 2008). On the contrary, there has been reported the induction of repetitive firing in response to short currents in the presence of the venom of scorpions as *Centruroides suffusus*, which contains β-NaTx in its venom (Couraud *et al.,* 1982).

Upon scrutinizing AP morphology, we note an alteration in repolarization when the venom was tested, characterized by an increase in slope and a decrease in duration (Figure 3E and F). However, it could be expected that the repolarization slope should decrease rather than increase because of TchKTx5 presence. This outcome diverges from the hypothesized result, yet it is conceivable that the influence of other toxins may obscure the overall repolarization effect of the venom.

In conclusion of this part, the decline in AP firing highlights the intricacies and potency of scorpion venom in disrupting neural excitability and, therefore, nervous system function. Results suggested that the most affected phase is depolarization, which agrees with the fact that most of the identified toxins so far in *T. championi* are putative NaTx (Díaz *et al.,* 2023).

Two types of Na^+ inward currents were identified in C1 neuron

The macroscopic Na^+ currents generated appeared to be composed by two different currents, each of them with different behavior, a faster transient current and a slower persistent one, the I_T and I_P, respectively. In our work, the I_T began to activate from -30 mV and reached its maximal magnitude at -20 mV, with a current close to 10 nA, which then becomes an output current with the E_{rev} of +40 mV (Fig. 6B). in the other hand, I_P has ten times less current (1 nA), its peak is at -10 mV, and its E_{rev} is close to 0 mV (Fig. 6C). This I_P is also found through $Na_V1.8$- and $Na_V1.9$-like channels in snail neurons, where the I_T is significantly larger, up to more than six times the I_P. Additionally, there is a notable shift in the E_{rev}, which is more positive in I_T than I_P. Emphasizing that I_T exhibits greater selectivity to Na^+ compared to I_P (Kiss *et al.,* 2012). In fact, I_P has been observed in gastropod neurons (Kiss, 2003; Staras *et al.,* 2002) and giant squid axons (Clay, 2003). Similarly, a slow inward current, referred to as I_B in some literature, was identified in mollusk cells, characterized by its significantly smaller amplitude, up to 100 times smaller than I_T, and a prolonged decay, lasting several seconds (Adams *et al.,* 1980). This current activates at more depolarized voltages, and run in parallel with larger currents, making individual observation challenging (Adams *et al.,* 1980). C1 in *H. aspersa*, these two inward currents overlapped. It is inferred that this current might be generated by a different channel with low or mixed specificity (Adams *et al.,* 1980), explaining the E_{rev} close to 0 mV. And they can contribute to a prolonged depolarization, leading to a faster frequency of spikes, and can increase excitatory stimulus through the summation of excitatory postsynaptic currents (Adams *et al.,* 1980).

In vertebrates, particularly in mammals, functional diversity arises from multiple genes. This situation contrasts with invertebrates, where fewer genes are present, and diversity is attributed mainly to alternative splicing and RNA editing (Goldin, 2001; Zakon, 2012). This could explain why there is just one reported isoform expressed, because of slight differences in sequences that can result in extensive changes in channel behavior. This observation correlates with findings from a previous study (Magistretti *et al.,* 1999) in which different channels, demonstrated by biophysical differences, mediate the I_P current, channels exhibiting fast kinetics possess a conductivity of approximately ~15 pS, whereas those with slower kinetics exhibit ~20 pS conductivity. It is well known that scorpion toxins have been invaluable tools for the purification, identification, and functional characterization of channels (García *et al.,* 2001). In this research,

we can also highlight the usefulness of *T. championi* toxins in detecting two currents, based on their different effects. For example, for Tch2 and Tch4, the I_T's voltage sensitivity was affected (Fig. 7A and E), which did not happen in the I_P (Fig. 7B and F). Furthermore, this difference between I_T and I_P becomes more noticeable when we see how Tch3 clearly affected the I_T but not the I_P (Fig. 7C and D).

In general, I_P can significantly influence several physiological functions (Goldin *et al.,* 2001), it is suggested to possess both a commanding and intrinsic modulatory role. The I_P current can enhance excitatory synaptic inputs, primarily by increasing both the amplitude and, more notably, the duration of the inputs. The I_P recorded in the C1 neuron, an interneuron within a neural network involved in foraging and salivation, may contribute significantly to signal integration and response modulation (Kiss*,* 2003).

The results obtained for I_T and I_P of C1 neurons resemble those obtained in other species. The supplementary Table SII summarizes several properties of both currents in different organisms. For example, for I_T, snails of the same genius, *H. pomatia* expressed $Na_V1.7$-like channels that showed similar behavior to the present study, a fast current with a maximal amplitude of approximately -24 nA at -20 mV and an E_{rev} of +20 mV (Kiss *et al.,* 2012). Other mollusks, such as freshwater *snail Lymnaea* sp., also exhibited a transient macroscopic Na^+ current of at least 40 nA at a membrane potential of -35 mV and an E_{rev} of +25 mV (Staras *et al.,* 2002). These Na^+ currents have also been studied in *Aplysia* sp. neurons and in the giant fiber lobe (GFL) neuron of the cephalopod *Loligo* sp., where they were activated at -30 mV, as in the case of this study, and reversed between +30 and +20 mV, respectively (Gilly *et al.,* 1997). Hence, it can be shown that the behavior of this I_T seems conserved in several orders of the phylum Mollusca.

Looking at the activation and inactivation kinetics reported in some studies in more detail, the LPa3 and RPa3 neurons of *H. pomatia*, have different activation voltage dependence and sensitivity, with a $V_{1/2}$ of -43 mV, and a k of 3.5 (Kiss, 2003), in comparison with -29.7 mV and 2.3, respectively in the present study. This negative shift in voltage sensitivity is also present in the inactivation kinetics, having a $V_{1/2}$ of -43.2 mV (Kiss, 2003) compared to a $V_{1/2}$ of -22.1 mV from our data. These variabilities may be due to differences in the cells studied, as there are differences in the expression of channel isoforms by cells in the ganglia (Kiss *et al.,* 2012).

Looking at the inactivation characteristic within other gastropods several similarities can be found with our data. For example, inactivation $V_{1/2}$ in *Aplysia* sp. had a value of -30 (Adams *et al.,* 1980), in *Pleurobranchea* sp. a value of -23.7 and in *Doripsilla* sp. a value of -25.3 mV (Gilly *et al.,* 1997), compared to the $V_{1/2}$ of -22.1 mV from our study.

Toxins effects on transient and persistent Na^+ currents

We will now discuss the activities of the toxins under investigation. Notably, Tch2 and Tch4 exhibited similar behaviors, both inducing a negative voltage shift. For instance, Tch2 was also found in the scorpions *T. jaimei* (called Tja2) and *T. desdoslargos* (called Tde2), and shares 91% homology with To6, a putative α-NaTxs (Guerrero-Vargas *et al.,* 2012; Diaz *et al.,* 2023). However, despite the high homology with α-NaTxs, our study suggests that it behaves more like a β-NaTxs. Both Tch2 and Tch4 evoked a shift in activation to more negative voltages after 5 and 10 min of treatment (Fig. 8A and C, Table II), a functional characteristic of β-NaTx (Catterall *et al.,* 2007). In *T. obscurus* this kind of effect was described for To4, classified as a β-NaTx, where there is a shift in $V_{1/2}$ to more hyperpolarized values in all human Na_V isoforms (Duque *et al.,* 2017). Also, in the β-NaTxs, there is an additional reported effect, a reduction in Na^+ conductance (Duque *et al.,* 2017). That is also evident for To1, which shows a negative shift and a decrease in macroscopic Na^+ current (Tibery *et al.,* 2019).

In our study, when the cells were exposed to Tch2 and Tch4 instead of a decrease, we saw a small increase in I_T (at -30 mV) and I_P. Intriguingly, there was an increase in I_P, in this matter, it has been reported that the toxin Tst1 causes incomplete inactivation of the $Na_V1.6$ isoform, resulting in a different behavior by slowing down the inactivation process (da Mata *et al.,* 2023). If this was our case, an incomplete inactivation in the $Na_V1.7$-like channel could contaminate the current from the I_P, which could explain why an increase in I_P was observed.

A similar case, a toxin that shared sequence homology with α-NaTx but presented β-NaTx effect has been illustrated by the case of Ts17 toxin from *T. serrulatus* venom. Despite Ts17 sequence identity with Ts5 and Ts3 (both α-NaTx) from the same species, detailed electrophysiological investigations unambiguously characterized Ts17 as a β-NaTx (Menezes *et al.,* 2023). This divergence was attributed to the highly conserved three-dimensional structure of

both scorpion toxin groups, characterized by α-helices and 3 to 4 antiparallel β-sheets, featuring cysteine residues critical for disulfide bridge formation (Quintero-Hernández *et al.,* 2013). Noteworthy insights arise from molecular dynamics simulations conducted by Chen and Chung, indicating that both α- and β-NaTx bind to receptor sites 3 and 4 respectively, in a consistent orientation within the binding pocket (Chen & Chung, 2012). This underscores that distinctions in functional outcomes may be more closely associated with specific amino acid residues pivotal for interactions in the specific receptor site.

Upon comparison with toxins such as AaHIT from *Androctonus australis*, recognized as a β-NaTx selective for insects, CssII and CssIV from *C. suffusus*, β-NaTx selective for mammals, and TsVII from *T. serrulatus*, which is β-like (selective for mammals and insects), all of these demonstrate, an increase in the inward current by up to 5, 3, 9, and 6 times more than the control at -40 mV (Bosmans *et al.,* 2007). Similarly, in our data Tch2 and Tch4 toxins induced Na^+ current increase at a fixed voltage of −30 mV.

The mechanism by which β-NaTx interacts with Na_V channels is known as the voltage sensor-trapping model. In this model, the toxin anchors to the loops between segments S4 and S5 of motive II, keeping the channel in a pre-active state, and making it more sensitive to voltage depolarization (Zhang *et al.,* 2012). Indeed, there is an increase in $V_{1/2}$ by up to 10 and 5 mV more negative for Tch2 and Tch4, respectively, thereby making it more responsive to voltage changes and consequently inducing channel opening earlier than the control. This increase in the probability of channel opening could be associated with an excitatory effect of the toxin, similar to the effects observed with toxins like AaHIT from *Androctonus australis* and Bj-xtrlT from *Buthotus judaicus* (Bosmans *et al.,* 2007). In these cases, an immediate and reversible effect of rapid contraction paralysis occurs, inducing spastic paralysis attributed to the general activation of skeletal musculature due to an excitatory presynaptic action on motor nerves that leads to repetitive firing (Oren *et al.,* 1998).

We observed that the window current increases but reverses its effect after 20 min of exposure to Tch2, exhibiting a fast and reversible effect, however, it does not return to a control state. This partial recovery behavior has also been reported for some α-NaTxs, such as Tc49b and Ts4 (Batista *et al.,* 2002b; Pucca *et al.,* 2015). From an evolutionary point of view, it can be associated with the immediate time of the effect being sufficient for the scorpion to immobilize its

invertebrate prey with its pincers, and there might not be a strong selection for insect-selective toxins with excessively high binding affinity. However, it cannot be ruled out that Tch2 and Tch4 toxins can affect also mammals, as the effect of β-NaTx has been linked to defensive behavior, affecting channels expressed in humans such as $Na_V1.4$ in skeletal muscle and $Na_V1.6$ in the central nervous system, as seen with To1, Tma1, and Tpa2 (Rincón-Cortés *et al.,* 2019). The reversibility of the toxins is consistent with observations that venom from *T. obscurus* shows a systemic effect hours after injection and reverses after 3 h in over 50% of animals (Santos da Silva *et al.,* 2017).

The inactivation of the current was influenced by the Tch2 and Tch4 toxins, with an increase in the k, indicating a reduced voltage dependence for inactivation. Simultaneously, a higher sensitivity was observed, with more negative $V_{1/2}$ values and increased time constants (Table III). In a study of the β-NaTx Tst1 purified from *T. stigmurus* venom on different Na_V isoforms, it was found that in three out of seven isoforms, $V_{1/2}$ becomes more negative than in control (da Mata *et al.,* 2023), resembling the case of Tch2 and Tch4. Additionally, for the Ts17 toxin, a more hyperpolarized $V_{1/2}$ is observed for $Na_V1.7$ channels (Menezes *et al.,* 2023).

An interesting observation is that in various studies, the k of inactivation, associated with voltage dependence, increases (da Mata *et al.,* 2023; Menezes *et al.,* 2023). Consistently, in our two β-NaTx, Tch2 and Tch4, there is an increase in the k, thus a decrease in voltage dependence, as evidenced by the less steep slope of the inactivation curve. It is noteworthy that, in most Na_V isoforms exposed to the Ts17 toxin (except for $hNa_V1.5$), the inactivation curve shows a decrease in k (Menezes *et al.,* 2023). However, in the case of the Tst1 toxin, most isoforms exhibit an increase in k (da Mata *et al.,* 2023). This suggests that despite the conservation of the sequence or the proximity of species, there is a specificity of action and isoform tart of these toxins.

Now, analyzing Tch3 toxin, we observed a remarkable one-third reduction in the I_T after a 20-min exposure at -30 and -20 mV, while the inward I_P remained mostly unaffected. This reduction can be elucidated by studying open probability graphs, revealing a diminished probability of channel opening, due to a positive shift, causing channels to open at more depolarized potentials. There was also a reduction in the voltage dependence, requiring a greater voltage change to transition between states. Furthermore, not only did it require a larger change to initiate channel opening, but inactivation occurred at more negative potentials, evident as a

negative shift and a less steep slope. Collectively, these alterations led to less than half of the window current, culminating in a reduction in macroscopic I_T.

Discovered by Díaz and colleagues, Tch3 was proposed to function as a modulator of Na_Vs, as confirmed in this study. In their investigation, the toxin was also found in *T. jaimei* (called Tja3) and *T.dedoslargos* (called Tde3), and an 88% homology was found with To7 toxin from *T. obscurus* (Díaz *et al.,* 2023). To7 shares 69 and 63% identity with the neurotoxins TdNa10 and TdNa9 from *T. discrepans* (Guerrero-Vargas *et al.,* 2012). All these sequences display a resemblance to α-NaTx. These toxins have a core domain, similar to Old World scorpion toxins (Gordon *et al.,* 2007). These Old World buthid species, that possess α-NaTx and high specificity for receptor site 3, induce the most significant harmful effects in children (Amr *et al.,* 2021). However, it is important to highlight that the α-NaTx characterization was made mostly regarding effects on mammalian channels, not in mollusk channels, so, we cannot categorize the effect of our Tch3 toxin as an α-NaTx, even though there are sequence similarities with various scorpions from the same genus. This underscores the significance of the development of functional electrophysiological research on different animal models, like our research, and the improvement of toxins classification.

Investigations involving *T. obscurus* shed light on the behavior of the Tc49b toxin, which deviates from the conventional characteristics of a typical scorpion α-NaTx. Notably, it exerts an almost complete blocking effect on the current at a concentration of 100 nM in rat cerebellar granule cells (Batista *et al.,* 2002b). This agrees with our findings, where we observe a reduction in current. This suggests that the ambiguity in classification is not exclusive to Tch3. Drawing parallels with pore-blocking peptides, we could conceptualize Tch3 as a blocking peptide, akin to the *m*-conotoxin. This peptide impacts Na^+ permeation through the membrane and exhibits an affinity with another receptor site in the channel, specifically receptor site number 1 situated in the pore-forming loop responsible for the ionic selectivity filter (Moczydlowski *et al.,* 1986; Chahine *et al.,* 1995; Dudley *et al.,* 1995). The incompleteness of the effect can be explained by variations in toxin binding within specific receptor site residues (Dudley *et al.,* 1995; Chahine *et al.,* 1995; Moczydlowski *et al.,* 1986; Yanagawa *et al.,* 1986). However, we cannot conclude that blocking is the main mechanism since this toxin affected biophysical channel characteristics.

A distinct toxin, derived from a tarantula, named ProTx-II, provides intriguing insights. Classified as a Na^+ channel blocker, ProTx-II exhibits noteworthy specificity for human $Na_V1.7$

channels in comparison to other isoforms. Notably, it induces a significant shift in activation towards more positive potentials, similar to the impact observed with our Tch3 toxin. Moreover, it substantially reduces channel conductance (Schmalhofer *et al.,* 2008). In 2019, Xu and collaborators proposed that ProTx-II acts as an electrostatic gating modifier. This mechanism involves the introduction of positive charges into the S3-S4 loop of the voltage sensor domain 2 (VSD2), identified as receptor site 4. The toxin neutralizes acidic residues with basic side chains, impeding the movement of S4 (Xu *et al.,* 2019). This revelation unveils the binding mechanisms between toxins and $Na_V1.7$, elucidating how a toxin can influence kinetics while simultaneously exerting an overall blocking effect.

A similar trend is observed with the local anesthetic QX-314, a derivative of lidocaine. QX-314 induces a shift in the activation $V_{1/2}$ to more positive voltages while simultaneously capable of inhibiting peak current in $Na_V1.7$ channels (Klasfauseweh *et al.,* 2022). Through mutant analysis, Klasfauseweh and colleagues conclude that pore blocking and restriction of the voltage sensor S4 movement can occur through multiple interactions between the positive charges of QX-314 and the negatively charged residues of the channel (Klasfauseweh *et al.,* 2022). Such convergence in the mechanisms of action between analgesics and scorpion toxins opens possibilities, proposing these toxins as potential agents for pathologies associated with pain and nociception.

Regarding the time required to obtain these effects, Tch3 induced a significant change in activation and inactivation after 20 min of exposure, indicating a non-immediate response (Krisch *et al.,* 1989). This latency in the toxin's effect has also been identified in studies with prey insects, exposing crickets to Tma2 and Tma3 (classified as insect α-NaTx), where initial symptoms of disorientation and paralysis are observed, and insect death is recorded up to 4 h later (Rincón-Cortés *et al.,* 2019). This effect is non-lethal at the moment but sufficient to facilitate predation on the animal.

Moreover, the recovery from inactivation was examined after exposure to the three toxins, and it was concluded that all of them affect the availability of closed channels (Fig. 10). Similar observations were made for the Ts17 toxin, where recovery from inactivation was affected (Menezes *et al.,* 2023). This indicates that akin to Ts17, these toxins stabilize a population of

channels in an inactive state, hindering their recovery to the closed state and subsequent opening upon further depolarizations.

Interestingly, even if Tch2 and Tch4 increase Na_Vs voltage sensitivity, decreasing recovery from inactivation their final effect will be a reduction in cellular AP firing. Together with the inhibitory effects of the Tch3 toxin, all these *T. championi* NaTxs reduce cellular excitability.

TchKTx5 effect on macroscopic K^+ current.

Lastly, it is known that the venom of *T. championi* does not exclusively contain NaTxs; rather, it is a complex mixture of more than 10 different molecules (Supplementary Table SI), including KTxs. In our case, we attested the dominant K^+ toxin, called TchKTx5 (Díaz *et al.,* 2023). The same sequence is found in TjaKTx5 of *T. jaimei* and TdeKTx5 of *T. dedoslargos*, with homology to peptides from *T. obscurus* (Díaz *et al.,* 2023).

A decrease in the K^+ outward current was evident with just 2 min of exposure, a fast effect compared with the NaTxs presented here. The presence of K_V channels in C1 metaneuron of *Helix* is known (Brenes *et al.,* 2022), suggesting that the macroscopic K^+ current in the steady-state is mainly generated from voltage-dependent channels, and we showed how the toxin affects these channels. This agrees with literature reports, where KTxs primarily act as blockers of the current from K_Vs. For instance, Ts6, known as butantoxin, has a blocking effect on more than five different K_V isoforms (the most affected were Kv1.1, 1.2, and 1.3). In this Ts6 toxin, a shift in the activation curve to more depolarized potentials was observed, accompanied by a decrease in k (Cerni *et al.,* 2014).

It has been proposed that these toxins block conductance by occluding the extracellular region of the channel pore, involving a lysine and a hydrophobic residue that are fully exposed to interact with the channel (Srinivasan *et al.,* 2002). This is a well-known molecular couple that disrupts K^+ conduction (Banerjee *et al.,* 2013), where electrostatic and hydrophobic interactions occlude the channel pore with their side chain (Lange *et al.,* 2006). Over 120 K^+ blockers from scorpion venom have been identified and classified into around 22 families with distinct primary and secondary structures and distinct target channels have been described (Cologna *et al.,* 2011). We can theorize that the overall effect is similar, a blockage.

Some families exhibit higher affinity, resulting in complete blockage (α-KTx) while others, like in our case, show lower affinity causing partial blockage (*k*-KTx) in specific regions where the target channels are expressed (Jiménez-Vargas *et al.,* 2017). Martin-Euclaire and collaborators reviewed that depending on the toxin and its target (i.e., specific isoforms of K^+ channels affected), the phenotypic effects can range from cardiovascular and muscular to immune system impacts (Martin-Eauclaire *et al.,* 2016).

Therefore, Na_V and K_V toxins in the venom do not compete; rather, they affect both Na^+ and K^+ currents in different ways, ultimately having different functional and pathological effects that serve the scorpion in its attack or defense mechanisms. Any disruption in the normal functioning of these channels can lead to neural activity disorders, muscle contraction issues, and nociceptor activity, etc. (Santos da Silva *et al.,* 2017). The sequences of these toxins show homology with those from scorpions such as *T. obscurus*, known for causing a significant number of sting incidents in the Amazon (Pardal *et al.,* 2003, 2014). While there are differences in epidemiology—mainly due to the lower probability of encounters between scorpions and humans in Costa Rica—the toxins and their effects are similar. This supports the hypothesis by Díaz and colleagues, who attribute the low incidence of severe scorpionism cases in Costa Rica to this reduced likelihood of interaction, as these species are allopatric in Costa Rican forests (Díaz *et al.,* 2023). However, it cannot be ruled out that, interspecific variations caused by geographical isolation could influence the severity of stings, as these variations may be reflected in differences in specific amino acids (Nishikawa *et al.,* 1994) or in the presence of distinct toxin profiles within the venom of *Tityus* species.

CONCLUSIONS

This study provides functional evidence of the effects of venom and specific toxins from the Costa Rican scorpion *T. championi* on mollusk neurons and their Na_V and K_V channels, which had not been previously reported in the literature.

We showed how the *T. championi* venom exerted an inhibitory effect on cellular excitability, primarily through changes in the AP time course, at least partially induced by the Tch3 toxin, and during repetitive firing affected by Tch2 and Tch4 toxins.

We showed that Tch3 toxin exhibited an inhibitory effect in all the Na_V characteristics analyzed. While Tch2 and Tch4 demonstrated excitatory effects in IV relationship, but an inhibitory effect of channel availability, with one of them (Tch2) showing reversible actions.

Additionally, we confirmed the presence of a functional inhibitory KTx (TchKTx5) in *T. championi* venom, although this toxin seems to have no contributions to the venom effects on C1 AP repolarization.

Furthermore, our findings suggest that the conventional classification of scorpion toxins targeting Na_V may be inadequate to fully explain the toxin effects on different channels.

Finally, this research described the macroscopic Na^+ currents in the C1 neuron of *H. aspersa*, allowing a better understanding of the cellular functioning and thereby enhancing its value as a model for future studies, such as pharmacological screening.

CAPÍTULO II

Effect of the venom and selected fractions of Costa Rican scorpion *Tityus championi* on voltage-gated ion channels from mammals and insects

Galit Akerman-Sánchez[1,2], Steve Peigneur[3], Kathleen Carter[3], Cecilia Díaz[4,5], Jan Tytgat[3], Oscar Brenes[1,6]

[1] Department of Physiology, School of Medicine, University of Costa Rica, San José, Costa Rica

[2] Postgraduate Study System, School of Biology, University of Costa Rica, San José, Costa Rica

[3] Toxicology and Pharmacology, Department of Pharmaceutical and Pharmacological Sciences, University of Leuven (KU Leuven), Leuven, Belgium

[4] Clodomiro Picado Institute, Faculty of Microbiology, Univesity of Costa Rica, Coronado, Costa Rica

[5] Department of Biochemistry, School of Medicine, University of Costa Rica, San José, Costa Rica

[6] Neuroscience Research Center, University of Costa Rica, San José, Costa Rica

ABSTRACT

Identifying the target channel isoforms of scorpion toxins is crucial for unraveling the mechanisms by which scorpions utilize their venom, as well as for channeling their potential pharmaceutical applications. In this study, we expressed various isoforms of voltage-gated sodium and potassium channels in *Xenopus laevis* oocytes to investigate the effects of *Tityus championi´*s whole venom and fractions separated by reverse-phase HPLC. The protein sequences of key components were identified through mass spectrometry analysis. Our findings revealed that the venom of *Tityus championi* exerts a potent blocking effect on the human Kv1.2 channel and a partial blockage of the *Drosophila* ShakerIR potassium channel. These effects were primarily attributed to the scorpion toxins TchKTx3, and a novel toxin identified in this study, named TchKTx7. Additionally, the venom contained classical scorpion alpha-toxins that affect Na$_V$1.6, Na$_V$1.7, and the cockroach BgNa$_V$1 channels. It is worth noticing that the venom exhibited both excitatory and inhibitory effects, either enhancing and reducing the current depending on the channel and the venom fraction tested. These results provide better insights on the functional role of the venom in natural conditions for *T. championi*, and the complex interplay between venom components and ion

channels. Finally, we point to Tch3 as, at least, one of the responsible peptides for the inhibitory activity on nociceptive channel Nav1.7 and highlight its potential pharmacological application.

INTRODUCTION

*Tityus championi***,** a scorpion endemic to Costa Rica and Panama, is a compelling subject of study due to its distinct ecological distribution and the varying severity of scorpionism cases in these two regions. In 2023, Díaz and colleagues, presented the first list of toxins found in *T. championi* venom from Costa Rica, identifying multiple putative sodium (NaTx) and potassium (KTx) channel toxins. That same year, Salazar *et al*., demonstrated that both the venom and the toxin-containing fractions from *T. championi* from Panama exhibit toxicity in mammals and insects (Salazar *et al.,* 2023). While severe cases of scorpionism in Costa Rica are rare, likely due to the low frequency of human-scorpion encounters (Díaz *et al.,* 2023), Panama has seen an increase in morbidity and fatalities, with *T. championi* recognized as a medically significant species (Ministry of Health, 2017). The venom's LD50 of *T. championi* from Panama is lower (3 mg/kg) compared to Costa Rica (4 mg/kg) (Brenes & Gómez, 2016), and human-scorpion interactions are more frequent in Panama (Salazar *et al.,* 2023). These findings, alongside the growing number of severe scorpionism cases in Panama, make investigating the venom of *T. championi* particularly relevant.

Although it is known from our work (Akerman-Sánchez *et al.,* unpublished), that the toxins in *T. championi* venom target sodium (Nav) and potassium (Kv) channels in mollusks, the isoforms these toxins act upon in mammals and insects remain unidentified. Determining these molecular targets is crucial for understanding the mechanisms behind envenomation's neuronal and systemic effects (Isbister & Bawaskar, 2014; Godoy *et al.,* 2021) and the identification of these targets could open the way for exploring potential clinical applications. Several scorpion toxins, such as chlorotoxin, maurotoxin, and BmK AGAP, have followed this research path and now show therapeutic potential, offering promising insights into treatments for conditions such as cancer, autoimmune diseases, and neurological disorders (Molavinia *et al.,* 2024; Shakeel *et al.,* 2023; Todesca *et al.,* 2024; Kampo *et al.,* 2019). This study aims to characterize the electrophysiological

impact of *T. championi* venom and some of its fractions on mammal and insect Na_V and K_V channel isoforms expressed in a heterologous model.

EXPERIMENTAL PROCEDURES

Venom

The venom of *T. championi* was obtained from the Dangerous Animals Research Laboratory (LIAP) at the Clodomiro Picado Institute (ICP). This part of the study was approved by the Biodiversity Commission of University of Costa Rica (No. 293-2021). Venom recollected from several specimens maintained in their animal facility was pulled, lyophilized, and diluted in autoclaved distilled water to achieve a concentration of 7.5 mg/ml.

Separation of the major components of the venom through RP-HPLC

A total amount of 7.5 µg crude venom of *T. championi* was further separated by reversed-phase HPLC using a Shim-pack Arata C18 column with dimensions of 4.6 × 250 mm and particle size of 5 µM with a linear gradient from 0% to 60% of solution B (0.1% TFA in ACN, vol/vol) in solution A (0.1% TFA in water, vol/vol) at a flow rate of 1 mL/min over 80 min. The absorbance was monitored at wavelengths of 214 and 280 nm. Eluting compounds were collected in fractions and dried with the Speed-Vac (Genevac™ model miVac DNA 23050-B0). Each dried fraction was then resuspended in 30 uL of ND96 buffer (96 mM NaCl, 2 mM $MgCl_2$, 2 mM KCl, and 5 mM HEPES; pH 7.5), and kept at -20 °C until electrophysiological evaluations.

Identification of the major components of the venom

Following HPLC, venom fractions were separated by SDS-PAGE (15-20% gradient polyacrylamide commercial gel) under reducing conditions (prior step of 10 min at 98 °C with 5% 2-mercaptoethanol) (Isotemp, Fischer Scientific). The low molecular weight ladder BLUeye Prestained Protein (94964, Sigma-Aldrich) was used. Subsequently, the gel was allowed to run for one hour at 150 V using a Mini-Protean Tetra System coupled with PowerPac Basic power supply (BioRad), and proteins were stained with Coomassie Blue R-250.

SDS-PAGE bands were excised from gels and subjected to reduction with dithiothreitol (10 mM) and alkylation with iodoacetamide (50 mM), followed by overnight in-gel digestion with sequencing-grade bovine trypsin (Sigma Chemical Co.) in an automated workstation (Intavis). The resulting peptides were analyzed by nESI--MS/MS using a nano-Easy® 1200 chromatograph and a Q-Exactive Plus® mass spectrometer (Thermo). 5 µL of each tryptic digest were loaded on a C18 trap column (75 µm × 2 cm, 3 µm particle; PepMap, Thermo), washed with 0.1% formic acid (solution A), and separated at 200 nL/min with a 3 µm particle, 15 cm × 75 µm C18 Easy-spray® analytical column using the following gradient toward solution B (80% acetonitrile, 0.1% formic acid): 1-5% B in 1 min, 5-25% B in 30 min, 25-79% B in 6 min, 79-99% B in 2 min, and 99% B in 6 min, for a total time of 45 min (Lomonte and Fernández, 2022). MS spectra were acquired in positive mode at 1.9 kV, with a capillary temperature of 200°C, using 1 scan at 400-1600 m/z, maximum injection time of 100 msec, AGC target of 3×106, and orbitrap resolution of 70,000. The top 10 ions with 2-5 positive charges were fragmented with AGC target of 1×105, maximum injection time of 110 msec, resolution of 17,500, loop count of 10, isolation window of 1.4 m/z, and a dynamic exclusion time of 5 sec. MS/MS spectra were processed for the assignment of peptide matches to known protein families by similarity with sequences contained in the UniProt/SwissProt database (Scorpion, 2024) using Peaks X® (Bioinformatics Solutions). Cysteine carbamidomethylation was set as a fixed modification, while deamidation of asparagine or glutamine and methionine oxidation were set as variable modifications, allowing up to 3 missed cleavages by trypsin.

Xenopus laevis frogs and the isolation of oocytes by partial ovariectomy

All experiments conducted in this study received approval from the Ethical Committee for Animal Research at KU Leuven. Overall experiments and procedures involving *Xenopus laevis* frogs were performed as previously described (Peigneur *et al.,* 2012b). Briefly, before harvesting stage V-VI oocytes from ovarian tissue, adult female *X. laevis* frogs underwent immersion in an aqueous solution containing 0.1% buffered tricaine (ethyl 3-aminobenzoate methanesulfonate, 1 g/L, Sigma-Aldrich, USA) and NaHCO3 (sodium bicarbonate, 1 g/L; Sigma-Aldrich, USA) in aquarium water (pH 7.5) for a duration of 20 min. Following the recovery period, the frogs were monitored daily and returned to their tanks at the Aquatic Facility of KU Leuven. The surgically

removed ovarian lobes underwent enzymatic defolliculation in a Ca^{2+}-free ND96 solution (96 mM NaCl, 2 mM KCl, 2 mM $MgCl_2$, and 5 mM HEPES), supplemented with collagenase from *Clostridium histolyticum* type IA, 1.5 mg/mL; Sigma-Aldrich, USA) on a rocker platform at 16 °C for 2.5 h. Following enzymatic defolliculation, the oocytes were transferred to a calcium containing ND96 buffer (96 mM NaCl, 2 mM $MgCl_2$, 2 mM KCl, 5 mM HEPES, and 1.8 mM $CaCl_2$; pH 7.5) supplemented with gentamicin (100 mg/L; Schering-Plough, Belgium) and theophylline (90 mg/L; ABC chemicals, Belgium) at 16 °C.

In vitro transcription of cDNA clones

Molecular biology techniques (subcloning, transformation, linearization and transcription) were used to make RNA encoding: (1) voltage-gated sodium channels (rNav1.2, rNav1.3, rNav1.4, hNav1.5, rNav1.6, rNav1.7, and BgNav) and their auxiliary subunits rβ1, hβ1, and TiPE β and, (2) potassium channels (hKv1.1, hKv1.2, hKv1.3, hKv1.4, hKv1.5, hKv1.6, hKv10.1, and ShakerIR) (Table SI). Plasmids corresponding to each channel underwent linearization using specific restriction enzymes and subsequent transcription with the T7 or SP6 mMESSAGE mMACHINE transcription kit (Ambion, USA). Depending on the channel type, defolliculated oocytes were injected with 5–20 nL of cRNA at a concentration of 1 ng/nL using a micro-injector (Micro2T SmarTouch™, World Precision Instruments). Electrophysiological experiments were conducted following cRNA injection, with an incubation period of 1–5 days at 16 °C in ND96 buffer.

Electrophysiological recordings with a two-electrode voltage-clamp (TEVC)

A two-electrode voltage-clamp (TEVC) system was performed with a GeneClamp 500 amplifier (Molecular Devices, Downingtown, PA, USA), under the control of pClamp data acquisition system (Axon Instruments, USA), and pClamp Clampex 10.4 software (Axon Instruments®, USA). This setup was employed to measure currents across the cell membrane. The whole-cell currents from the oocytes were recorded at room temperature (18-22 °C). Two microelectrodes, comprising voltage and current electrodes, were crafted from borosilicate glass capillaries (1.14 mm outside diameter, 0.7 mm inside diameter), pulled using a microelectrode puller, PUL-1 (World Precision Instruments, USA). These electrodes were filled with 3 M KCl

using a MicroFill needle, and their resistance was maintained between 0.5 and 1.5 MΩ. Throughout the measurements, oocytes were positioned in a 200 µL recording chamber. A membrane test was initially conducted to adjust measurement parameters based on the membrane quality. After the expression check of the voltage-gated ion channel, the venom of its fractions was applied until a stable effect on the channel was reached. In all experiments, 0.6 µg of the venom from *T. championi* was directly pipetted into the bath, resulting in a final concentration of 0.15 µg/µL tested and the fractions were tested at a final concentration of 2 µM.

For voltage-gated sodium and potassium channel protocols, the recorded currents were sampled at 20 kHz for Na_Vs and BgNav1, and 10 kHz for K_V and ShakerIR. Via a four-pole low-pass Bessel filter, the currents were filtered at 2 kHz for Na_Vs, and 500 MHz for K_Vs, and ShakerIR. Leak subtraction was performed using a −P/4 protocol. Na_V traces used to monitor effects were generated through 100 ms depolarizations to 0 mV from a baseline of -90 mV. Standard current-voltage (IV) relationships for Na^+ and K^+ channels, were performed using 50 ms step depolarizations ranging from −90 to +65 mV with 5 and 10 mV increments, respectively from a baseline of -90 mV.

A two-step protocol was used for steady-state inactivation analyzes, involving a 100 ms pulse from −90 to 0 mV with a 5 mV step, followed immediately by a test pulse to 0 mV. To obtain the channel opening probability, the conductance (g_{Na}) was calculated as $g_{Na} = \frac{I_{peak}}{(V_m - V_{rev})}$, where I_{peak} is the peak current recorded, V_m is the voltage step and V_{rev} is the reversal potential. The opening probability (Po) was calculated by the normalization of the conductance with the maximum conductance and was plotted as a function of voltage. The data were fitted using the Boltzmann equation $I(V) = \frac{Imax}{1+e^{\left(\frac{V-V1/2}{k}\right)}}$, where $V_{1/2}$ represents the voltage where half of the channels are activated, and k is the slope factor.

Data and statistical analysis of the electrophysiological experiments

All data were presented as the means ± standard error of the mean (s.e.m.). All experiments were replicated at least three times (n≥3). GraphPad Prism version 10 (GraphPad Software, USA) was employed for parametric statistical analysis. The normal distribution was assessed by

Kolmogorov–Smirnov and Shapiro–Wilk normality tests and the two-way ANOVA followed by Bonferroni post-hoc test was performed to assess significance between groups. Non-parametric statistical analysis was performed in RStudio (Version 2023.06.0+421) using the paired Wilcoxon test. Significance level was set at $p \leq 0.05$, and denoted as follows: *$p \leq 0.05$, **$p < 0.01$, ***$p < 0.001$, and ****$p < 0.0001$. The specific results of the statistical tests, including F values, degrees of freedom, and p-values, are reported in the text as "exp" for venom exposure and "int" for the interaction between voltage and venom exposure.

RESULTS

Using heterologous expression in frog oocytes and TEVC, the effect of venom at an approximate concentration of 2 μM was evaluated on different isoforms of ion channels. For K_V channels, the venom had a significant impact on six of the eight tested channels (K_V1.1-1.3, K_V1.5-1.6, and ShakerIR) (Fig. 1). In the case of the K_V1.1 channel, exposure to the venom resulted in up to 7% reduction in current compared the control ($F_{(1,112)\,exp} = 40.8$, $p < 0.0001$; $F_{(15,112)\,int} = 2.37$, $p = 0.0052$). The K_V1.2 channel exhibited the most substantial effect, with up to a 70% reduction in current compared to the control ($p_{\,wilcoxon} = 0.0006$) (Fig. 1 and Fig. 2, left panel). For the K_V1.3 channel, only half of the venom concentration was applied, leading up to a 12% decrease in current at the highest depolarized voltages ($F_{(1,16)\,exp} = 146$, $p < 0.0001$; $F_{(15,16)\,int} = 4.95$, $p = 0.0014$). The venom's effect on the K_V1.5 channel was distinct from the others in two key ways: first, the current was only affected at positive voltages, and second, the venom increased the outward current, with an up to 9% change ($F_{(1,88)\,exp} = 19.5$, $p < 0.0001$; $F_{(15,88)\,int} = 1.17$, $p = 0.3124$).

For the K_V1.6 channel, differences in current amplitude were observed from -20 mV, with the inhibition becoming more pronounced as the cell depolarized ($F_{(1,91)\,exp} = 147$, $p < 0.0001$; $F_{(15,91)\,int} = 12.1$, $p < 0.0001$), reaching up to a 10% reduction. In the case of K_V10.1, no effects were observed. The venom's effect was also tested on an invertebrate K_V channel, the ShakerIR from *D. melanogaster*, where a pronounced inhibition was observed, with up to 31% reduction in current compared to control conditions ($F_{(1,48)\,exp} = 95.5$, $p < 0.0001$; $F_{(15,48)\,int} = 5.53$, $p < 0.0001$). In some cells, the current was inhibited up to 50% following venom exposure (Fig. 2, right panel).

After studying the effect of the complete venom, the next step was to separate some of its principal fractions to identify the toxins that could been generating the effect observed on $K_V1.2$ and ShakerIR channels. Chromatographic runs were carried out, successfully separating the components into fractions. One representative chromatogram is shown in Figure 3, small individual peaks were observed with an elution time from minute 29 to minute 37. After this, additional peaks with higher absorbance are detected until minute 48.

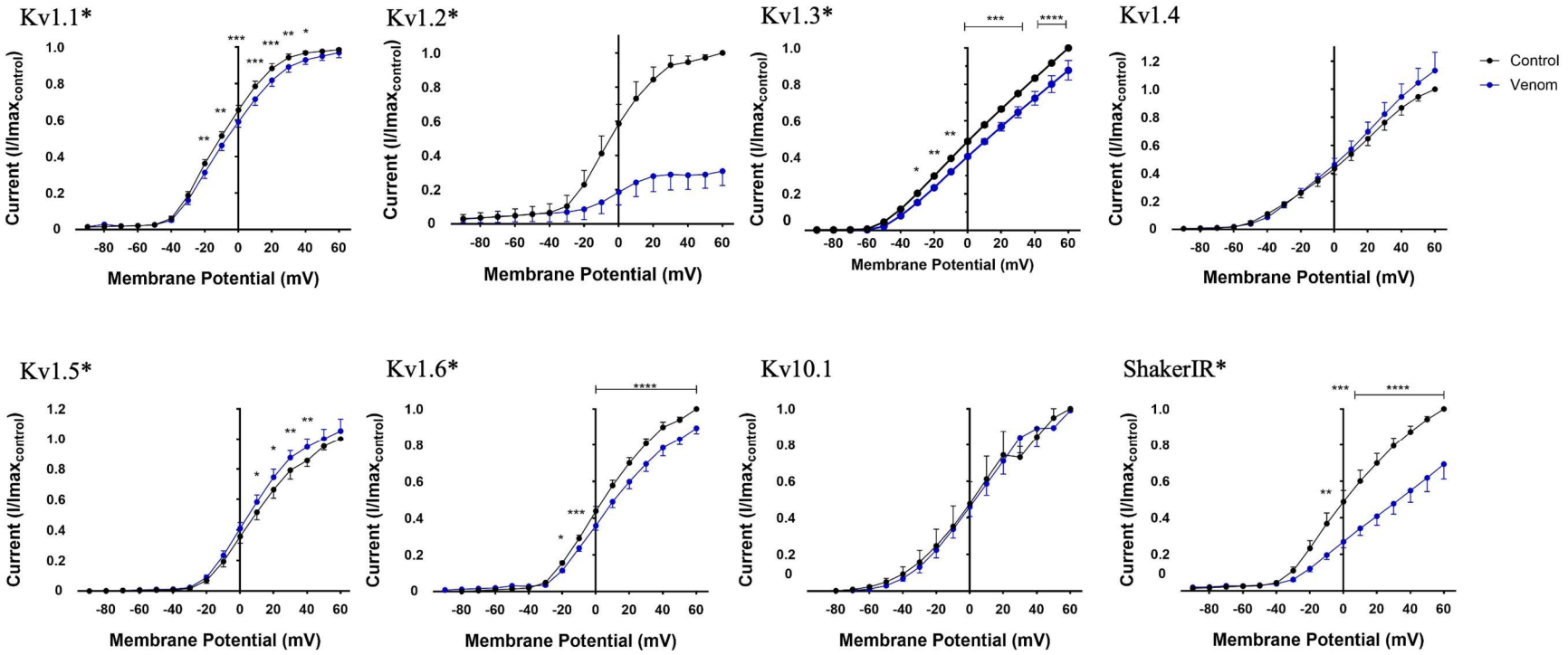

Figure 1. Effect of *Tityus championi* venom on expressed isoforms of Kv from human and insect. All channels were tested using a concentration of 0.15 µg/µL (approximately 2 µM), except for the Kv1.3 channel, where half of the venom concentration, 0.075 µg/µL (approximately 1 µM), was used. Control conditions are shown in black and venom exposure in blue. Kv1.1 (n=8), Kv1.2 (n=3), Kv1.3 (n=2), Kv1.4 (n=4), Kv1.5 (n=7), Kv1.6 (n=7), Kv10.1 (n=3), and ShakerIR (n=4). Each value indicates mean ± s.e.m.

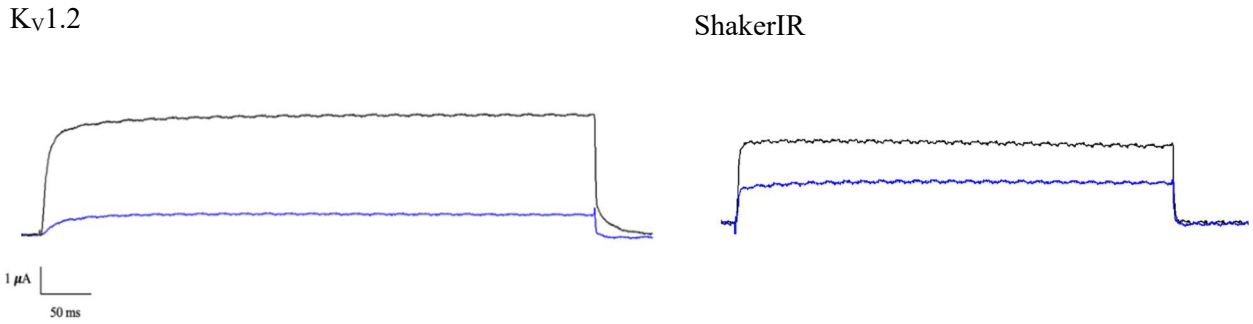

Figure 2. Representative currents of the Kv1.2 and ShakerIR channels. These two channels exhibited the most significant reduction in current following venom exposure (blue recording) regarding control conditions (black recording).

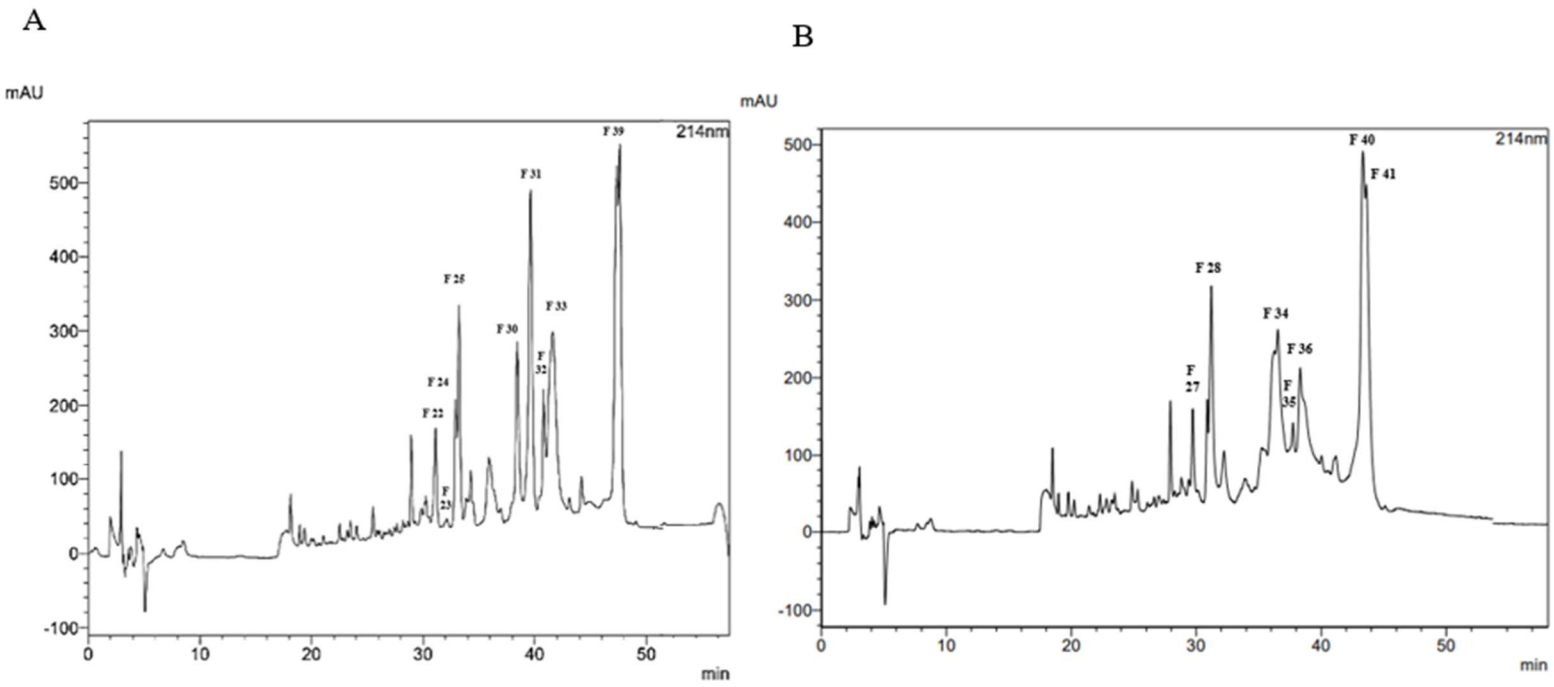

Figure 3. RP-HPLC separation of *T. championi* venom using a linear acetonitrile gradient. Panels A and B present two independent chromatographic runs conducted under identical conditions. The labeled peaks correspond to the fractions that were selected for further analysis.

Seven selected fractions were analyzed using TEVC and SDS-PAGE polyacrylamide gel electrophoresis. This allowed the correlation of the functional effects with the qualitative comparison of the molecular weights of the components in these fractions and an initial assessment of their purity. The main protein components of the fractions with functional effects on $K_V1.2$ and ShakerIR channels were sequenced, identifying potential neurotoxins by comparing their sequences with those reported in public protein databases.

Fractions 22 and 27 from two different chromatographic runs showed similar peaks in their chromatograms (with comparable retention times), both showed one single SDS-PAGE band (Fig. 4A) and shared similar effects on the channels tested. Fraction 22 showed an inhibitory effect, reducing the current through $K_V1.2$ channels by 80% at 0 mV (Fig. 4B), while in the ShakerIR channel, a 15% reduction in current was observed at 0 mV (Fig. 4C), a complete block does not occur. A similar pattern is observed in both channels tested with fraction 27, where the current decreased by approximately 10% across the tested membrane potentials (Fig. 4D and 4E).

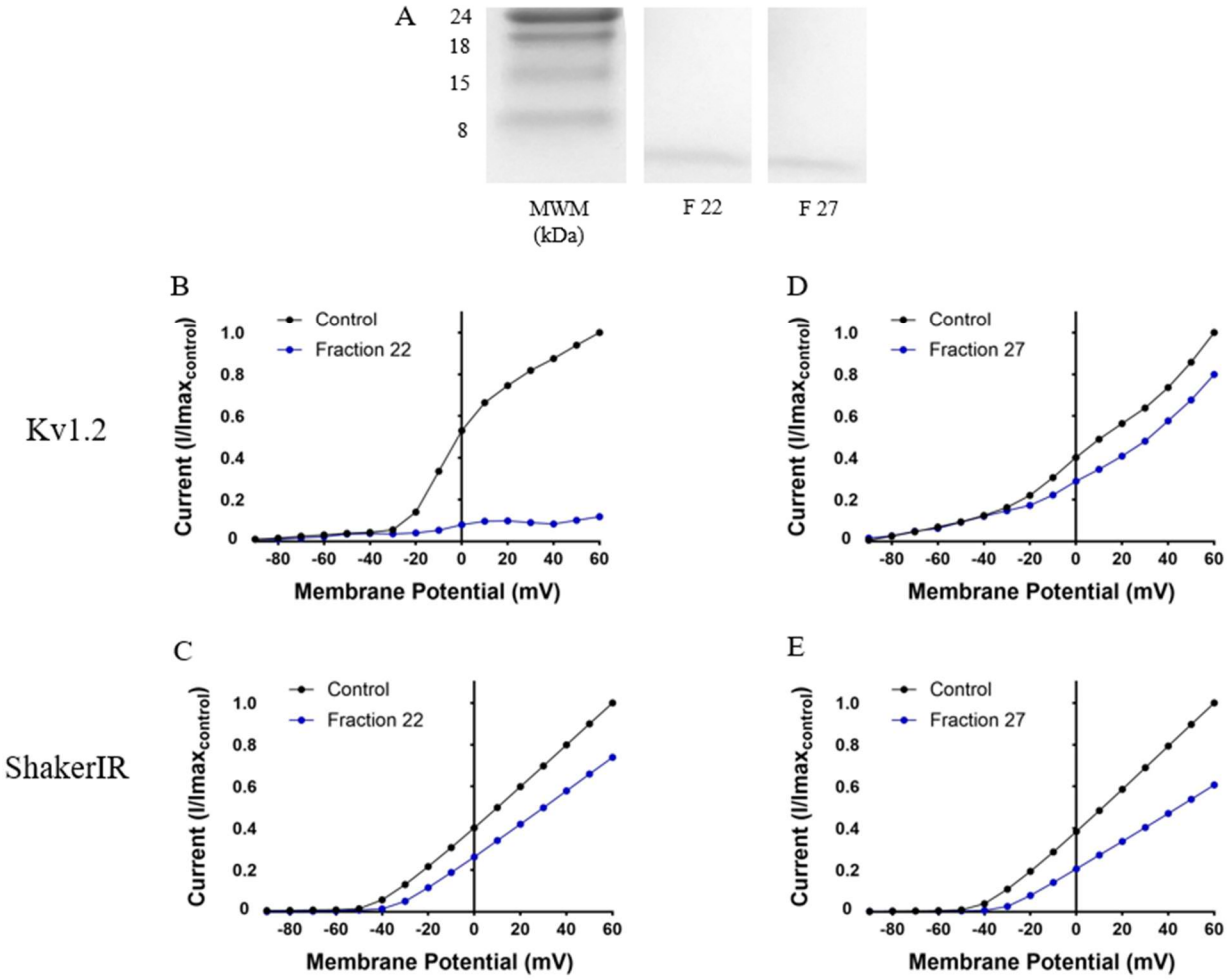

Figure 4. Effect of fractions 22 and 27 on Kv1.2 and ShakerIR channel currents. A. SDS-PAGE banding of individual fractions. B and C show the effect of fraction 22 (n=1), while D and E display the effect of fraction 27 (n=1).

Table I shows a series of alignments of the two main components from fractions 22 and 27. Component A is present in both fractions, while component B is found only in fraction 27. It appears that component B is a fragment of component A. Components A and B showed 100% similarity with other scorpion KTxs from the same genus, such as *T. obscurus* and *T. cisandinus*. The difference in sequences between components A and B is a tripeptide at the N-terminal end (SQQ), and an even shorter version of the whole toxin.

Among the initial peaks of the chromatograms, the fractions 23, 24, and 25 shared very similar retention times (31.5, 33.0, and 33.5 respectively), and presented comparable molecular weight single bands in the gel (Fig. 5A). Analyzing the individual effect of each of these fractions,

identical patterns were observed, which led us to the decision to combine the functional data. The resulting IV relationship showed a remarkable blocking effect on the $K_V1.2$ channel currents, with a reduction of over 40% at 0 mV (Wilcoxon $p < 0.0001$, Fig. 5B). In contrast, no differences were observed over ShakerIR channel currents ($F_{(15,32)\ exp} = 0.233$, $p > 0.05$; $F_{(15,32)\ int} = 5.63$, $p > 0.05$, Fig. 5C). Sequencing of the components from fraction 25 revealed two components, component A was the already identified *T. championi* KvTx, TchKTx3, while component B showed identity with toxins that target Na^+ channels (Table II).

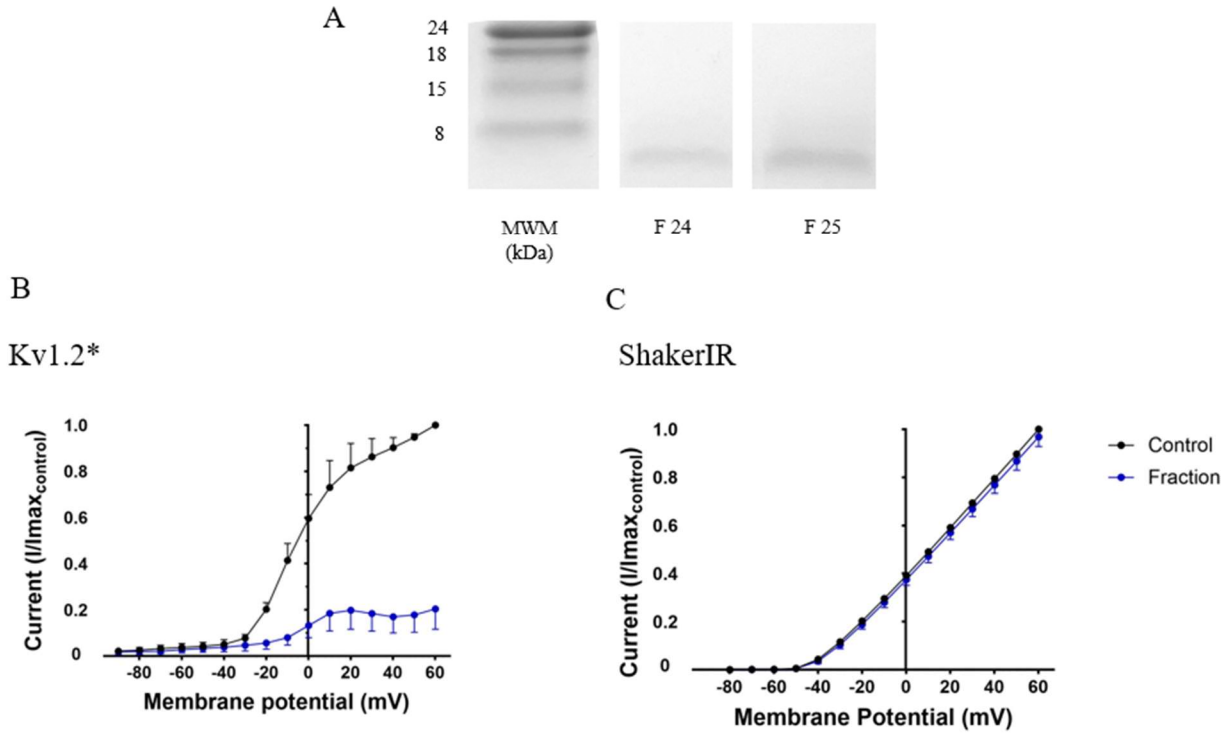

Figure 5. Combined effect of fractions 23, 24, and 25 on $K_V1.2$ and ShakerIR channel currents. A. SDS-PAGE banding of individual fractions (fraction 23 not shown due to low concentration loaded). B. Effect on the $K_V1.2$ channel. C. Effect on the ShakerIR channel. (n=3).

Table I. Sequenced components and alignment of fraction 22 and 27. The amino acid identities are highlighted in gray, and the proposed signal peptides are underlined according to the corresponding literature. Lysine (K, highlighted in blue) and tyrosine (Y, in green) refer to the functional dyad of KTx. "P" refers to direct protein sequencing, while "T" indicates that the protein sequence was obtained from transcriptomic data (from the transcript).

ID	Sequence	Identity (%)	Type	Accession
Component A *T. championi*	VFINVKCRGSKECLPACKAAVGK			
Component B *T.championi*	SQQVFINVKCR			
Tc30 *T. cambridgei*	VFINVKCRGSKECLPACKAAVGKAAGKCMNGKCKCYP	100	P	P60210.1
TdK1 *T. discrepans*	VFINVKCTGSKQCLPACKAAVGKAAGKCMNGKCKCYT	91.3	P	P59925.1
Tcis20 *T. cisandinus*	MKVVYVILMVFILCSMVDLSQQVFINVKCRGSKECLPACKAAVGKAAGKCMNGKCKCYP	100	T	WDU65865.1
Tcis21 *T. cisandinus*	MKVVYVILMVFILCSMVDLSQQVFINVKCTGSKQCLPACKAAVGKARGKCMNRKCKCYP	91.3	T	WDU65866.1
Tco30 *T. costatus*	MKAFYGVLIIFILISMLDLSQQVFINVKCRGSPECLPKCKE A I GKSAGKCMNGKCKCYP	82.6	T	Q5G8B6.1

Table II. Sequenced components and alignment of fraction 25. The amino acid identities are highlighted in gray. "P" refers to direct protein sequencing, while "T" indicates that the protein sequence was obtained from transcriptomic data (from the transcript).

ID	Sequence	Identity (%)	Type	Accession
Component A *T. championi*	CKPLNCAKXXXXXGKGTGYCDKDVCK			
TchKTx3 *T. championi*	SPFGKCKPLNCAK ECQER GKGTGYCDKDVCKCSEW	81	P	Díaz *et al.*, 2023
TjaKTx3 *T. championi*	SPFGKCKPLNCAK ECQER GKGTGYCDKDVCKCSEW	81	P	Díaz *et al.*, 2023
TdeKTx3 *T. championi*	SPFGKCKPLNCAK ECQER GKGTGYCDKDVCKCSEW	81	P	Díaz *et al.*, 2023
Tcis23 *T. cisandinus*	MHFSGIVLILISMTLINTFFSVMIVEATPFRNCKPLNCAKECQER GKGTGYCDKDVCKCSEWKR	81	T	WDU65869.1
KTx *T. metuendus*	TPFRYCNPRNCAK ECQGR GKE T TYCD E VCKCSGW	58	P	P0DQU3.1

Different isoforms of mammalian and insect Nav channels were also expressed to evaluate the effect of venom components on these targets. Significant effects on peak current were observed depending on the isoform analyzed (Fig. 6). The IV relationship is accompanied by the open probability plot, where the window current for each channel was displayed (Fig. 7).

Starting with the $Na_V1.2$ channel, venom exposure resulted in a significant increase in peak currents ($p_{Wilcoxon} = 0.0001$, Fig. 6). In the window current, a +4 mV positive shift was observed on the activation curve ($F_{(1,32)\ exp} = 5.64$, $p = 0.0238$; $F_{(15,32)\ int} = 1.54$, $p = 0.1492$) (Table III), and also +6 mV shift on the inactivation curve ($p_{Wilcoxon} = 0.0385$) (Table IV). The window current area appears to be similar, however, it is shifted towards slightly more positive voltages (Fig. 7). In the case of $Na_V1.4$, no significant differences were observed in peak currents, or the activation curve ($p>0.05$) (Table III).

For the $Na_V1.5$ channel, significant differences were found between the control and venom curves ($p_{Wilcoxon} < 0.0001$), even if the currents' differences after venom exposition are not evident. A small positive shift at the beginning of the activation curve makes the window smaller, however, this effect was not significant (Fig. 7). Additionally, the $V_{1/2}$ activation value showed a minimal change of +2 mV towards more depolarized voltages, with voltage dependence remaining practically unchanged (Table III). As for the inactivation curve, it appeared visually similar; however, significant differences were noted due to venom exposure ($F_{(1,133)\ exp} = 16.6$, $p < 0.0001$; $F_{(18,133)\ int} = 1.02$, $p = 0.4427$, Fig. 7), between -80 to -65 mV and a slightly more hyperpolarized $V_{1/2}$ was observed. While inactivation was affected, these effects seemed to precede the window current. The voltage dependence of inactivation also appears unchanged (Table IV).

In the case of $Na_V1.6$ channel, a significant increase in peak currents was observed, with at least a twofold increase in current magnitude compared to control conditions ($F_{(1,64)\ exp} = 356$, $p < 0.0001$; $F_{(31,64)\ int} = 11.7$, $p < 0.0001$, Fig. 6). The activation curve was not statistically affected ($p_{Wilcoxon} = 0.1819$); however, a positive shift in voltage sensitivity of +3.6 mV was observed, along with reduced voltage dependence (Table III). The most evident effect was observed in the inactivation, where partial inactivation occurred, and the curve never decreased below a relative conductance of 50% ($p_{Wilcoxon} = 0.0008$, Fig. 7). Both voltage sensitivity and dependence were slightly affected (Table IV). All these resulted in a large increase in the window current. Figure 8

provides a clearer visualization of the partial inhibition of inactivation of Na^+ current, accompanied by an almost 20-fold increase in the decay constant ($t = 4.77$, $df = 3$, $p = 0.0175$).

Next, we analyzed the $Na_V1.7$ channel, where despite a current reduction of more than 1/3 at voltages around -15 mV, this difference was not significant ($p_{Wilcoxon} = 0.0770$, Fig. 6). No strong effects were observed on activation in terms of relative conductance ($p_{Wilcoxon} = 0.3955$), voltage dependence or voltage sensitivity (Table III). Regarding inactivation, the inactivation gate remained slightly open even at depolarized voltages (relative conductance remained around 10%) ($F_{(1,114)\ exp} = 38$, $p < 0.0001$; $F_{(18,114)\ int} = 3.84$, $p < 0.0001$, Fig. 7), this difference became evident from -25 mV. This resulted in an increased window current where the channel remained active but not fully inactivated. A small negative shift in voltage sensitivity and an increase in inactivation k were observed (Table IV). Figure 7 shows the reduction in the peak currents with a 4.6-fold increase in decay time constant compared with control conditions (p Wilcoxon = 0.0078). Interestingly, the combination of these effects evoked an IV relationship with decreased currents around -15 mV, both increased currents around +20 mV (Fig. 7).

Finally, we analyzed the venom effects on the insect Na_V channel, BgNav1. In this cockroach channel, there was a significant increase in currents due to venom exposure, increasing by an average of 1.2 μA at -25 mV ($p_{Wilcoxon} = 0.0003$, Fig. 6). Regarding activation, there appeared to be a difference between control and venom conditions ($p_{Wilcoxon} = 0.0150$, Fig. 6). This difference in activation was likely due to a reduction in voltage dependence, as sensitivity remained practically unchanged (Table III). Regarding inactivation, a situation similar to NaV1.6 and 1.7 occurred. The inactivation was affected ($p_{Wilcoxon} < 0.0001$, Fig. 7), the inactivation curve with venom approached zero at a lower rate at less negative voltages, corroborated in part by an increase in k (Table IV), resulting in a larger window current compared to normal conditions. The decreased inactivation is clearly shown in Figure 8, where partial inactivation occurs, however, the decay tau does not present a significant difference ($p_{Wilcoxon} = 0.0547$), and probably the current goes back to zero over longer periods of time.

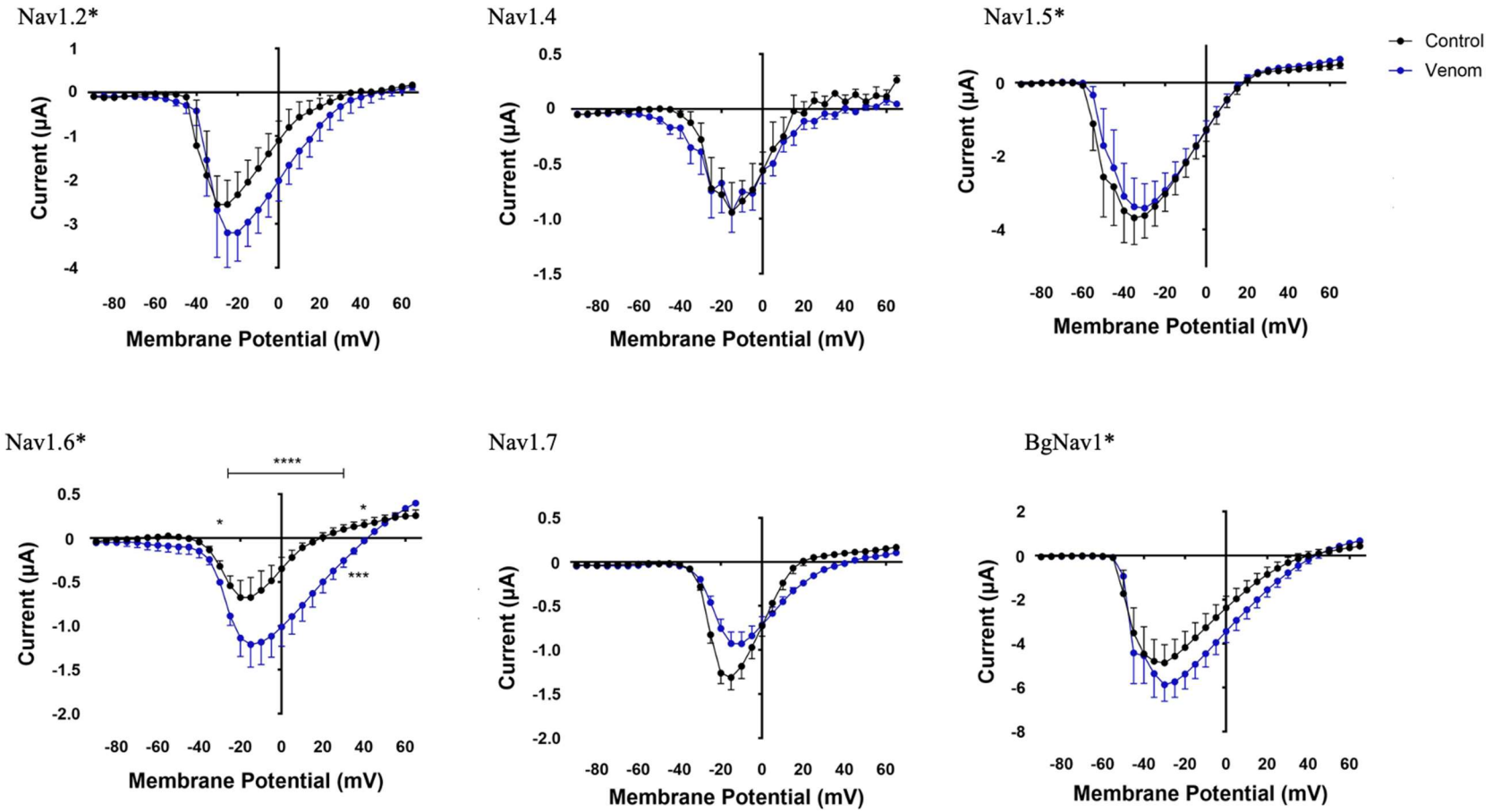

Figure 6. Effect of *T. championi* venom on expressed isoforms of Nav channels from mammals and insects. All channels were tested using a concentration of 0.15 µg/µL (approximately 2 µM). The currents were measured before (control, black lines) and after (blue lines) venom exposure. The number of replicates (n) for each channel is as follows: $Na_V1.2$ (n=3), $Na_V1.4$ (n=4), $Na_V1.5$ (n=9), $Na_V1.6$ (n=4), $Na_V1.7$ (n=8), and BgNav1 (n=9). Each value indicates mean ± s.e.m. The asterisk (*) next to the channel name indicates statistical significance between conditions with $p < 0.05$. In the curves * = $p < 0.05$, *** = $p < 0.001$, **** = $p < 0.0001$.

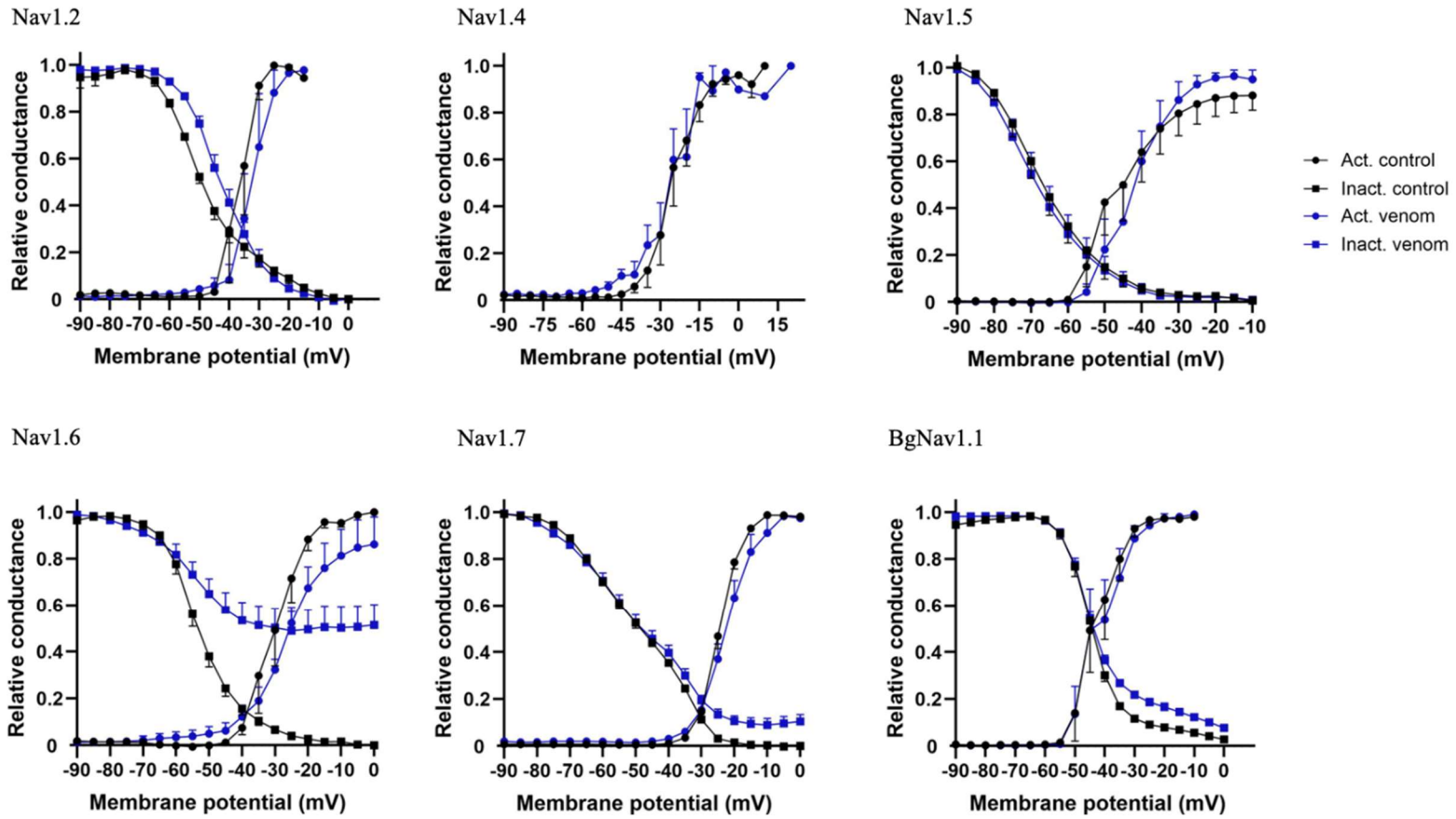

Figure 7. The window current is altered by the venom in different ways depending on the target Nav expressed. The window current is observed by combining the activation curves (●) generated as relative conductance (G/G_{max}), and inactivation curves (■) calculated as relative current (I/I_{max}) in the same graph. The open probabilities are reported before (control, black lines) and after (blue lines) venom exposure. The number of replicates (n) for each channel is as follows: Nav1.2 (n=3), Nav1.4 (n=4), Nav1.5 (n=9), Nav1.6 (n=4), Nav1.7 (n=8), and BgNav1 (n=9). Each value indicates mean ± s.e.m.

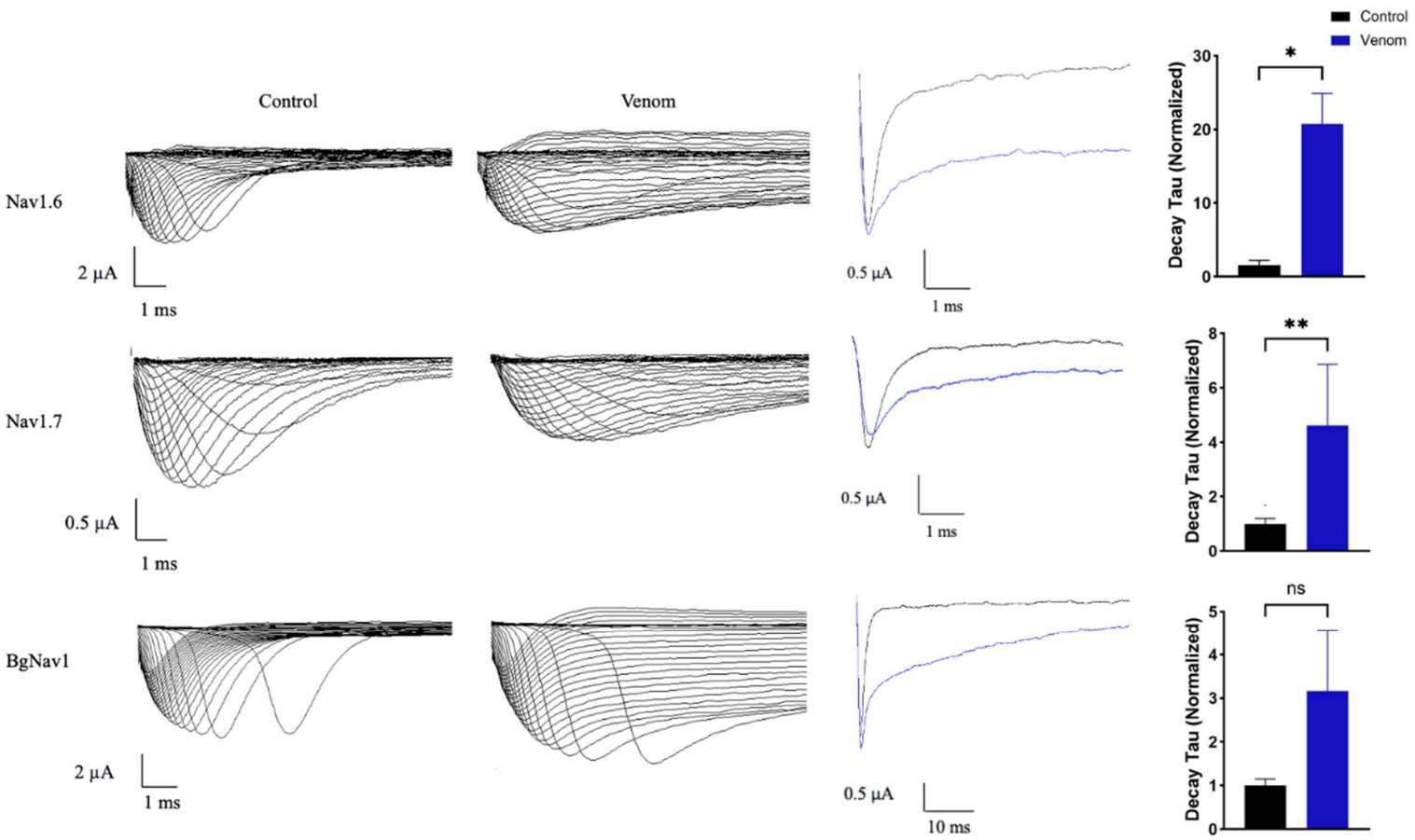

Figure 8. Inhibition of inactivation by venom in Nav1.6, Nav1.7, and BgNav1 channels. The top panel corresponds to Nav1.6, the middle panel to Nav1.7, and the bottom panel to BgNav1 currents. Representative Na^+ inward currents were evoked by a voltage-step protocol ranging from -90 to +65 mV for 50 ms, with a 5 mV increment. The Na^+ inward current traces at 0 mV under control conditions (black) and venom exposure (blue) are presented in the middle column. Bar graphs show the normalized decay tau to the maximum value for each cell, displayed as mean ± s.e.m. The number of replicates (n) is as follows: Nav1.6 (n=4), Nav1.7 (n=8), and BgNav1 (n=9), with control shown in black and venom in blue. Ns = no significant, * = $p < 0.05$, ** = $p < 0.01$

Table III. Open probability biophysical parameters derived from the mean activation curve using Boltzmann equation for each channel tested. $V_{1/2}$ is the voltage corresponding to half-maximal activation; k is the slope factor of activation.

Channel	Control		Venom		n
	$V_{1/2}$	k	$V_{1/2}$	k	
$Na_V1.2$	-36.18	3.21	-32.33	3.47	3
$Na_V1.4$	-26.16	4.78	-25.45	6.26	4
$Na_V1.5$	-46.93	5.88	-43.37	5.51	9
$Na_V1.6$	-30.32	4.50	-26.73	6.16	4
$Na_V1.7$	-24.67	3.05	-23.21	3.87	8
BgNav1	-43.87	4.21	-42.18	5.34	9

Table IV. Steady-state inactivation biophysical parameters derived from the mean curve using Boltzmann equation for each channel tested. $V_{1/2}$ is the voltage corresponding to half-maximal inactivation; k is the slope factor of inactivation.

Channel	Control		Venom		n
	$V_{1/2}$	k	$V_{1/2}$	k	
$Na_V1.2$	-48.38	8.09	-42.28	7.10	3
$Na_V1.5$	-68.63	9.21	-70.41	9.46	9
$Na_V1.6$	-52.85	6.29	-55.82	7.02	4
$Na_V1.7$	-48.37	11.71	-50.33	12.49	8
BgNav1	-44.47	4.44	-44.70	5.28	9

Ten different fractions were chosen to analyze the toxins evoking the reported effects on $Na_V1.6$ and $Na_V1.7$. However, we detected several sequences with identities matching various toxins in each fraction.

Eight of the fractions were tested in the cells expressing the $Na_V1.6$ channel. Six of the fractions tested evoked an increase in peak currents, while the remaining two had an inhibitory effect. For example, fraction 32 decreased the currents at negative voltages (Fig. 9, upper left panel), while fraction 33 increased the currents at most voltages (Fig. 9, upper middle panel). Interestingly, some of the fractions seemed to evoke a positive shift in the IV relationship, such as fraction 35 (Fig. 9 upper right panel).

Regarding the cells expressing the $Na_V1.7$, nine fractions were tested, five fractions evoked an increase in peak currents, while four of them had an inhibitory effect. For example, fraction 35 induced the inhibition of the peak currents at most voltages tested (Fig. 9 lower right panel), and on the other hand fraction 33 induced the increase in the peak currents at most voltages (Fig. 9 lower middle panel). Interestingly, some of the fractions induced a decrease in the currents just in the opening of the channel, such as fraction 32 (Fig. 9, lower left panel).

Revisiting the results from Figure 5, it is observed that the crude venom had differential effects between the two isoforms, increasing $Na_V1.6$ current while decreasing $Na_V1.7$. From the fractions analyzed, two exhibited this isoform-specific behavior, exemplified by fraction 35, which increased the current and shifted the voltage sensitivity to more positive potentials in $Na_V1.6$, while showing a clear reduction in $Na_V1.7$ currents (Fig. 9, right panels). The specific NaTxs present are still being identified for each fraction. Although, in the present work, the effect of the fractions cannot be attributed to a single toxin, interesting effects can be analyzed.

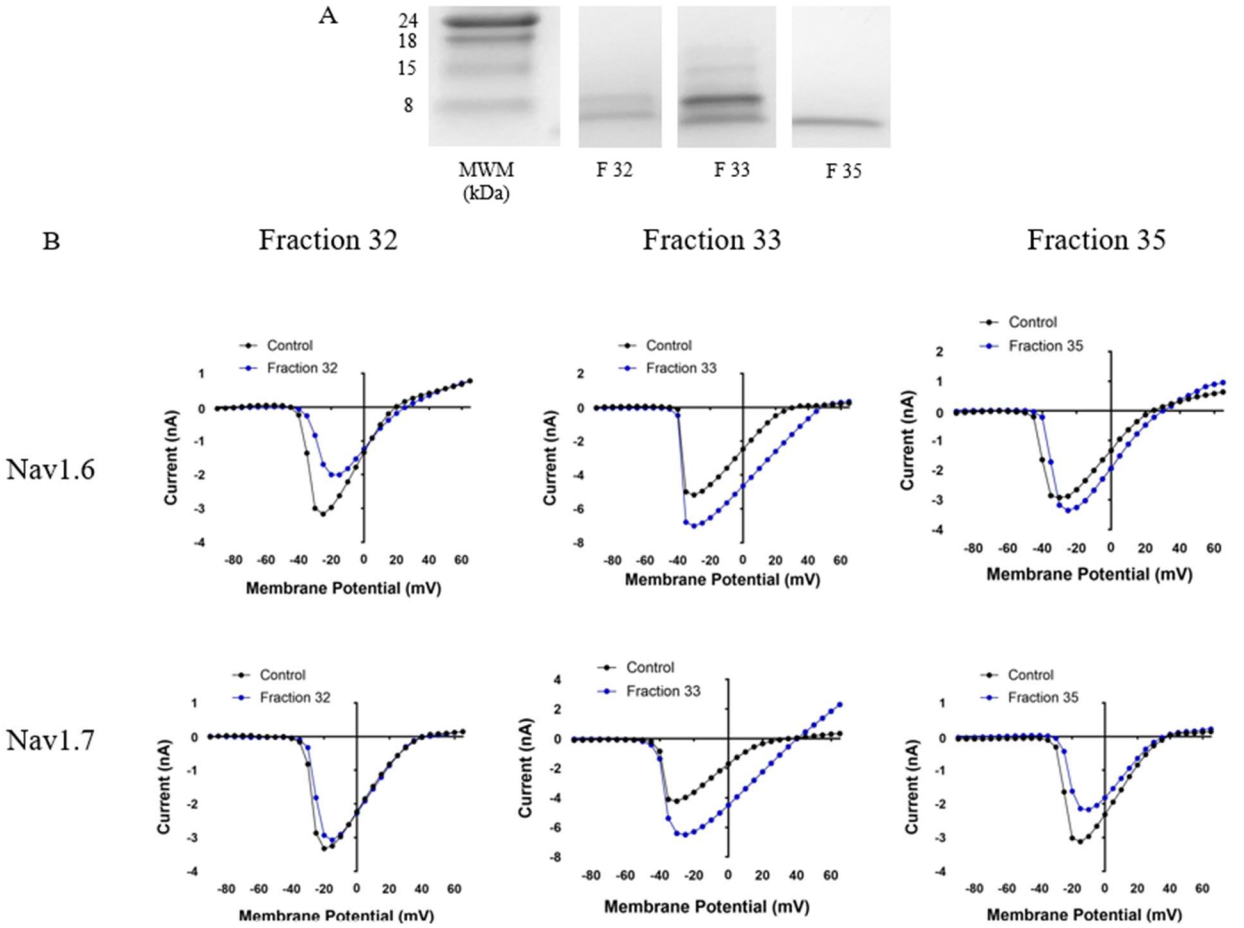

Figure 9. Differential effects of fractions 32, 33, and 35 on Nav1.6 and Nav1.7 channel currents. A. SDS-PAGE banding of individual fractions. B. All channels were tested using a concentration of 0.15 µg/µL (approximately 2 µM). The currents were measured before (control, black lines) and after (blue lines) venom exposure (n=1).

DISCUSSION

Venom-mediated inhibition of currents in human and insect K_V channels

Even with high homology among members of the K_V1 channel family (Capera *et al.,* 2022), scorpion toxins can interact differently in each isoform and modulate their current (Moczydlowski *et al.,* 1988). Here, we found that the venom of *T. championi* slightly influenced the current from the isoforms $K_V1.1$, $K_V1.3$, $K_V1.5$, and $K_V1.6$, and exerted a greater blocking effect over the current from $K_V1.2$ and ShakerIR channels (Fig. 1). The fact that the venom affects multiple

channels is expected, as it contains a variety of KTx peptides with different selectivity (Matsumura *et al.,* 2021). For instance, *Tityus serrulatus* venom, which includes Ts6 and Ts7, inhibits the same channels discussed in this study (Cerni *et al.,* 2014; Nencioni *et al.,* 2018). Also, similar current decrease over $K_V1.1$, $K_V1.2$, $K_V1.3$, and $K_V1.6$ have been observed when using the toxin AbeTx1 from *Actinia bermudensis* (Orts *et al.,* 2018). The fact that this response was seen with both a complex venom and a single toxin, may suggest a common underlying mechanism. These channels are expressed in the central nervous system (CNS) in various combinations of heterotetramers (Sheng *et al.,* 1993, Martel *et al.,* 2011). Their co-expression in the membrane might explain their collective susceptibility to toxins. Furthermore, all four channels function as low-threshold channels (Dodson *et al.,* 2023), which could also correlate with structural similarities and the shared effect of the venom.

Although statistically significant differences were observed between control and venom-treated conditions in the mentioned channels, it is important to highlight that within the physiological range of membrane potentials, the most affected channels by the venom were $K_V1.2$ and ShakerIR (Fig. 2). Toxins such as Mesomartoxin from *Mesobuthus martensii* and Agitoxin-2 from *Leiurus quinquestriatus hebraeus* (Yuan *et al.,* 2017), as well as Ts6 and Ts7 (*T. serrulatus*) (Cerni et al., 2014, 2016), similarly block both channels. $K_V1.2$, frequently targeted by a variety of scorpion toxins, including Ts19 from *T. serrulatus* (Cerni *et al.,* 2016), Tst26 from *T. stigmurus* (Papp *et al.,* 2009), Css20 from *C. suffuses suffusus* (Corzo *et al.,* 2008), AbeTx1 (*A. bermudensis*) (Orts *et al.,* 2018), Cm39 from *C. margaritatus* (Nassem *et al.,* 2023). This channel is predominantly expressed in the brain and heart, where it modulates neuronal excitability and prevents terminal hyperexcitability (Dodson *et al.,* 2003), playing a critical role in membrane repolarization as a delayed rectifier (Shieh *et al.,* 2000; Hatta *et al.,* 2002; McKeown *et al.,* 2008). Dysfunction in $K_V1.2$ has been strongly associated with epilepsy and ataxia (Robbins & Tempel, 2012). In the brain, $K_V1.2$ is highly expressed in regions such as the auditory brainstem, hippocampus (Dodson *et al.,* 2003), and cerebellum (Southan & Robertson, 1998). Studies in knockout mice have linked $K_V1.2$ deficiency to brainstem seizures and respiratory failure (Robbins & Tempel, 2012). Envenomation by *Tityus* scorpions often results in respiratory dysfunction (de Matos *et al.,* 2024), a symptom that can be potentially tied to $K_V1.2$ inhibition. Additionally, blocking $K_V1.2$ in cerebellar basket interneurons leads to increased GABA release onto Purkinje cells, likely contributing to motor coordination deficits (Southan & Robertson, 1998; Williams *et*

al., 2012). This may explain symptoms such as vertigo, dizziness, and loss of coordination reported by envenomated individuals, particularly in children (Xie *et al*., 2010), affectations possibly happening as well in small mammalian predators of these scorpions.

As mentioned, multiple scorpion toxins block ShakerIR channels. The Shaker channel from *Drosophila melanogaster* shares 68% identity with the human K_V1.2 channel (Jegla *et al.*, 2012; Capera *et al.*, 2022). For instance, Maurotoxin induces a 58% mean reduction in macroscopic current at 0 mV (Carlier *et al.*, 2000), while *T. championi* venom reduced current by 31% under the same membrane potential (Fig. 1), and in some cells, even half of the current was reduced (Fig. 2). Many scorpion toxins block insect K_V channels by inserting into the channel pore, effectively acting as a molecular "cork" (Carbone *et al.*, 1982; Banerjee *et al.*, 2013). The high affinity of these toxins for Shaker channels is likely due to their binding at the extracellular S1 site, which blocks cation flow without causing major conformational changes in the channel (Banerjee *et al.,* 2013). The blockage disrupts membrane potential repolarization, leading to paralysis and eventual death in the insect (Bergeron & Bingham, 2012; Zhang *et al.,* 2015). For example, the BoiTx1 blocks Shaker channels leading to repetitive firing and sustained action potential, which result in prolonged muscle contraction in *D. melanogaster* larvae (Kozminsky-Atias *et al.,* 2007).

Novel discovery of TchKTx7 and confirmation of TchKTx3 blocking effects on K_V1.2 and Shaker channels

During the initial venom separation, we identified a fragment of a KTx in the early eluted fractions 22 and 27 (Fig. 3, Table I). This fragment exhibits blocking activity on K_V1.2 channels and, to a lesser extent, on ShakerIR channels (Fig. 4). Sequence analysis shows 100% identity with toxins Tc30 from *T. obscurus* and TdK1 from *T. discrepans*, which are known to block over 70% of Shaker B channel activity (Suze et al., 1999; Batista et al., 2002a), confirming its selective effect on K_V channels. Additionally, this fragment shares high affinity with putative KTx toxins, Tcis20 and Tcis21 (Table I). The effect of Tco30 from *T. costatus* (81% sequence identity, Table I) is more comparable to that of the identified fragment, as it shows a lower blockage of about 44% on Shaker B channels at a concentration of 2.6 μM (Diego-García *et al.,* 2005). This is the first report of this toxin for *T. championi* and the first description of its functional blocking effect. Following the nomenclature proposed by Díaz *et al.,* for *T. championi* we suggest naming this toxin TchKTx7.

The 'functional dyad' in a KTxs sequence is critical for contacting the K_V channels, where a basic residue (K) and a hydrophobic residue (Y) plug into the pore (Matsumura *et al.,* 2021). As shown in Table I, Tc30 exhibits the highest affinity and contains the mentioned functional dyad (highlighted in green and blue) (Matsumura *et al.,* 2021), suggesting a pore-plugging mechanism of channel blockage for TchKTx7. Furthermore, Diego-García *et al.* (2005) identified a signal peptide region (residues 1-22), which includes the SQQ triad. This same triad is present in the peptide sequence we obtained for component B of the venom fraction (Table I). In scorpion toxins, the signal peptide is followed by a very small propeptide (PP) region. While the signal peptide is typically cleaved by endoproteolytic enzymes of the convertase family during toxin maturation (Delgado-Prudencio *et al.,* 2019), we propose that the SQQ triad might be part of the PP region, which sometimes remains uncleaved during venom processing. Additionally, other active post-translational cleavage processes in the venom could further target this triad (Zeng *et al.,* 2024).

The differences observed in Figure 4 between fractions 22 and 27 in $K_V1.2$ channel blockage may be due to intrinsic cellular variability. It is also important to note that we were unable to determine the exact concentration of toxins in the fractions applied to the cells, and different concentrations between fractions may have influenced the observed effects, as venom activity is concentration-dependent (data not shown).

We successfully separated (fractions 23, 24 and 25) and identified the recently discovered putative TchKTx3 (Table II) (Díaz *et al.*, 2023). This toxin shares high homology with TjaKTx3 and TdeKTX3 from Costa Rica, a similarity that may be attributed to comparable ecological pressures, as suggested by the authors. Our results confirm that TchKTx3 blocks K_V channels, reducing 60% of the current at 20 mV from the human $K_V1.2$ channel, with no observed effect on the insect ShakerIR channel (Fig. 5). Additionally, TchKTx3 shows 58% identity with a KTx from *T. metuendus*, whose venom injection shows hyperactivity, respiratory issues, paralysis, convulsions, and death in mice (Batista *et al.*, 2018). Furthermore, a fraction containing putative KTx from *T. championi* was tested in mice and crickets. A 1 µg intracranial dose was lethal to mice, whereas 5 µg had no significant effect on crickets (Salazar *et al.*, 2023). It is likely that TchKTx3 and TchKTx7 together influence the venom's activity on $K_V1.2$, while TchKTx7 also targets ShakerIR channels. However, further tests with isolated pure toxins will be necessary to determine their exact effects and specificity.

Venom modulation of macroscopic currents in mammalian Na$_V$ channels

By expressing multiple Na$_V$ channels heterologously in *Xenopus laevis* oocytes, we show the influence of *T. championi* venom on five out of six tested isoforms. Na$_V$1.2, Na$_V$1.6, and BgNav1 exhibited increased currents, while Na$_V$1.5 and Na$_V$1.7 showed reductions in current (Fig. 6).

Starting with Na$_V$1.2, we observed an increase in peak current (Fig. 6), along with a positive shift in the voltage sensitivity of both activation and inactivation, slightly moving the window current to more depolarized voltages (Fig. 7). The toxin MeuNaTxα-1 also increases Na$_V$1.2 currents with minimal effect on inactivation, as in our case (data not shown), which is linked to initiating nociceptor sensitization through indirect downstream mechanism (van Cann *et al.*, 2020). The venom's effects deviate from the classic classification of scorpion toxins, where β-scorpion toxins typically induce a shift toward more hyperpolarized potentials, such as Ts17 from *Tityus serrulatus* (*Santos-Menezes et al.*, 2023). Other toxins, including TsVII, Css VI, Css IV, and Css II, also shift voltage sensitivity toward hyperpolarization in the Na$_V$1.2 channel (Bosmans *et al.*, 2007), contrasting with the depolarizing shift we observed for *T. championi* venom (Fig. 7). Na$_V$1.2 is predominantly expressed during early development, where it is the primary Na$_V$ channel in axons, later it is replaced by Na$_V$1.6 (Spratt *et al.*, 2019). In adults, both Na$_V$1.2 and Na$_V$1.6 are located in the axon initial segment (AIS), but they serve different roles, where Na$_V$1.2 have a higher activation threshold (Hu *et al.*, 2009; Filipis *et al.*, 2023).

Interestingly, while MeuNaTxα-1 induces a threefold increase in Na$_V$1.2 current, it also significantly impairs inactivation in Na$_V$1.6 currents (van Cann *et al.*, 2020), which is consistent with our findings with the venom (Fig. 8). Actually, in the tested membrane potentials the open probability of the inactivation gate of this channel is always above 50% (Fig. 7). Inhibition of inactivation is a hallmark of α-toxin action, commonly seen in venoms from the Buthidae family (Mendes *et al.*, 2023). These toxins bind to receptor site 3 in the IV motive of the Na$_V$ channel's α-subunit, preventing the outward movement of the voltage sensor and thus blocking inactivation (Rogers *et al.*, 1996; Bosmans & Tytgat, 2007; Martin-Eauclaire *et al.*, 2019). Examples of such toxins include Lqh2, LqhaIT, Lqh3 (Mendes *et al.*, 2023), and Ts4 (Pucca *et al.*, 2015a), all of

which similarly inhibit inactivation, and increase inactivation time constant, as with the venom tested (Fig. 8, right upper panel).

Nav1.6 is the most abundantly expressed Na_V channel in the CNS and peripheral nervous system (PNS), especially in regions such as the AIS and nodes of Ranvier (Goldin, 2001). It plays a crucial role in lowering the voltage threshold for action potential (AP) generation (Li *et al.*, 2023) and is implicated in increased neuronal hyperexcitability during epileptogenesis (Hargus *et al.*, 2013). An inhibition of inactivation, and the consequent increase in current, could lead to prolonged depolarizations in axon terminals and elevated neurotransmitter release (Reis *et al.*, 2019). Moreover, there is evidence suggesting that heightened activation of $Na_V1.6$ can promote inflammation (Alrashdi *et al.*, 2019), a critical mechanism deployed by scorpion venom (Reis *et al.*, 2019).

Tityus venom displayed an intriguing dual effect over $Na_V1.7$. First, it inhibited inactivation (Fig. 8), which would typically prolong AP and increase neuronal excitability. This is similar to the effects of Ts2 and Ts5, which inhibit the rapid inactivation of both $Na_V1.6$ and $Na_V1.7$ (Pucca *et al.*, 2015b). However, we also observed a reduction in $Na_V1.7$ peak current at negative voltages (Fig. 6). Although inhibition of inactivation could theoretically enhance excitability, the overall decrease in current likely dominates, leading to a macroscopic reduction in channel activity.

$Na_V1.7$ is primarily expressed in peripheral somatic neurons and plays a pivotal role in regulating sensory neuron excitability. This channel has a critical role in pain perception (Dib-Hajj *et al.*, 2013). Gain-of-function mutations in the *SCN9A* gene, which encodes $Na_V1.7$, are linked to neuropathic pain conditions, while loss-of-function mutations cause congenital insensitivity to pain (Vetter *et al.*, 2017). Although inhibition of inactivation prolongs APs and enhances nociceptive neuron spike frequency, leading to acute pain (Jami *et al.*, 2023; Lu *et al.*, 2022), the reduction in peak current we observed in $Na_V1.7$ by the crude venom suggests a dampening effect that could have analgesic potential, as the inhibiting Na^+ current scorpion toxin BmK IT2 (Wang *et al.*, 2000; Zhang *et al.*, 2003; Zhao *et al.*, 2008). Additionally, it is interesting to note that while the venom increased current in channels such as $Na_V1.2$ and $Na_V1.6$—possibly contributing to excitatory and inflammatory responses—it reduced $Na_V1.7$ activity. This suggests a potential dual

role for *T. championi* venom: it may have pro-excitatory effects through certain channels while inhibitory effects through Na$_V$1.7.

Akerman-Sánchez *et al*. (unpublished) determined that one of the toxins present in the tested venom, the TCh3, exhibited an inhibitory effect on the Na^+ current of snail C1 neurons, which exclusively express Na$_V$1.7-like channels. This finding is consistent with the results of this study (Fig. 6), providing valuable insights into the selective effect of the venom or toxin on this isoform across two distant taxa, mollusks and mammals. Furthermore, at the level of APs, the venom also appears to have an inhibitory effect, reducing the C1 cell ability to fire APs, likely due to specific inhibition of Na$_V$1.7 and a dominant effect of this toxin in the overall venom. As pointed before, this inhibition could potentially result in reduced nociceptive signaling. As for Na$_V$1.5, although the potential effects on this channel are of interest, the differences observed are minimal and likely to have limited physiological significance.

Fractions reveal distinct effects compared to crude venom, highlighting additional functional complexity

In the present work, we explored the effects of specific venom fractions (Fig. 9), showing that the same fraction containing NaTxs can either increase or decrease currents depending on the isoform tested. For example, fraction 32 inhibited both channels, with a stronger effect on Na$_V$1.6. Fraction 33 induced one third increase in current for both channels, and also inhibited inactivation (data not shown), possibly containing excitatory toxins for neurons in the CNS and nociceptors in the PNS. Lastly, fraction 35 had distinct effects, it increased current in Na$_V$1.6 with a slight positive shift in the activation $V_{1/2}$ (Table III), but reduced currents in Na$_V$1.7. These findings support the idea that toxins can interact with Na$_V$ subtypes and exert distinct effects (*Gordon et al.*, 2002). Moreover, the overall effect depends on the relative concentration of each toxin in the venom at any given moment. Ongoing efforts are focused on identifying the exact toxins responsible for these varying effects across the different venom fractions.

T. championi venom targeted both mammalian and insect Na$_V$ channels, demonstrating non-exclusive selectivity

Another Na_V channel tested was the cockroach channel BgNav1, where an increase in current was observed, along with inhibition of inactivation, although the decay time constant is not different from the control condition (Fig. 6 and 8, inferior panel). Toxins such as AaH II and LqhαIT2 also inhibit the inactivation of BgNav1 currents, leading to prolonged APs in isolated giant cockroach axons (Gordon *et al.*, 1996). The latter toxin induces flaccid paralysis in fly larvae (Eitan *et al.*, 1990; Loret *et al.*, 1991; Zhu *et al.*, 2020). Also, fractions of crude venom from the *Latrodectus geometricus* spider demonstrated inhibition of inactivation in insect Na_V channels (Khamtorn *et al.*, 2021). Since venoms are complex mixtures of toxins, it is necessary to identify whether this effect is caused by a toxin with high selectivity for insects, which could make it a potential candidate for insecticide development (Gordon *et al.*, 2007; Peigneur & Tytgat, 2012).

T. championi´s venom containing NaTxs has been studied by Salazar *et al.* (2023). In their study, a fraction containing the sequence found in our Fractions 32 and 33 (not shown) was shown to be lethal when injected intracranially in mice (1 μg), caused severe effects when injected intraperitoneally (50 μg), and induced paralysis in cricket for two hours, during which the insect lost complete mobility. This suggests that the venom may exert a paralyzing effect on insects, likely by inhibiting Na_V channel inactivation and blocking Shaker channels. Such paralysis could allow the scorpion to feed on the immobilized prey. Regarding the effects observed in mice, the severe toxicity resulted in breathing difficulties and paralysis of the limbs, though recovery was seen after 24 hours. This mechanism may offer the scorpion an advantage in predatory situations by incapacitating its attacker long enough to escape.

CONCLUSIONS

This study provides novel insights into the differential modulation of human and insect K_V and Na_V channels by *Tityus championi* venom. Our findings reveal a significant inhibitory effect on $K_V1.2$ and Shaker IR channels, confirming the presence of specific KTx toxins with selective affinity. The newly identified toxin TchKTx7, which exhibits pore-blocking activity, is reported for the first time for this species, offering new evidence of this scorpion venom's ability to selectively target channel subtypes. Additionally, the venom's dual action on Na_V channels, enhancing $Na_V1.2$ and $Na_V1.6$ currents while reducing $Na_V1.7$ activity highlights its complex role in modulating neuronal excitability, with potential analgesic effects. The identification of these

distinct mechanisms across both mammalian and insect ion channels underscores the venom's evolutionary adaptation for predation and defense. These discoveries open new avenues for therapeutic applications targeting specific K_V and Na_V channel subtypes, particularly in the context of neurological disorders and pain management. Further identification and characterization of isolated toxins will be essential to elucidate their precise pharmacological profiles and clinical potential.

GENERAL CONCLUSIONS

This work represents the first electrophysiological characterization into the venom of *T. championi* and some of its neurotoxins, demonstrating its inhibitory effects on neuronal excitability. Specifically, we have shown a decreasing AP firing in mollusk neurons and that inhibitory effect can be associated with the suppression of Na^+ currents mediated by $Na_V1.7$-like channels, and K^+ currents through channels yet to be identified in this organism, but likely related with $K_V1.2$, since this venom proved to have strong inhibitory effects in this K_V isoform.

Of particular note is the NaTx, termed Tch3, which exhibited potential pharmacological properties by inhibiting ion channels expressed in mammalian nociceptors. The venom's broad inhibitory profile extends across various Na_V and K_V isoforms in both mammals and insects, including a confirmed effect on rat $Na_V1.7$ channels. Additionally, the presence of α-toxins in the venom exerted significant effects on $Na_V1.6$ channels, linked to epilepsy in the literature, while the venom's influence on cockroach channels probed its non-selectivity across species. Importantly, the venom affected most human K_V isoforms tested, with a pronounced impact on $K_V1.2$ channels, a key regulator of respiratory function in the brainstem. This discovery enhances our understanding of the clinical manifestations following a scorpion sting and sheds light on the predator-prey dynamics of these animals.

Moreover, the KTxs tested exhibited effects on insect channels, such as ShakerIR, further demonstrating the venom's broad selectivity. Lastly, this thesis uncovered a new KTx from *T. championi*, that we called TchKTx7, that had potent inhibitory effect on $K_V1.2$ and ShakerIR channels.

It is important to point out the convergence of findings using two distinct electrophysiological methodologies and two animal models in this thesis, offering an integrated understanding of neurotoxins. This work not only deepened the knowledge of *T. championi* venom but also expanded the understanding of ion channel diversity in a widely studied model, such as the C1 neuron of *H. aspersa*. Most compellingly, these findings highlight the promising potential for Costa Rican scorpion neurotoxins in the development of novel pain management therapies.

ANEXOS

SUPPLEMENTARY MATERIALS

CAPÍTULO I

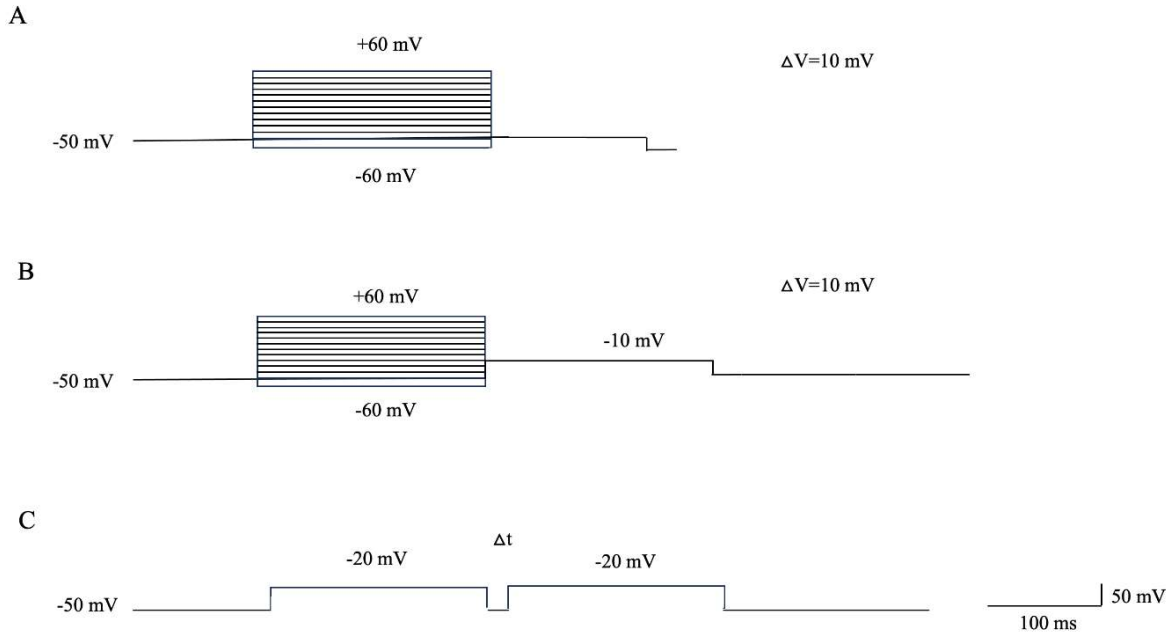

Figure S1. Voltage-clamp stimulation protocols on *Helix aspersa* C1 neurons in whole-cell patch-clamp configuration. (A) Voltage-dependent activation protocol for recording Na^+ and K^+ currents. (B) Voltage-dependent activation from hyperpolarization for recording Na^+ currents. (C) Steady-state inactivation protocol for recording Na^+ currents. (D) Recovery from inactivation protocol for Na^+ channels. The inset values indicate the voltages (mV) of each step.

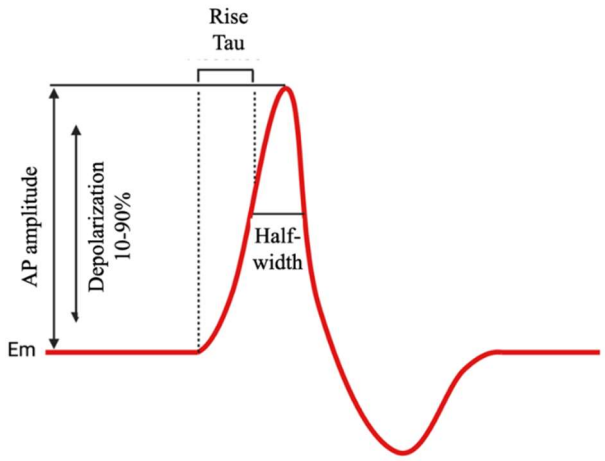

Figure S2. Representation of some of the reported action potential parameters.

$$f(t) = \sum_{i=1}^{n} A_i \, e^{-t/\tau_i} + C \qquad \text{SE.1}$$

Where τ_i represents the time constant of current inactivation.

$$g_{Na} = \frac{I_T}{(V_m - V_{rev})} \qquad \text{SE.2}$$

Where I_T is the maximal transient current, V_m corresponds to the membrane potential of the pulse and V_{rev} corresponds to the experimental reversal potential (the voltage at which the current is equal to 0 pA).

$$Po = \frac{g(V)}{g_{max}} \qquad \text{SE.3}$$

Where g(V) is the conductance calculated with SE.2 at each voltage step, and g_{max} is the maximal conductance.

$$I(V) = \frac{Imax}{1 + e^{\left(\frac{V - V1/2}{k}\right)}} \qquad \text{SE.4}$$

Where I_{max} represents the maximum current, V is the voltage, $V_{1/2}$ is the voltage of half-maximal activation or inactivation, and k is the slope factor of the voltage dependence of open probability.

Table SI. Protein families, identified by mass spectrometry, present in the venom of the scorpion T. championi.

Protein family	Presence
Potassium channel toxin	√
Sodium channel toxin	√
Calcium channel toxin	-
Metalloproteinase	√
Hyaluronidase	√
Cysteine-rich protein	√
Serine proteinase	√
Endothelin-converting enzyme	√
Monooxygenase	√
Angiotensin-converting enzyme	√
Neprilysin	-
Amylase	√
Phosphodiesterase	√
IGF-binding protein	√
G protein-coupled receptor	-
Peptidase inhibitor	√
Cytokinin RF domain-containing protein	√
Lectin	√
Putative phospholipase A2	-
Antimicrobial peptide	-
CRISP/Allergen/PR-1-like	√
Endopeptidase	-
Peptidase M14	-
Peptidyl-prolyl isomerase	-
Vasoactive peptide	-
Hypotensin-like	√
Vasopressin/Oxytocin	-
Calycin	-
Acid phosphatase	-
Glycosyl transferase	-
Putative secreted protein	√
U8-agatoxin-like	-
Hemocyanin	√
Transferrin	-

Table SII. Comparative analysis of distinct properties of IT and IP Na+ currents in various organisms.

Cell/ Channel	Current	Specie	Opening Potential (mV)	Peak Potential (mV)	Peak Amplitude (nA)	E_{rev} (mV)	Reference
C1 Nav1.7-like	I_T	*H. aspersa*	-30	-20	10	+40	Present Article
C1 Nav1.7-like	I_P	*H. aspersa*	-30	-10	2	0	Present Article
GFL of stellate ganglion	I_T	*Loligo opalescens*	-35	-5	~8	+20	Gilly *et al.,* 1997
Pedal ganglion	I_T	*Aplysia californica*	-30	0	~8	+30	Gilly *et al.,* 1997
Nav Cerebral Giant Cell	I_T	*Lymnaea*	-58	-35	~45	+25	Staras, 2002
Nav Cerebral Giant Cell	I_P	*Lymnaea*	-90	0	5	-	Staras, 2002
LPa3 y RPa3	I_T	*H. pomatia*	-45 y -40	-10	-20	+40	Kiss, 2003
LPa3 y RPa3	I_P	*H. pomatia*	-55	-20	-4	0	Kiss, 2003
EC layer II principal neuron	I_P	*Rattus rattus*	-65	-30	-96.5 +- 61.5 pA	+63	Magistretti & Alonso. 1999
Nav1.7	I_P	*H. pomatia*	-	-65	-4	-13.5	Kiss *et al.,* 2012
Nav1.7	I_T	*H. pomatia*	-	-20	-24	+20	Kiss *et al.,* 2012
Nav 1.8	I_T	*H. pomatia*	-	-20	-55	+20	Kiss *et al.,* 2012
Nav 1.8	I_P	*H. pomatia*	-	-35	-4	-14	Kiss *et al.,* 2012
Nav 1.9	I_T	*H. pomatia*	-	-20	-200	+20	Kiss *et al.,* 2012
Nav 1.9	I_P	*H. pomatia*	-	-30	-18	-23	Kiss *et al.,* 2012

CAPÍTULO II

Table SI. Isoforms of channels heterologously expressed in this study and their organism of origin.

Channel Isoform	Organism	Species	Reference
Nav1.2	Rat	*Mus musculus*	Lee *et al.,* 2014
Nav1.4	Rat	*Mus musculus*	Silver *et al.,* 2005
Nav1.5	Human	*Homo sapiens sapiens*	Fan *et al.,* 2010
Nav1.6	Rat	*Mus musculus*	Okura *et al.,* 2014
Nav1.7	Rat	*Mus musculus*	Okura *et al.,* 2014
Bgv1	Cockroach	*Blatella germanica*	Peigneur *et al.,* 2012a
Kv1.1	Human	*H. sapiens sapiens*	Gigolaev *et al.,* 2022
Kv1.2	Human	*H. sapiens sapiens*	Gigolaev *et al.,* 2022
Kv1.3	Human	*H. sapiens sapiens*	Gigolaev *et al.,* 2022
Kv1.4	Human	*H. sapiens sapiens*	Rolf *et al.,* 2000
Kv1.5	Human	*H. sapiens sapiens*	Rolf *et al.,* 2000
Kv1.6	Human	*H. sapiens sapiens*	Gigolaev *et al.,* 2022
Kv10.1	Human	*H. sapiens sapiens*	Moreels *et al.,* 2017
ShakerIR	Housefly	*Drosophila melanogaster*	Timpe *et al.,* 1998

REFERENCIAS

Abroug, F., Ouanes-Besbes, L., Tilouche, N., & Elatrous, S. (2020). Scorpion envenomation: state of the art. *Intensive care medicine*, *46*(3), 401-410.

Adams, D.J; Smith, S.J & Thompson, S.H (1980). Ionic currents in molluscan soma. *Annual Review Neuroscience*. 3: 141–167.

Alexandrou, A. J., Brown, A. R., Chapman, M. L., Estacion, M., Turner, J., Mis, M. A., ... & Stevens, E. B. (2016). Subtype-selective small molecule inhibitors reveal a fundamental role for Nav1. 7 in nociceptor electrogenesis, axonal conduction and presynaptic release. *PloS one*, *11*(4), e0152405.

Alrashdi, B., Dawod, B., Schampel, A., Tacke, S., Kuerten, S., Marshall, J. S., & Côté, P. D. (2019). Nav1. 6 promotes inflammation and neuronal degeneration in a mouse model of multiple sclerosis. *Journal of Neuroinflammation*, *16*, 1-13.

Amr, Z. S., Baker, M. A. A., Al-Saraireh, M., & Warrell, D. A. (2021). Scorpions and scorpion sting envenoming (scorpionism) in the Arab Countries of the Middle East. *Toxicon*, *191*, 83-103.

B. Orts, D. J., Peigneur, S., Silva-Gonçalves, L. C., Arcisio-Miranda, M., PW Bicudo, J. E., & Tytgat, J. (2018). AbeTx1 is a novel sea anemone toxin with a dual mechanism of action on shaker-type K+ channels activation. *Marine Drugs*, *16*(10), 360.

Banerjee, A., Lee, A., Campbell, E., & MacKinnon, R. (2013). Structure of a pore-blocking toxin in complex with a eukaryotic voltage-dependent K+ channel. *Elife*, *2*, e00594.

Banerjee, A., Lee, A., Campbell, E., & MacKinnon, R. (2013). Structure of a pore-blocking toxin in complex with a eukaryotic voltage-dependent K+ channel. *Elife*, *2*, e00594.

Batista, C. V. F., Martins, J. G., Restano-Cassulini, R., Coronas, F. I., Zamudio, F. Z., Procópio, R., & Possani, L. D. (2018). Venom characterization of the Amazonian scorpion Tityus metuendus. *Toxicon*, *143*, 51-58.

Batista, C. V., Gómez-Lagunas, F., de la Vega, R. C. R., Hajdu, P., Panyi, G., Gáspár, R., & Possani, L. D. (2002a). Two novel toxins from the Amazonian scorpion Tityus cambridgei that block Kv1. 3 and Shaker B K+-channels with distinctly different affinities. *Biochimica et Biophysica Acta (BBA)-Proteins and Proteomics*, *1601*(2), 123-131.

Batista, C. V., Zamudio, F. Z., Lucas, S., Fox, J. W., Frau, A., Prestipino, G., & Possani, L. D. (2002b). Scorpion toxins from Tityus cambridgei that affect Na+-channels. *Toxicon*, *40*(5), 557-562.

Bergeron, Z. L., & Bingham, J. P. (2012). Scorpion toxins specific for potassium (K+) channels: a historical overview of peptide bioengineering. *Toxins*, *4*(11), 1082-1119.

Borges, A., Graham, M. R., Cândido, D. M., & Pardal, P. P. (2021). Amazonian scorpions and scorpionism: integrating toxinological, clinical, and phylogenetic data to combat a human health crisis in the world's most diverse rainforest. *Journal of Venomous Animals and Toxins including Tropical Diseases*, *27*, e20210028.

Borges, A., Lomonte, B., Angulo, Y., de Patiño, H. A., Pascale, J. M., Otero, R., ... & Caro-López, J. A. (2020). Venom diversity in the Neotropical scorpion genus Tityus: Implications for antivenom design emerging from molecular and immunochemical analyses across endemic areas of scorpionism. *Acta Tropica*, *204*, 105346.

Bosmans, F., & Tytgat, J. (2007). Voltage-gated sodium channel modulation by scorpion α-toxins. *Toxicon*, *49*(2), 142-158.

Bosmans, F., Martin-Eauclaire, M. F., & Tytgat, J. (2007). Differential effects of five 'classical'scorpion β-toxins on rNav1. 2a and DmNav1 provide clues on species-selectivity. *Toxicology and applied pharmacology*, *218*(1), 45-51.

Brenes, E., & Gómez, A. (2016). Scorpion maintenance in captivity for venom extraction in Costa Rica. *Revista Biología Tropical, 64*(3), 1019-1027.

Brenes, O. (2022). Invertebrate neurons as a simple model to study the hyperexcitable state of epileptic disorders in single cells, monosynaptic connections, and polysynaptic circuits. *Biophysical Reviews*, *14*(2), 553-568.

Capera, J., Navarro-Pérez, M., Moen, A. S., Szabó, I., & Felipe, A. (2022). The mitochondrial routing of the Kv1. 3 channel. *Frontiers in oncology*, *12*, 865686.

Carbone, E., Wanke, E., Prestipino, G., Possani, L. D., & Maelicke, A. (1982). Selective blockage of voltage-dependent K+ channels by a novel scorpion toxin. *Nature*, *296*(5852), 90-91.

Carlier, E., Geib, S., De Waard, M., Avdonin, V., Hoshi, T., Fajloun, Z., ... & Kharrat, R. (2000). Effect of maurotoxin, a four disulfide-bridged toxin from the chactoid scorpion Scorpio maurus, on Shaker K+ channels. *The Journal of Peptide Research*, *55*(6), 419-427.

Catterall, W. A., Cestèle, S., Yarov-Yarovoy, V., Frank, H. Y., Konoki, K., & Scheuer, T. (2007). Voltage-gated ion channels and gating modifier toxins. *Toxicon*, *49*(2), 124-141.

Cerni, F. A., Pucca, M. B., Amorim, F. G., Bordon, K. D. C. F., Echterbille, J., Quinton, L., ... & Arantes, E. C. (2016). Isolation and characterization of Ts19 Fragment II, a new long-chain potassium channel toxin from Tityus serrulatus venom. *Peptides*, *80*, 9-17.

Cerni, F. A., Pucca, M. B., Peigneur, S., Cremonez, C. M., Bordon, K. C., Tytgat, J., & Arantes, E. C. (2014). Electrophysiological characterization of Ts6 and Ts7, K+ channel toxins isolated through an improved Tityus serrulatus venom purification procedure. *Toxins*, *6*(3), 892-913.

Chahine, M., Chen, L. Q., Fotouhi, N., Walsky, R., Fry, D., Santarelli, V., ... & Kallen, R. G. (1995). Characterizing the mu-conotoxin binding site on voltage-sensitive sodium channels with toxin analogs and channel mutations. *Receptors & channels*, *3*(3), 161-174.

Chen, M., Lu, M., Feng, X., Wu, M., Luo, X., Xiang, R., ... & Zhou, X. (2023). LmNaTx15, a novel scorpion toxin, enhances the activity of Nav channels and induces pain in mice. *Toxicon*, *236*, 107331.

Chen, R., & Chung, S. H. (2012). Binding modes and functional surface of anti-mammalian scorpion α-toxins to sodium channels. *Biochemistry*, *51*(39), 7775-7782.

Chippaux, J. P., & Goyffon, M. (2008). Epidemiology of scorpionism: a global appraisal. *Acta tropica*, *107*(2), 71-79.

Chow, C. Y., Chin, Y. K. Y., Walker, A. A., Guo, S., Blomster, L. V., Ward, M. J., ... & King, G. F. (2019). Venom peptides with dual modulatory activity on the voltage-gated sodium channel NaV1. 1 provide novel leads for development of antiepileptic drugs. *ACS Pharmacology & Translational Science*, *3*(1), 119-134.

Clairfeuille, T., Cloake, A., Infield, D. T., Llongueras, J. P., Arthur, C. P., Li, Z. R., ... & Payandeh, J. (2019). Structural basis of α-scorpion toxin action on Nav channels. *Science*, 363(6433).

Collaço, RdC. O., Hyslop, S., Dorce, V. A., Antunes, E., & Rowan, E. G. (2019). Scorpion venom increases acetylcholine release by prolonging the duration of somatic nerve action potentials. *Neuropharmacology*, 153, 41-52.

Cologna, C. T., Peigneur, S., Rosa, J. C., Selistre-de-Araujo, H. S., Varanda, W. A., Tytgat, J., & Arantes, E. C. (2011). Purification and characterization of Ts15, the first member of a new α-KTX subfamily from the venom of the Brazilian scorpion Tityus serrulatus. *Toxicon*, *58*(1), 54-61.

Corzo, G., Papp, F., Varga, Z., Barraza, O., Espino-Solis, P. G., de la Vega, R. C. R., ... & Possani, L. D. (2008). A selective blocker of Kv1. 2 and Kv1. 3 potassium channels from the venom of the scorpion Centruroides suffusus suffusus. *biochemical pharmacology*, *76*(9), 1142-1154.

Couraud, F., Jover, E., Dubois, J. M., & Rochat, H. (1982). Two types of scorpion toxin receptor sites, one related to the activation, the other to the inactivation of the action potential sodium channel. *Toxicon*, 20(1), 9-16.

D'Suze, G., Zamudio, F., Gómez-Lagunas, F., & Possani, L. D. (1999). A novel K+ channel blocking toxin from Tityus discrepans scorpion venom. *FEBS letters*, *456*(1), 146-148.

da Mata, D. O., Tibery, D. V., Fernandes-Pedrosa, M. F., & Schwartz, E. F. (2023). Modulation of hNav by Tst1, a β-toxin purified from the scorpion Tityus stigmurus. *Biochimie*, *204*, 118-126.

de la Vega, R. C. R., & Possani, L. D. (2005). Overview of scorpion toxins specific for Na+ channels and related peptides: biodiversity, structure–function relationships and evolution. *Toxicon*, *46*(8), 831-844.

de la Vega, R. C. R., & Possani, L. D. (2007). Novel paradigms on scorpion toxins that affects the activating mechanism of sodium channels. *Toxicon*, *49*(2), 171-180.

de Matos, I. M., Santos, F. F., Marçal, F. L., Silva, L. D., & Silva, M. (2024). Clinical manifestations and management of Tityus species envenoming: A systematic review. *Research, Society and Development*, *13*(2), e1302345161-e1302345161.

de Oliveira, U. C., Nishiyama Jr, M. Y., Dos Santos, M. B. V., Santos-da-Silva, A. D. P., Chalkidis, H. D. M., Souza-Imberg, A., ... & Junqueira-de-Azevedo, I. D. L. M. (2018). Proteomic endorsed transcriptomic profiles of venom glands from Tityus obscurus and T. serrulatus scorpions. *PloS one*, *13*(3), e0193739.

Delgado-Prudencio, G., Possani, L. D., Becerril, B., & Ortiz, E. (2019). The dual α-amidation system in scorpion venom glands. *Toxins*, *11*(7), 425.

Díaz, C., Serna-Gonzalez, M., Chang-Castillo, A., Lomonte, B., Bonilla, F., Alfaro-Chinchilla, A., ... & Sasa, M. (2023). Proteomic profile of the venom of three dark-colored Tityus (Scorpiones: Buthidae) from the tropical rainforests of Costa Rica. *Acta Tropica*, *248*, 107031.

Dib-Hajj, S. D., Yang, Y., Black, J. A., & Waxman, S. G. (2013). The Na v 1.7 sodium channel: From molecule to man. In *Nature Reviews Neuroscience* (Vol. 14, Issue 1, pp. 49–62). https://doi.org/10.1038/nrn3404

Diego-García, E., Batista, C. V., García-Gómez, B. I., Lucas, S., Candido, D. M., Gómez-Lagunas, F., & Possani, L. D. (2005). The Brazilian scorpion Tityus costatus Karsch: genes, peptides and function. *Toxicon*, *45*(3), 273-283.

Dodson, P. D., Billups, B., Rusznák, Z., Szucs, G., Barker, M. C., & Forsythe, I. D. (2003). Presynaptic rat Kv1. 2 channels suppress synaptic terminal hyperexcitability following action potential invasion.

Doyle, D. A., Cabral, J. M., Pfuetzner, R. A., Kuo, A., Gulbis, J. M., Cohen, S. L., ... & MacKinnon, R. (1998). The structure of the potassium channel: molecular basis of K+ conduction and selectivity. *science*, *280*(5360), 69-77.

Dudley, S. C., Todt, H., Lipkind, G., & Fozzard, H. A. (1995). A mu-conotoxin-insensitive Na+ channel mutant: possible localization of a binding site at the outer vestibule. *Biophysical Journal*, *69*(5), 1657-1665.

Duque, H. M., Mourão, C. B. F., Tibery, D. V., Barbosa, E. A., Campos, L. A., & Schwartz, E. F. (2017). To4, the first Tityus obscurus β-toxin fully electrophysiologically characterized on human sodium channel isoforms. *Peptides*, *95*, 106-115.

Eitan, M., Fowler, E., Herrmann, R., Duval, A., Pelhate, M., & Zlotkin, E. (1990). A scorpion venom neurotoxin paralytic to insects that affects sodium current inactivation: purification, primary structure, and mode of action. *Biochemistry*, *29*(25), 5941-5947.

Fan, X. R., Ma, J. H., Zhang, P. H., & Xing, J. L. (2010). Blocking effect of methylflavonolamine on human NaV1. 5 channels expressed in Xenopus laevis oocytes and on sodium currents in rabbit ventricular myocytes. *Acta Pharmacologica Sinica*, 31(3), 297-306.

Filipis, L., Blömer, L. A., Montnach, J., Loussouarn, G., De Waard, M., & Canepari, M. (2023). Nav1. 2 and BK channel interaction shapes the action potential in the axon initial segment. *The Journal of Physiology*, *601*(10), 1957-1979.

Garcia, M. L., Gao, Y. D., McManus, O. B., & Kaczorowski, G. J. (2001). Potassium channels: from scorpion venoms to high-resolution structure. *Toxicon*, *39*(6), 739-748.

Ghosh, A., Roy, R., Nandi, M., & Mukhopadhyay, A. (2019). Scorpion venom–toxins that aid in drug development: a review. *International journal of peptide research and therapeutics*, *25*, 27-37.

Gigolaev, A. M., Kuzmenkov, A. I., Peigneur, S., Tabakmakher, V. M., Pinheiro-Junior, E. L., Chugunov, A. O., ... & Vassilevski, A. A. (2020). Tuning scorpion toxin selectivity: switching from KV1.1 to KV1.3. *Frontiers in Pharmacology, 11*, 551725.

Gilly, W. F., Gillette, R., & McFarlane, M. (1997). Fast and slow activation kinetics of voltage-gated sodium channels in molluscan neurons. *Journal of neurophysiology*, 77(5), 2373-2384.

Godoy, D. A., Badenes, R., Seifi, S., Salehi, S., & Seifi, A. (2021). Neurological and systemic manifestations of severe scorpion envenomation. *Cureus, 13*(4).

Goldin, A. L. (2001). Resurgence of sodium channel research. *Annual review of physiology*, 63(1), 871-894.

Gómez, C. E., Pascal, J. C., Jimenez, J. F., & Esteban, P. (2010). Heterogeneous systems verification on hiles designer tool. In *IECON 2010-36th Annual Conference on IEEE Industrial Electronics Society* (pp. 132-137). IEEE.

Gordon D, Karbat I, Ilan N, Cohen L, Kahn R, et al. (2007) The differential preference of scorpion alpha-toxins for insect or mammalian sodium channels: implications for improved insect control. Toxicon 49: 452–472.

Gordon, D. A. L. I. A., Gilles, N. I. C. O. L. A. S., Bertrand, D. A. N. I. E. L., Molgo, J. O. R. D. I., Nicholson, G. M., Sauviat, M. P., ... & Heinemann, S. H. (2002). Scorpion toxins differentiating among neuronal sodium channel subtypes: nature's guide for design of selective drugs. *Perspectives in molecular toxinology*, 215-238.

Gordon, D., & Gurevitz, M. (2003). The selectivity of scorpion α-toxins for sodium channel subtypes is determined by subtle variations at the interacting surface. *Toxicon*, *41*(2), 125-128.

Gordon, D., Karbat, I., Ilan, N., Cohen, L., Kahn, R., Gilles, N., ... & Gurevitz, M. (2007). The differential preference of scorpion α-toxins for insect or mammalian sodium channels: implications for improved insect control. *Toxicon*, *49*(4), 452-472.

Gordon, D., Martin-Eauclaire, M. F., Cestele, S., Kopeyan, C., Carlier, E., Khalifa, R. B., ... & Rochat, H. (1996). Scorpion toxins affecting sodium current inactivation bind to distinct homologous receptor sites on rat brain and insect sodium channels. *Journal of Biological Chemistry*, *271*(14), 8034-8045.

Goudet, C., Chi, C. W., & Tytgat, J. (2002). An overview of toxins and genes from the venom of the Asian scorpion Buthus martensi Karsch. *Toxicon*, *40*(9), 1239-1258.

Guerra-Duarte, C., Horta, C. C. R., Oliveira-Mendes, B. B. R., de Freitas Magalhães, B., Costal-Oliveira, F., Stransky, S., ... & Chávez-Olórtegui, C. (2019). Determination of hyaluronidase activity in Tityus spp. Scorpion venoms and its inhibition by Brazilian antivenoms. *Toxicon*, *167*, 134-143.

Guerra-Duarte, C., Saavedra-Langer, R., Matavel, A., Oliveira-Mendes, B. B., Chavez-Olortegui, C., & Paiva, A. L. B. (2023). Scorpion envenomation in Brazil: Current scenario and perspectives for containing an increasing health problem. *PLoS neglected tropical diseases*, *17*(2), e0011069.

Guerrero-Vargas, J. A., Mourao, C. B., Quintero-Hernandez, V., Possani, L. D., & Schwartz, E. F. (2012). Identification and phylogenetic analysis of Tityus pachyurus and Tityus obscurus novel putative Na+-channel scorpion toxins. *PLoS One*, *7*(2), e30478.

Gwee, M. C., Nirthanan, S., Khoo, H. E., Gopalakrishnakone, P., Kini, R. M., & Cheah, L. S. (2002). Autonomic effects of some scorpion venoms and toxins. *Clinical and experimental pharmacology and physiology*, *29*(9), 795-801.

Hanck, D. A., & Sheets, M. F. (2007). Site-3 toxins and cardiac sodium channels. *Toxicon*, *49*(2), 181-193.

Hargus, N. J., Nigam, A., Bertram III, E. H., & Patel, M. K. (2013). Evidence for a role of Nav1. 6 in facilitating increases in neuronal hyperexcitability during epileptogenesis. *Journal of neurophysiology*, *110*(5), 1144-1157.

Hedrich, U. B., Lauxmann, S., Wolff, M., Synofzik, M., Bast, T., Binelli, A., ... & Lerche, H. (2021). 4-Aminopyridine is a promising treatment option for patients with gain-of-function KCNA2-encephalopathy. *Science translational medicine*, *13*(609), eaaz4957.

Herzog, R. I., Cummins, T. R., Ghassemi, F., Dib-Hajj, S. D., & Waxman, S. G. (2003). Distinct repriming and closed-state inactivation kinetics of Nav1. 6 and Nav1. 7 sodium channels in mouse spinal sensory neurons. *The Journal of physiology*, *551*(3), 741-750.

Housley, D. M., Housley, G. D., Liddell, M. J., & Jennings, E. A. (2017). Scorpion toxin peptide action at the ion channel subunit level. *Neuropharmacology*, *127*, 46-78.

Hu, W., Tian, C., Li, T., Yang, M., Hou, H., & Shu, Y. (2009). Distinct contributions of Nav1. 6 and Nav1. 2 in action potential initiation and backpropagation. *Nature neuroscience*, *12*(8), 996-1002.

Ierusalimsky, V. N., Roshchin, M. V., & Balaban, P. M. (2020). Immediate-Early Genes Detection in the CNS of Terrestrial Snail. *Cellular and Molecular Neurobiology*, *40*(8), 1395-1404.

Isbister, G. K., & Bawaskar, H. S. (2014). Scorpion envenomation. *New England Journal of Medicine, 371*(5), 457-463.

Jami, S., Deuis, J. R., Klasfauseweh, T., Cheng, X., Kurdyukov, S., Chung, F., ... & Vetter, I. (2023). Pain-causing stinging nettle toxins target TMEM233 to modulate NaV1. 7 function. *Nature Communications*, *14*(1), 2442.

Jegla, T., Marlow, H. Q., Chen, B., Simmons, D. K., Jacobo, S. M., & Martindale, M. Q. (2012). Expanded functional diversity of shaker K+ channels in cnidarians is driven by gene expansion. *PloS one*, *7*(12), e51366.

Jiménez-Vargas, J. M., Possani, L. D., & Luna-Ramírez, K. (2017). Arthropod toxins acting on neuronal potassium channels. *Neuropharmacology*, *127*, 139-160.

Kampo, S., Ahmmed, B., Zhou, T., Owusu, L., Anabah, T. W., Doudou, N. R., ... & Wen, Q. P. (2019). Scorpion venom analgesic peptide, BmK AGAP inhibits stemness, and epithelial-mesenchymal transition by down-regulating PTX3 in breast cancer. *Frontiers in Oncology, 9*, 21.

Khamtorn, P., Peigneur, S., Amorim, F. G., Quinton, L., Tytgat, J., & Daduang, S. (2021). De novo transcriptome analysis of the venom of Latrodectus geometricus with the discovery of an insect-selective Na channel modulator. *Molecules*, *27*(1), 47.

Kirsch, G. E., Skattebøl, A., Possani, L. D., & Brown, A. M. (1989). Modification of Na channel gating by an alpha scorpion toxin from Tityus serrulatus. *The Journal of general physiology*, *93*(1), 67-83.

Kiss, T. (2003). Evidence for a persistent Na-conductance in identified command neurones of the snail, Helix pomatia. *Brain research*, *989*(1), 16-25.

Kiss, T., László, Z., & Pirger, Z. (2012). Cellular localization and kinetic properties of NaV1. 9-, NaV1. 8-, and NaV1. 7-like channel subtypes in Helix pomatia. *Neuroscience*, *203*, 78-90.

Klasfauseweh, T., Israel, M. R., Ragnarsson, L., Cox, J. J., Durek, T., Carter, D. A., ... & Deuis, J. R. (2022). Low potency inhibition of NaV1. 7 by externally applied QX-314 via a depolarizing shift in the voltage-dependence of activation. *European Journal of Pharmacology*, *925*, 175013.

Kozminsky-Atias, A., Somech, E., & Zilberberg, N. (2007). Isolation of the first toxin from the scorpion Buthus occitanus israelis showing preference for Shaker potassium channels. *FEBS letters*, *581*(13), 2478-2484.

Kuang, Q., Purhonen, P., & Hebert, H. (2015). Structure of potassium channels. *Cellular and molecular life sciences*, *72*, 3677-3693.

Lange, A., Giller, K., Hornig, S., Martin-Eauclaire, M. F., Pongs, O., Becker, S., & Baldus, M. (2006). Toxin-induced conformational changes in a potassium channel revealed by solid-state NMR. *Nature*, *440*(7086), 959-962.

Lee, J. H., Liu, J., Shin, M., Hong, M., Nah, S. Y., & Bae, H. (2014). Metergoline inhibits the neuronal Nav1. 2 voltage-dependent Na+ channels expressed in Xenopus oocytes. *Acta Pharmacologica Sinica, 35*(7), 862-868.

Li, Y., Yuan, T., Huang, B., Zhou, F., Peng, C., Li, X., Qiu, Y., Yang, B., Zhao, Y., Huang, Z., & Jiang, D. (2023). Structure of human NaV1.6 channel reveals Na+ selectivity and pore blockade by 4,9-anhydro-tetrodotoxin. *Nature Communications*, *14*(1).

Loret, E. P., Martin-Eauclaire, M. F., Mansuelle, P., Sampieri, F., Granier, C., & Rochat, H. (1991). An anti-insect toxin purified from the scorpion Androctonus australis Hector also acts on the. alpha.-and. beta.-sites of the mammalian sodium channel: sequence and circular dichroism study. *Biochemistry*, *30*(3), 633-640.

Lu, W., Cheng, X., Chen, J., Wang, M., Chen, Y., Liu, J., ... & Cao, P. (2022). A Buthus martensii Karsch scorpion sting targets Nav1. 7 in mice and mimics a phenotype of human chronic pain. *Pain*, *163*(2), e202-e214.

Lukyanetz, E. A., & Sotkis, A. V. (1996). Characterization of single K+ channels in Helix pomatia neurons. *Neurophysiology*, *28*(6), 193-201.

Luna-Ramirez, K., Csoti, A., McArthur, J. R., Chin, Y. K., Anangi, R., del Carmen Najera, R., ... & Finol-Urdaneta, R. K. (2020). Structural basis of the potency and selectivity of Urotoxin, a potent Kv1 blocker from scorpion venom. *Biochemical Pharmacology, 174*, 113782.

Magistretti, J., Ragsdale, D. S., & Alonso, A. (1999). High conductance sustained single-channel activity responsible for the low-threshold persistent Na+ current in entorhinal cortex neurons. *Journal of Neuroscience*, *19*(17), 7334-7341.

Martin-Eauclaire, M. F., Adi-Bessalem, S., Hammoudi-Triki, D., Laraba-Djebari, F., & Bougis, P. E. (2019). Serotherapy against voltage-gated sodium channel-targeting α-toxins from androctonus scorpion venom. *Toxins*, *11*(2), 63.

Martin-Eauclaire, M. F., Pimenta, A. M., Bougis, P. E., & De Lima, M. E. (2016). Potassium channel blockers from the venom of the Brazilian scorpion Tityus serrulatus (). *Toxicon*, *119*, 253-265.

Matsumura, K., Yokogawa, M., & Osawa, M. (2021). Peptide toxins targeting KV channels. *Pharmacology of Potassium Channels*, 481-505.

McDermott, L.A.; Weir, G.A.; Themistocleous, A.C.; Segerdahl, A.R.; Blesneac, I.; Baskozos, G.; Clark, A.J.; Millar, V.; Peck, L.J.; Ebner, D.; et al. (2019). Defining the functional role of Na(V)1.7 in human nociception. *Neuron*, 101, 905–919.e908.

Mckeown, L., Swanton, L., Robinson, P., & Jones, O. T. (2008). Surface expression and distribution of voltage-gated potassium channels in neurons (Review). In *Molecular Membrane Biology* (Vol. 25, Issue 4, pp. 332–343). https://doi.org/10.1080/09687680801992470

Mendes, L. C., Viana, G. M. M., Nencioni, A. L. A., Pimenta, D. C., & Beraldo-Neto, E. (2023). Scorpion peptides and ion channels: an insightful review of mechanisms and drug development. *Toxins*, *15*(4), 238.

Menezes, L. F. S., Maranhão, M. M., Tibery, D. V., de Souza, A. C. B., da Mata, D. O., Campos, L. A., ... & Schwartz, E. F. (2023). Ts17, a Tityus serrulatus β-toxin structurally related to α-scorpion toxins. *Biochimica et Biophysica Acta (BBA)-Biomembranes*, *1865*(1), 184057.

Menezes, L. F. S., Maranhão, M. M., Tibery, D. V., de Souza, A. C. B., da Mata, D. O., Campos, L. A., ... & Schwartz, E. F. (2023). Ts17, a Tityus serrulatus β-toxin structurally related to α-scorpion toxins. *Biochimica et Biophysica Acta (BBA)-Biomembranes*, *1865*(1), 184057.

Ministerio de Salud, 2017. Situación Epidemiológica de las Picaduras de Alacrán en la República de Panamá. Anos: ˜ 2000-2016 (p) 2017. http://www.%20Minsa.gob. pa/nformacion-salud/epidemiologia.

Moczydlowski, E., Olivera, B. M., Gray, W. R., & Strichartz, G. R. (1986). Discrimination of muscle and neuronal Na-channel subtypes by binding competition between [3H] saxitoxin and mu-conotoxins. *Proceedings of the National Academy of Sciences*, *83*(14), 5321-5325.

Molavinia, S., Salehcheh, M., Baradaran, M., Karimi, M. A., Pirmoradi, G., & Mohammadi, E. (2024). The effects of chlorotoxin and its derivatives on glioma cells: a systematic review of in vitro studies. *Toxin Reviews, 43*(2), 255-263.

Moreels, L., Peigneur, S., Yamaguchi, Y., Vriens, K., Waelkens, E., Zhu, S., ... & Tytgat, J. (2017). Expanding the pharmacological profile of κ-hefutoxin 1 and analogues: A focus on the inhibitory effect on the oncogenic channel Kv10. 1. *Peptides, 98*, 43-50.

Mouhat, S., Andreotti, N., Jouirou, B., & Sabatier, J. M. (2008). Animal toxins acting on voltage-gated potassium channels. *Current pharmaceutical design*, *14*(24), 2503-2518.

Narahashi, T. O. S. H. I. O., Shapiro, B. I., Deguchi, T. A. K. E. H. I. K. O., Scuka, M., & Wang, C. M. (1972). Effects of scorpion venom on squid axon membranes. *American Journal of Physiology-Legacy Content,* 222(4), 850-857.

Naseem, M. U., Gurrola-Briones, G., Romero-Imbachi, M. R., Borrego, J., Carcamo-Noriega, E., Beltrán-Vidal, J., ... & Panyi, G. (2023). Characterization and chemical synthesis of Cm39 (α-KTx 4.8): a scorpion toxin that inhibits voltage-gated K+ channel KV1. 2 and small-and intermediate-conductance Ca2+-Activated K+ channels KCa2. 2 and KCa3. 1. *Toxins*, *15*(1), 41.

Nencioni, A. L. A., Beraldo Neto, E., Freitas, L. A. D., & Dorce, V. A. C. (2018). Effects of Brazilian scorpion venoms on the central nervous system. *Journal of venomous animals and toxins including tropical diseases*, *24*, 3.

Nishikawa, A. K., Caricati, C. P., Lima, M. L. S. R., Dos Santos, M. C., Kipnis, T. L., Eickstedt, V. R. D., ... & Da Silva, W. D. (1994). Antigenic cross-reactivity among the venoms from several species of Brazilian scorpions. *Toxicon*, *32*(8), 989-998.

Okura, D., Horishita, T., Ueno, S., Yanagihara, N., Sudo, Y., Uezono, Y., & Sata, T. (2014). The endocannabinoid anandamide inhibits voltage-gated sodium channels Nav1. 2, Nav1. 6, Nav1. 7, and Nav1. 8 in Xenopus oocytes. *Anesthesia & Analgesia*, 118(3), 554-562.

Oliveira-Mendes, B. B. R. D., Miranda, S. E. M., Sales-Medina, D. F., Magalhaes, B. D. F., Kalapothakis, Y., Souza, R. P. D., ... & Horta, C. C. R. (2019). Inhibition of Tityus serrulatus venom hyaluronidase affects venom biodistribution. *PLoS neglected tropical diseases*, *13*(4), e0007048.

Oren, D. A., Froy, O., Amit, E., Kleinberger-Doron, N., Gurevitz, M., & Shaanan, B. (1998). An excitatory scorpion toxin with a distinctive feature: an additional α helix at the C terminus and its implications for interaction with insect sodium channels. *Structure*, *6*(9), 1095-1103.

Pardal, P. P. D. O., Castro, L. C., Jennings, E., Pardal, J. S. D. O., & Monteiro, M. R. D. C. D. C. (2003). Aspectos epidemiológicos e clínicos do escorpionismo na região de Santarém, Estado do Pará, Brasil. *Revista da Sociedade Brasileira de Medicina Tropical*, *36*, 349-353.

Pardal, P. P., Ishikawa, E. A., Vieira, J. L., Coelho, J. S., Dórea, R. C., Abati, P. A., ... & Chalkidis, H. M. (2014). Clinical aspects of envenomation caused byTityus obscurus (Gervais, 1843) in two distinct regions of Pará state, Brazilian Amazon basin: a prospective case series. *Journal of Venomous Animals and Toxins including Tropical Diseases*, *20*, 1-7.

Peigneur, S., & J, Tytgat. (2012). The Sophisticated Peptide Chemistry of Venomous Animals as a Source of Novel Insecticides Acting on Voltage-Gated Sodium Channels. *Insecticides—Advances in Integrated Pest Management; IntechOpen: London, UK*, 213-250.

Peigneur, S., Béress, L., Möller, C., Marí, F., Forssmann, W. G., & Tytgat, J. (2012a). A natural point mutation changes both target selectivity and mechanism of action of sea anemone toxins. *The FASEB Journal, 26*(12), 5141-5151.

Peigneur, S., Sevcik, C., Tytgat, J., Castillo, C., & D'Suze, G. (2012b). Subtype specificity interaction of bactridines with mammalian, insect and bacterial sodium channels under voltage clamp conditions. *The FEBS Journal*, *279*(21), 4025-4038.

Pucca, M. B., Cerni, F. A., Peigneur, S., Bordon, K. C., Tytgat, J., & Arantes, E. C. (2015a). Revealing the function and the structural model of Ts4: insights into the “non-toxic” toxin from Tityus serrulatus venom. *Toxins*, *7*(7), 2534-2550.

Pucca, M. B., Peigneur, S., Cologna, C. T., Cerni, F. A., Zoccal, K. F., de CF Bordon, K., ... & Arantes, E. C. (2015b). Electrophysiological characterization of the first Tityus serrulatus alpha-like toxin, Ts5: Evidence of a pro-inflammatory toxin on macrophages. *Biochimie*, *115*, 8-16.

Quintero-Hernández, V., Jiménez-Vargas, J. M., Gurrola, G. B., Valdivia, H. H., & Possani, L. (2013). Scorpion venom components that affect ion-channels function. *Toxicon*, *76*, 328-342.

Reis, M. B., Zoccal, K. F., Gardinassi, L. G., & Faccioli, L. H. (2019). Scorpion envenomation and inflammation: Beyond neurotoxic effects. *Toxicon*, *167*, 174-179.

Rincón-Cortés, C. A., Olamendi-Portugal, T., Carcamo-Noriega, E. N., Santillán, E. G., Zuñiga, F. Z., Reyes-Montaño, E. A., ... & Possani, L. D. (2019). Structural and functional characterization of toxic peptides purified from the venom of the Colombian scorpion Tityus macrochirus. *Toxicon*, *169*, 5-11.

Robbins, C. A., & Tempel, B. L. (2012). Kv1. 1 and Kv1. 2: similar channels, different seizure models. *Epilepsia*, *53*, 134-141.

Rogers, J. C., Qu, Y., Tanada, T. N., Scheuer, T., & Catterall, W. A. (1996). Molecular determinants of high affinity binding of α-scorpion toxin and sea anemone toxin in the S3-S4 extracellular loop in domain IV of the Na+ channel α subunit. *Journal of Biological Chemistry*, *271*(27), 15950-15962.

Rolf, S., Haverkamp, W., Borggrefe, M., Mußhoff, U., Eckardt, L., Mergenthaler, J., ... & Madeja, M. (2000). Effects of antiarrhythmic drugs on cloned cardiac voltage-gated potassium channels expressed in Xenopus oocytes. *Naunyn-Schmiedeberg's archives of pharmacology, 362*, 22-31.

Salazar, M. H., Arenas, I., Corrales-García, L. L., Miranda, R., Vélez, S., Sánchez, J., ... & Acosta, H. (2018). Venoms of Centruroides and Tityus species from Panama and their main toxic fractions. *Toxicon*, *141*, 79-87.

Salazar, M. H., Ortíz, M. H., Encarnación, S., Zamudio, F., Possani, L. D., Cleghorn, J., ... & Corzo, G. (2023). A proteomic overview of the major venom components from Tityus championi from Panama. *Toxicon*, *227*, 107082.

Santos-da-Silva, A. d. P., Candido, D. M., Nencioni, A. L. A., Kimura, L. F., Prezotto-Neto, J. P., Barbaro, K. C., ... & Dorce, V. A. C. (2017). Some pharmacological effects of Tityus obscurus venom in rats and mice. *Toxicon*, *126*, 51-58.

Schmalhofer, W. A., Calhoun, J., Burrows, R., Bailey, T., Kohler, M. G., Weinglass, A. B., ... & Priest, B. T. (2008). ProTx-II, a selective inhibitor of NaV1.7 sodium channels, blocks action potential propagation in nociceptors. *Molecular pharmacology*, *74*(5), 1476-1484.

Silver, K., & Soderlund, D. M. (2005). State-dependent block of rat Nav1. 4 sodium channels expressed in Xenopus oocytes by pyrazoline-type insecticides. *Neurotoxicology, 26*(3), 397-406.

Shakeel, K., Olamendi-Portugal, T., Naseem, M. U., Becerril, B., Zamudio, F. Z., Delgado-Prudencio, G., ... & Panyi, G. (2023). Of seven new K+ channel inhibitor peptides of *Centruroides bonito*, α-KTx 2.24 has a picomolar affinity for Kv1.2. *Toxins, 15*(8), 506.

Sheng, M., Liao, Y. J., Jan, Y. N., & Jan, L. Y. (1993). Presynaptic A-current based on heteromultimeric K+ channels detected in vivo. *Nature*, *365*(6441), 72-75.

Southan, A. P., & Robertson, B. (2000). Electrophysiological characterization of voltage-gated K+ currents in cerebellar basket and Purkinje cells: Kv1 and Kv3 channel subfamilies are present in basket cell nerve terminals. *Journal of Neuroscience*, 20(1), 114-122.

Spratt, P. W., Ben-Shalom, R., Keeshen, C. M., Burke, K. J., Clarkson, R. L., Sanders, S. J., & Bender, K. J. (2019). The autism-associated gene Scn2a contributes to dendritic excitability and synaptic function in the prefrontal cortex. *Neuron*, *103*(4), 673-685.

Srinivasan, K. N., Gopalakrishnakone, P., Tan, P. T., Chew, K. C., Cheng, B., Kini, R. M., ... & Brusic, V. (2002). SCORPION, a molecular database of scorpion toxins. *Toxicon*, *40*(1), 23-31.

Srinivasan, K. N., Sivaraja, V., Huys, I., Sasaki, T., Cheng, B., Kumar, T. K. S., ... & Gopalakrishnakone, P. (2002). κ-hefutoxin1, a novel toxin from the scorpionheterometrus fulvipes with unique structure and function: importance of the functional diad in potassium channel selectivity. *Journal of Biological Chemistry*, *277*(33), 30040-30047.

Staras, K., Győri, J., & Kemenes, G. (2002). Voltage-gated ionic currents in an identified modulatory cell type controlling molluscan feeding. *European Journal of Neuroscience*, *15*(1), 109-119.

Stevens, M., Peigneur, S., & Tytgat, J. (2011). Neurotoxins and their binding areas on voltage-gated sodium channels. Frontiers in pharmacology, 2, 71.

Terlau, H., Shon, K. J., Grilley, M., Stocker, M., Stühmer, W., & Olivera, B. M. (1996). Strategy for rapid immobilization of prey by a fish-hunting marine snail. *Nature*, *381*(6578), 148-151.

Tibery, D. V., Campos, L. A., Mourão, C. B. F., Peigneur, S., e Carvalho, A. C., Tytgat, J., & Schwartz, E. F. (2019). Electrophysiological characterization of Tityus obscurus β toxin 1 (To1) on Na+-channel isoforms. *Biochimica et Biophysica Acta (BBA)-Biomembranes*, *1861*(1), 142-150.

Timpe, L. C., Schwarz, T. L., Tempel, B. L., Papazian, D. M., Jan, Y. N., & Jan, L. Y. (1988). Expression of functional potassium channels from Shaker cDNA in Xenopus oocytes. *Nature*, *331*(6152), 143-145.

Todesca, L. M., Gerke, M., Bulk, E. E., Bachmann, M., Rudersdorf, A., Antonuzzo, L., ... & Schwab, A. (2024). Targeting KCa3.1 channels to overcome erlotinib resistance in non-small cell lung cancer cells. *Cell Death Discovery, 10*(1), 2.

van Cann, M., Kuzmenkov, A., Isensee, J., Andreev-Andrievskiy, A., Peigneur, S., Khusainov, G., ... & Hucho, T. (2021). Scorpion toxin MeuNaTxα-1 sensitizes primary nociceptors by selective modulation of voltage-gated sodium channels. *The FEBS Journal*, *288*(7), 2418-2435.

Vetter, I., Deuis, J. R., Mueller, A., Israel, M. R., Starobova, H., Zhang, A., ... & Mobli, M. (2017). NaV1. 7 as a pain target–from gene to pharmacology. *Pharmacology & therapeutics*, *172*, 73-100.

Wang, C. Y., Tan, Z. Y., Chen, B., Zhao, Z. Q., & Ji, Y. H. (2000). Antihyperalgesia effect of BmK IT2, a depressant insect-selective scorpion toxin in rat by peripheral administration. *Brain research bulletin*, *53*(3), 335-338.

Williams, M. R., Fuchs, J. R., Green, J. T., & Morielli, A. D. (2012). Cellular mechanisms and behavioral consequences of Kv1. 2 regulation in the rat cerebellum. *Journal of Neuroscience*, 32(27), 9228-9237.

Xie, G., Harrison, J., Clapcote, S. J., Huang, Y., Zhang, J. Y., Wang, L. Y., & Roder, J. C. (2010). A new Kv1. 2 channelopathy underlying cerebellar ataxia. *Journal of Biological Chemistry*, *285*(42), 32160-32173.

Xu, H., Li, T., Rohou, A., Arthur, C. P., Tzakoniati, F., Wong, E., ... & Payandeh, J. (2019). Structural basis of Nav1. 7 inhibition by a gating-modifier spider toxin. *Cell*, *176*(4), 702-715.

Yanagawa, Y., Abe, T., & Satake, M. (1986). Blockade of [3H] lysine-tetrodotoxin binding to sodium channel proteins by conotoxin GIII. *Neuroscience letters*, *64*(1), 7-12.

Yuan, S., Gao, B., & Zhu, S. (2017). Molecular dynamics simulation reveals specific interaction sites between scorpion toxins and Kv1. 2 channel: implications for design of highly selective drugs. *Toxins*, *9*(11), 354.

Zakon, H. H. (2012). Adaptive evolution of voltage-gated sodium channels: the first 800 million years. *Proceedings of the National Academy of Sciences*, *109*(supplement_1), 10619-10625.

Zeng, L., Zhang, C., Yang, M., Sun, J., Lu, J., Zhang, H., ... & Jiang, Z. (2024). Unveiling the Diversity and Modifications of Short Peptides in Buthus martensii Scorpion Venom through Liquid Chromatography-High Resolution Mass Spectrometry. *Toxins*, *16*(3), 155.

Zhang, J. Z., Yarov-Yarovoy, V., Scheuer, T., Karbat, I., Cohen, L., Gordon, D., ... & Catterall, W. A. (2012). Mapping the interaction site for a β-scorpion toxin in the pore module of domain III of voltage-gated Na+ channels. *Journal of Biological Chemistry*, *287*(36), 30719-30728.

Zhang, S., Gao, B., & Zhu, S. (2015). Target-driven evolution of scorpion toxins. *Scientific Reports*, *5*(1), 14973.

Zhang, S., Gao, B., & Zhu, S. (2015). Independent Origins of Scorpion Toxins Affecting Potassium and Sodium Channels. *Evolution of Venomous Animals and Their Toxins, 1–16.*

Zhang, X. Y., Bai, Z. T., Chai, Z. F., Zhang, J. W., Liu, Y., & Ji, Y. H. (2003). Suppressive effects of BmK IT2 on nociceptive behavior and c-Fos expression in spinal cord induced by formalin. *Journal of neuroscience research*, *74*(1), 167-173.

Zhao, R., Zhang, X. Y., Yang, J., Weng, C. C., Jiang, L. L., Zhang, J. W., ... & Ji, Y. H. (2008). Anticonvulsant effect of BmK IT2, a sodium channel-specific neurotoxin, in rat models of epilepsy. *British journal of pharmacology*, *154*(5), 1116-1124.

Zhu, S., Gao, B., Peigneur, S., & Tytgat, J. (2020). How a scorpion toxin selectively captures a prey sodium channel: the molecular and evolutionary basis uncovered. *Molecular Biology and Evolution, 37*(11), 3149-3164.